



Fall 2022

Modeling 21st century peak streamflows in the Stillaguamish Watershed using dynamically downscaled general circulation model projections

James Marcell Robinson
Western Washington University, jmrobins@mtu.edu

Follow this and additional works at: <https://cedar.wwu.edu/wwuet>



Part of the [Geology Commons](#)

Recommended Citation

Robinson, James Marcell, "Modeling 21st century peak streamflows in the Stillaguamish Watershed using dynamically downscaled general circulation model projections" (2022). *WWU Graduate School Collection*. 1150.

<https://cedar.wwu.edu/wwuet/1150>

This Masters Thesis is brought to you for free and open access by the WWU Graduate and Undergraduate Scholarship at Western CEDAR. It has been accepted for inclusion in WWU Graduate School Collection by an authorized administrator of Western CEDAR. For more information, please contact westerncedar@wwu.edu.

**Modeling 21st Century Peak Streamflows in the Stillaguamish Watershed Using
Dynamically Downscaled General Circulation Model Projections**

By

James M. Robinson

Accepted in Partial Completion
of the Requirements for the Degree
Master of Science

ADVISORY COMMITTEE

Dr. Robert J. Mitchell, Chair

Dr. Allison M. Pfeiffer

Dr. Guillaume S. Mauger

GRADUATE SCHOOL

David L. Patrick, Dean

Master's Thesis

In presenting this thesis in partial fulfillment of the requirements for a master's degree at Western Washington University, I grant to Western Washington University the non-exclusive royalty-free right to archive, reproduce, distribute, and display the thesis in any and all forms, including electronic format, via any digital library mechanisms maintained by WWU.

I represent and warrant this is my original work, and does not infringe or violate any rights of others. I warrant that I have obtained written permissions from the owner of any third party copyrighted material included in these files.

I acknowledge that I retain ownership rights to the copyright of this work, including but not limited to the right to use all or part of this work in future works, such as articles or books.

Library users are granted permission for individual, research and non-commercial reproduction of this work for educational purposes only. Any further digital posting of this document requires specific permission from the author.

Any copying or publication of this thesis for commercial purposes, or for financial gain, is not allowed without my written permission.

James M. Robinson

December 7, 2022

**Modeling 21st Century Peak Streamflows in the Stillaguamish Watershed Using
Dynamically Downscaled General Circulation Model Projections**

A Thesis
Presented to
The Faculty of
Western Washington University

In Partial Fulfillment
Of the Requirements for the Degree
Master of Science

by
James M. Robinson
December 2022

Preamble

This document has two parts: this primary document which was written in journal manuscript format, and a Supplemental Materials document which describes additional information related to the research. The primary document is a complete narrative and can be read on its own. The Supplemental Materials provide background information, a more thorough methods description, and additional results. It should be read in conjunction with the primary document, but it does include its own table of contents, tables, and figures.

Abstract

Climate change is projected to increase river flooding in the Puget Sound region of Washington State by reducing snowpack and yielding more intense storm events. Pairing meteorological forcings from general circulation models (GCMs) with a physically based hydrologic model is a robust method of assessing watershed response to projected climate. Before GCM forcings can be applied to regional hydrologic models, some form of downscaling or regionalization is required. Dynamical downscaling is a means of incorporating mesoscale atmospheric processes within GCM-informed boundary conditions. Here I apply climate projections, dynamically downscaled using the Weather Research and Forecasting model (WRF), to the Stillaguamish watershed in northwest Washington State using the physically based Distributed Hydrology Soil Vegetation Model (DHSVM). I simulate hourly streamflow for 12 high emissions scenarios (i.e., Representative Concentration Pathway 8.5) throughout the 1,724-square-kilometer basin from 1970 through 2099 and analyze climate and hydrologic trends, with a particular emphasis on peak flows. My projections indicate that as the climate warms, snowpack will recede to higher elevations and the basin will shift from transitional to rain-dominant, leading to an increase in average winter streamflows and a decline in spring and summer streamflows. Peak streamflow magnitude in the Stillaguamish River will increase by about +26.5% across the assessed return intervals (2 to 100 years) and flow durations (3 hours to 1 week) by the 2080s. Similarly, modern day peak flow magnitudes will recur more frequently. Flow generating mechanisms also change, with rain-on-snow events decreasing in likelihood while extreme precipitation events become more common and more severe. These shifts have wide ranging implications for flooding within the developed lowlands of the watershed, and for threatened salmonid populations which are culturally and economically critical to the region.

Acknowledgements

This research would not have been possible without the funding and support provided by the Stillaguamish Tribe of Indians and the Bureau of Indian Affairs Branch of Tribal Climate Resilience. Thanks especially to Kip Killebrew, former Fisheries Biologist at the Tribe, for his long support of our lab's research. This work was also supported by the U.S. Geological Survey Northwest Climate Adaptation Science Center award G17A000218 which provided funding and training on co-producing actionable science. The Geologic Society of America also provided funding. Regional climate model simulations were provided by Ruby Leung at Pacific Northwest National Laboratory and Cliff Mass at the University of Washington Department of Atmospheric Sciences. This work was completed in tandem with similar research conducted by Guillaume Mauger, Jason Won, and Nicoleta Cristea for the Snohomish Watershed. Both projects were supported by Snohomish County through a grant from the Washington State Floodplains by Design Program.

Thank you to Dr. Guillaume Mauger and Jason Won for providing many insights on climate model downscaling and analytical methods. Thank you to Dr. Allison Pfeiffer for her geomorphic insights and encouragement throughout the project. Working with my advisor, Dr. Robert Mitchell, was the impetus of my move from New York City to Bellingham and attendance at WWU. His teaching and support were excellent, and I am honored to be a part of his lab group. Thanks also to Kate Clarke, Kyra Freeman, Ryan Murphy, Susan Dickerson-Lange, and Stephanie Truitt who all contributed methods and R scripts to improve DHSVM processing. A big thanks also goes out to Dr. Jimmy Diehl (WWU Geology Alumnus), my undergraduate geophysics professor and Dr. Robert Mitchell's MS advisor. Without his recommendation, I might not have stumbled upon this opportunity. Thanks also to the WWU Geology program at large for fostering a supportive and fun environment to learn about rocks and water.

Finally, thanks to my friends and cohort mates in the WWU Geology department. It was a grand time, and I am incredibly grateful to have worked alongside you all. Dr. Julie Morris, my fiancé and best friend pushed me across this MS finish line. Without her, I would be lost in most things, and more relevantly, all the figures herein would be uglier. Lastly, thanks to my parents for their unyielding support.

Table of Contents

1	Introduction	1
1.1	The Stillaguamish Watershed.....	2
1.2	Peak Flows	3
2	Methods	4
2.1	Gridded Meteorological Forcings	4
2.2	Hydrologic Model	6
2.3	Hydrologic Model Calibration	6
2.4	Quantifying Projected Changes in Peak Flow Magnitude	8
2.5	Quantifying Projected Changes in Peak Flow Frequency.....	9
2.6	Assessing Peak Flow Generating Mechanisms.....	10
3	Results	11
3.1	Changes in Climate	11
3.2	Changes in Hydrology.....	11
3.3	Changes in Peak Flow Magnitude.....	13
3.4	Changes Peak Flow Frequency	13
3.5	Changes in Flow Generating Mechanisms.....	14
4	Discussion.....	14
5	Conclusions	17
6	References	19

Tables

Figures

Supplemental Materials

List of Tables and Figures

Table 1: Parent GCMs Downscaled with WRF

Table 2: Bias-corrections Applied to Historical Meteorologic Forcings

Table 3: Model Evaluation Scores for the Stillaguamish DHSVM

Table 4: Difference in 3-hour Peak Flow Change, 1990s to 2050s and 2080s

Figure 1: The Stillaguamish Watershed DHSVM

Figure 2: Calibration Hydrographs at Silvana

Figure 3: Cumulative Probability Plots, 3-hour flows at Silvana

Figure 4: Flow Generating Mechanism Decision Tree

Figure 5: Simulated Annual Hydrograph at Stanwood, 1990s, 2050s, and 2080s

Figure 6: Basin-Mean Snow Water Equivalent, 1990s, 2050s, and 2080s

Figure 7: Map of April 1 Snowline, 1990s, 2050s, 2080s, ACCESS 1.0

Figure 8: Basin-Mean Snow Melt, 1990s, 2050s, and 2080s

Figure 9: Discharge vs Return Period, 3-hour flows, 1990s, 2050s, 2080s

Figure 10: Percent Change in 3-hour, 10-year Peak Flow Magnitude

Figure 11: Frequency of 3-hour, 10-year Peak Flow Occurrence per 30-year Climate Normal

Figure 12: Discharge vs Frequency by Flow Generating Mechanism, 1990s, 2050s, and 2080s

1 Introduction

In the Salish Sea region of Washington State and British Columbia, peak streamflow magnitude and frequency are increasing as the climate warms, particularly in transitional rain-snow basins like that of the Stillaguamish River (Hamlet and Lettenmaier, 2007; Lee et al., 2018; Chegwiddden et al., 2020). Two primary mechanisms are at work: changes in rain-snow partitioning elevation (Mote et al., 2018) and more intense winter rain events (Warner et al., 2015).

Snowpack in mountainous regions of the Pacific Northwest acts as a natural reservoir – snow accumulates throughout cold winter months, when the majority of annual precipitation falls (Neiman et al., 2008), and melts during drier spring and summer months, wetting soils and supplying summer streamflow (Stewart et al., 2004; Hamlet et al., 2013). As the climate warms, snowlines are retreating to higher elevations, exposing a greater proportion of landscape to winter rainfall rather than snow (Ikeda et al., 2019), resulting in higher peak winter streamflow and lower summer streamflow.

Intense winter storm events in the Salish Sea Region are typically attributable to atmospheric rivers (Ralph et al., 2017) – narrow bands of water vapor lasting on the order of hours to days that produce heavy rain and snow when they flow over the high relief of the Cascade Mountain Range (Rutz et al., 2014). As the climate warms, the amount of water vapor atmospheric rivers carry is projected to increase, yielding not only greater precipitation but also rainier versus snowier storms (Warner et al., 2015). Modeling indicates this will result in higher winter peak streamflow, particularly in basins that have historically been snowier but by the end of the century will be increasingly rainier due to rising winter air temperatures (Hamlet et al., 2013).

In this study I assess changes in peak streamflow by applying an ensemble of general circulation model (GCM) projections that were dynamically downscaled with the Weather Research and Forecasting model (WRF; Skamarock et al., 2008) to a calibrated distributed-hydrology-soil-vegetation model (DHSVM; Wigmosta et al., 1994). I evaluate changes in peak streamflow magnitude and frequency from 1980 through 2099 for each downscaled GCM and evaluate how peak-flow generating mechanisms change through time. This research is novel in its incorporation of dynamically downscaled meteorological projections. Whereas other similar studies incorporated statistically downscaled projections, which typically have limited temporal

resolution (Hamlet et al., 2013; Dickerson-Lange and Mitchell, 2013; Freeman, 2020; Clarke, 2020), the projections used in this study have native sub-hourly temporal resolution. This is critical for incorporating intense short-duration rainfall events like atmospheric rivers (Salathe et al., 2014) that can yield extreme peak flows. This research also advances methods for coupling WRF outputs with DHSVM. Both models are complex and require significant time investments to learn and calibrate.

1.1 The Stillaguamish Watershed

The Stillaguamish River discharges a 1724 km² watershed in the Puget Sound region of northwest Washington State and has a mean annual discharge of about 95 cubic meters per second (m³s⁻¹, 3400 cubic feet per second [cfs], USGS, 2016, Figure 1). The Stillaguamish River has three primary tributaries: Pilchuck Creek to the north, the North Fork of the Stillaguamish River to the northeast, and the South Fork of the Stillaguamish River to the south. The North and South Forks of the Stillaguamish River have high relief (elevation ranges from about 15 to 2,000 meters above sea level [USGS, 2001]), and are dominated by coniferous forests. The North and South Forks are transitional rain-snow basins and maintain significant winter snowpack above approximately 1,000 m. Pilchuck Creek drains a lower relief, rain-dominated section of the basin (elevation ranges from about 5 to 1,100 meters above sea level) and contains a greater proportion of developed lands (e.g., agriculture, urban, residential).

Near-surface geology in the valleys of the Stillaguamish watershed is dominated by unconsolidated alluvial and glacial deposits. These deposits are Pleistocene in age or younger and were deposited during the recession of the Cordilleran ice sheet which retreated about 13,000 years ago, or subsequently due to fluvial processes. The Vashon Drift unit which includes advance, lacustrine, proglacial, outwash, till and recessional deposits is the dominant surficial geologic unit within the watershed (Booth et al., 2003). This unit is a common source of post-glacial landslides in the region such as the devastating Oso landslide which occurred in March 2014 along the North Fork of the Stillaguamish River (USGS, 2017; Wartman et al., 2016). Bedrock in the watershed comprises Mesozoic subduction-borne metamorphic units which are exposed in high relief sections of the watershed (Booth et al., 2003).

The Stillaguamish watershed experiences a Pacific maritime climate with cool wet winters and warm dry summers. Precipitation is highly variable across the watershed due to high relief (Roe et al., 2003) and the surrounding regional topography, which includes the Olympic

Mountain range to the southwest and the Cascades Mountain range to the east (Mass, 1981; Whitney et al., 1993, Minder et al., 2008). Within the historical record, annual precipitation magnitude in the Stillaguamish watershed ranges from less than one meter in the lowlands to over three meters in the highlands (PRISM Climate Group, 2014). Approximately 75% of precipitation in the watershed falls between October and March. The watershed periodically receives heavy winter precipitation from atmospheric rivers – bands of warm, wet air that cross the Pacific Ocean and create heavy precipitation along the west coast of the North America (Lorente-Plazas et al., 2018). Studies examining the prevalence of atmospheric river landfalls suggest they will become more frequent and intense in a warmer future climate (Gao et al., 2015; Warner et al., 2015).

From 1895 to 2014 average air temperatures in the Puget Sound region increased by about 0.7 °C (Abatzglou et al., 2014). This upward trend is projected to continue or increase through the coming decades in part due to the accumulation of anthropogenically generated greenhouse gases such as carbon dioxide, methane, and others which absorb infrared radiation that is reflected from and emitted by Earth’s surface (IPCC, 2021). Modeling efforts aimed at quantifying future air temperatures of the western Cascades project further warming ranging from about 1.9 °C (in a low emissions scenario) to about 4.8 °C in a high emissions scenario by the 2080s, relative to the period 1950 to 1999 (Rogers and Mauger, 2021).

1.2 Peak Flows

Peak flows are high magnitude, short duration streamflows that last on the order of hours to days (Ryberg et al., 2017). Extreme peak flows can lead to flooding, the second most deadly weather-related phenomena in the United States (extreme heat being the deadliest; Ashley and Ashley, 2008; NWS, 2021; Han and Sharif, 2021), and cause significant infrastructure damage (Jongman et al., 2012, Winsemius et al., 2016). In the Puget Sound region, increasing peak-flow magnitude and increasing flow variability are depleting threatened salmonids (Embrey, 1987; Beamer and Pess, 1999; Greene et al., 2005; Mantua et al., 2010; Ward et al., 2015) which are culturally and economically critical to local Indigenous peoples. Despite these negative outcomes, peak flows also perform functions critical to river evolution (Friedman and Lee, 2002; Richter and Thomas, 2007) and ecosystem health by connecting floodplains to streams (Beechie et al., 2013) and maintaining a diverse variety of habitats (Leibowitz et al., 2018). The balance point between negative and beneficial consequences of peak flows correlates with magnitude –

very high magnitude peak flows (>100-year flows) are detrimental to both the human environment and ecosystem health (Lapointe et al., 2000; Thomaz et al., 2007) whereas smaller magnitude peak flows (<10-year flows) have neutral to positive outcomes for a variety of ecosystem services (Talbot et al., 2018). Studies examining peak flows in the Puget Sound region project increases in both flood magnitude and frequency as a function of climate change (Hamlet and Lettenmaier, 2007; Salathé et al., 2014; Lee et al., 2018; Berghuijs et al., 2016; S. Chegwiddden et al., 2020), suggesting peak flows will become more detrimental to both the human environment and aquatic ecosystems by the end of the century.

2 Methods

I paired dynamically downscaled regional climate projections generated with the Weather Research and Forecasting model, (WRF; Skamarock et al., 2008) from 12 high-emissions general circulation models (GCM) with a calibrated physically based hydrologic model -- the Distributed Hydrology Soil Vegetation Model (DHSVM; Wigmosta et al., 1994; Wigmosta et al., 2002), to produce streamflow projections from 1980 through 2099 in the Stillaguamish Watershed. Quantifying changes in peak streamflows was the focus of the analysis. To quantify changes in peak flow magnitude and frequency over time I performed flood frequency analysis on simulated streamflows within three climate normals: the 1990s (water years 1981-2010), 2050s (water years 2040-2069), and 2080s (water years 2070-2099). To examine trends in peak flow generating processes, I linked annual maximum flows (AMF) to antecedent watershed conditions.

2.1 Gridded Meteorological Forcings

The historical meteorologic forcings used for hydrologic model calibration, hereafter referred to as PNNL-Obs, were generated by Ruby Leung and colleagues at the Pacific Northwest National Laboratory using WRF model version 3.2 (Chen et al., 2018). The lateral boundary conditions and sea surface temperature for this WRF implementation were derived from the North America Regional Reanalysis (NARR; Mesinger et al., 2006). Reanalysis datasets are internally consistent gridded collections of weather observations created by combining available historical data and past short-range weather forecasts. The NARR-forced historical WRF simulation used to calibrate the model had a spatial resolution of 6 kilometers (km), a timestep of 1-hour, and a simulation spanning from 1981 through 2015.

The dynamically downscaled climate projections used in this study were generated by Cliff-Mass's research group at the University of Washington Atmospheric Sciences Department using WRF model version 3.2 (Mass et al., 2022). For each WRF simulation, lateral boundary conditions and sea surface temperature were applied from a parent GCM, similar to NARR and PNNL-Obs. The lateral resolution of the WRF projections (hereafter referred to as WRF-GCM) was set to 12-km. Prior to applying the WRF-GCM projections to the Stillaguamish DHSVM, their native 12-km grid was transferred via bilinear interpolation to a 6-km grid matching PNNL-Obs. To reduce biases between WRF-GCMs (e.g., cold, hot, wet, or dry biases), spatial bias-correction factors were made by comparing mean annual meteorology at a given grid cell for a WRF-GCM projection to the respective grid cell of PNNL-Obs. The bias correction factors were calculated for water years 1981-2015, and they were applied to each grid cell for a given WRF-GCM projection prior to forcing the Stillaguamish DHSVM. All parent GCMs in this study were obtained from the Climate Model Inter-comparison Project, phase 5 (CMIP5; Taylor et al., 2011). A total of twelve high-emissions Representative Concentration Pathway (RCP) 8.5 (Van Vuuren et al., 2011) GCMs are included in the model ensemble (Table 1). These GCMs were selected based on Brewer and Mass (2016) who evaluated and ranked GCMs based on their ability to reproduce the climate of the Pacific Northwest. The projections used in this study were also used in Lorente-Plazas et al. (2018).

Climate projections derived from GCMs have coarse spatial (>100 kilometers) resolutions which limit their viability for watershed-specific hydrological modeling. Downscaling is a means of improving spatial resolution based on historical observations (i.e., statistical downscaling) or physical relationships through numerical modeling (i.e., dynamic downscaling; Widmann et al., 2003). A novel aspect of this study is that I used dynamically downscaled historical meteorology (PNNL-Obs) to calibrate my hydrologic model and then applied dynamically downscaled climate projections (WRF-GCM) over the same meteorologic forcing grid. This has several advantages. First, all meteorologic forcings in this study have a native 1-hour timestep. This ensures that the hydrologic model is calibrated for near-instantaneous flows – the basis for many hydraulic regulations and design standards (Chen et al., 2017). Second, regional atmospheric models like WRF account for weather processes in complex topography and they are not limited by the sparsity of weather observations in remote areas (Salathé et al., 2014). Finally, by using the same regional climate model to generate both the

historical calibration and the future projected meteorologic forcings, the hydrologic model is well adapted to reflect the implications of climate change on streamflows rather than the implications of forcing format or downscaling method.

2.2 Hydrologic Model

The DHSVM is a hydrologic model that simulates dynamic (one day or shorter time step) soil moisture, snow cover, evapotranspiration, and runoff production at the grid scale within a watershed (Wigmosta et al., 1994; Wigmosta et al., 2002). It has been widely applied in mountainous regions around the world (e.g., Storck et al., 1998, Bowling and Lettenmaier, 2001; Du et al., 2014; Zhang et al., 2016) and used to assess climate change and landcover impacts on streamflow (e.g., Elsner et al., 2010; Dickerson-Lange and Mitchell, 2013; Lundquist et al., 2013; Cristea et al., 2014). The DHSVM consists of a two-layer canopy to model evapotranspiration, a two-layer energy balance model for snow accumulation and melt, a multilayer unsaturated soil model, a saturated subsurface flow model, and an overland flow and stream routing model. Model inputs include grided timeseries of near-surface meteorology (precipitation, temperature, wind speed, humidity, shortwave and longwave radiation); static grids for topography, soil type, soil thickness, and landcover type; and a stream channel network based on topography (Figure 1 and SM Figures 1-4). In this study, model layers and the stream channel network were built at 150-meter resolution using publicly available data as described in the Supplemental Materials (Section SM 2.1). Channel geometries in the DHSVM are user specified. My calibration includes 36 distinct channel classifications with hydraulic geometries and Mannings n values that correspond to drainage area and slope (steeper slopes have higher Mannings n values and narrower channels; larger drainage areas have larger channels; refer to SM Table 5). The downscaled climate projections from the WRF-GCM simulations were applied at 144 grid points across the watershed at a 6-kilometer horizontal resolution.

2.3 Hydrologic Model Calibration

Hydrologic model calibration involved bias correcting the historical representation of observed climate (PNNL-Obs) and optimizing hydrologic variables such as meteorological constants (e.g., temperature lapse rate, rain/snow partitioning thresholds), soil parameters (e.g., saturated lateral hydraulic conductivity, porosity), and landcover characteristics (e.g., canopy height, leaf area index) to produce the closest match in simulated to observed streamflows.

Simulated snow accumulation was also calibrated by comparing April 1st snow water equivalent (SWE) within a discrete elevation band to nearby SNOTEL stations with similar geographic settings. The Stillaguamish basin lacks a SNOTEL station.

The PNNL-Obs dataset was evaluated in comparison to weather observations from 35 weather stations in and around the Stillaguamish watershed. Biases between PNNL-Obs and regional weather observations were quantified for annual averages, seasonal averages, and extremes of temperature, precipitation, wind speed, and humidity. Generally, PNNL-Obs compared well with observations, but small corrections were applied uniformly across the basin to bias correct all grid cells and timesteps (Table 2). Additional details on the historical meteorology bias correction are provided in the Supplemental Materials (section SM 2.2).

The PNNL-Obs dataset was used to force the Stillaguamish DHSVM throughout the bias-correction process to evaluate meteorological data bias and ensure proper WRF-DHSVM data coupling. For the DHSVM calibration, parameters and constants for meteorology, soil, and landcover were adjusted until achieving a satisfactory model skill. Kling-Gupta efficiency (KGE; Gupta et al., 2009) and Nash-Sutcliffe efficiency (NSE; Nash and Sutcliffe, 1970) were the primary statistical determinants of model skill. The baseline (pre-calibration) DHSVM parameterization was informed by other DHSVM-based studies in similar western Cascade watersheds (Dickerson-Lange and Mitchell, 2013; Freeman, 2019; Clarke, 2020) and sensitivity studies in similar geographies and hydroclimates (Du et al., 2014; Sun et al., 2019). Parameters were modified manually and through automated simulations via a multi-objective complex evolution global optimization method (Yapo et al., 1998). Simulated streamflows were compared to observed streamflows at four stream-gauging stations within the watershed which are equipped with continuous flow monitoring devices (Figure 1). The calibration period was water years (from October 1st through September 30th) 2005 (the start of automated streamflow data recording) through 2015 (the end of the PNNL-Obs timeseries) for three of four gauging stations (NF_Arlington, SF_JordanRd, and Pilchuck626) and 2010 through 2015 for the furthest downstream gauging station (Silvana). Overall, model skill across the basin ranks from “satisfactory” to “good” based on percent bias, NSE, and KGE values (Moriassi, et al., 2007; Moriassi, et al., 2015, Knoben et al., 2019; Table 3; Figure 2 and SM Figures 9-12). A more thorough explanation of the calibration process, including details on April 1 snowpack calibration and evaluation, is provided in the Supplemental Materials (SM 2.2.2).

Calibrating a hydrologic model to peak flows is complicated by two factors: 1) potential data recording errors at gauging sites during peak flows and 2) the limitations of simplified channel geometry and flow logic which are inherent to watershed scale hydrologic models like the DHSVM. During peak flows, stream channels fill above their typical levels and alter stream morphology, invoking potential issues for automated data logging devices and rating curves which are typically calibrated during non-extreme flow events (Turnipseed and Sauer, 2010). This can yield significant errors in stream discharge like when streams breach levees and flow around gauging equipment or stream channels incise, aggrade, or meander. In the DHSVM, all simulated streamflow is retained within stream channels unless it intercepts an unsaturated grid cell (Wigmosta et al., 2002). During peak flows, grid cells adjacent to a stream channel are likely to be fully saturated, meaning all flow directed to a stream channel will be retained within the channel. This means the DHSVM will not simulate overbank flooding which could reduce downstream discharge. I focused DHSVM calibration on overall flows, with a bias towards higher flow volumes. The peak flows predicted by my calibrated model are generally biased high compared to observed flows. This could be caused by gauging data that is biased low during peak flows or by DHSVM limitations which cannot reproduce floodplain storage or bank overtopping. It could also be caused by poor model calibration. Regardless, the objective treatment of flows in DHSVM allowed me to analyze flow changes through time independent of localized channel effects, recording device errors, and imperfect model calibration. In other words, although my calibrated model may be imperfect in absolute terms, the relative changes in simulated streamflow it yields should be informative. This assumes that the calibrated model is sensitive to climate change (i.e., it is not missing key processes or cancelling biases) and that the climate projections applied to the model are accurate. Neither of these assumptions were rigorously tested in this study.

2.4 Quantifying Projected Changes in Peak Flow Magnitude

I quantified changes in peak flow magnitude within each of the 12 WRF-GCM simulations described in section 2.1 (Table 1). Each of these simulations are based on a parent GCM with its own downscaled gridded meteorological timeseries. I used statistical techniques on annual maximum flows (AMF; i.e., the maximum peak stream discharge within a water year at a given reach) over three distinct climate normals: 1981-2010 (the 1990s), 2040-2069 (the 2050s), and 2070-2099 (the 2080s) to quantify changes in peak flow magnitude over time. Each

30-year sample AMF series was fit to an empirical Gumbel extreme value function (Gumbel, 1941) via L-moment parameterization (Hosking 1990), following methods similar to Salathe et al. (2014) and Tohver et al. (2014). Whereas those studies used empirical generalized extreme value (GEV) distributions defined by bootstrap sampling with replacement, I elected to use only my raw simulated results with the Gumbel distribution because of its simpler form and effective performance with small datasets (Cunnane, 1989). In my iterative testing of Gumbel, GEV and Log-Pearson Type 3 distributions, each generated near equivalent results in terms of peak flow change over time. I automated my statistical analysis using R (R Core Team, 2020) and the lmom package (Hosking, 2019). A thorough description of the statistical techniques I used is provided in the Supplemental Materials (SM 2.4). Individual cumulative probability versus discharge plots were created for each DHSVM simulation forced by a WRF-GCM (Figure 3). Cumulative probability describes the likelihood of an AMF being less than or equal to specified discharge for a given climate normal and parent GCM.

Peak flow likelihood can be expressed in decimal or fractional form on an annual basis (i.e., 1% likelihood) or based on return period (i.e., 100-year flow). In this study I use the latter nomenclature. Return period for a given flow magnitude is defined below:

$$RP = \frac{1}{1 - P}$$

Where RP is return period and P is the cumulative probability at a given flow magnitude. Peak flow magnitudes were computed from empirical Gumbel extreme value functions for 2-year, 10-year, 20-year, and 100-year events for average flow durations of 1 hour, 3 hours, 24 hours, 72 hours (3 days), and 168 hours (1 week) for each downscaled WRF-GCM simulation. To quantify peak flow change over time, I calculated percent change in magnitude within individual WRF-GCM simulations (i.e., 10-year peak flows from the 2050s and 2080s climate normal were compared to 10-year peak flows from the 1990s normal). This helps to overcome systematic biases that may be present in individual downscaled GCMs.

2.5 Quantifying Projected Changes in Peak Flow Frequency

A simple method of quantifying changes in peak flow frequency is to count the number of exceedances of a peak flow threshold through time. The threshold I elected is the 10-year peak flow magnitude of the calibrated model forced by PNNL-Obs. This threshold was calculated using the same techniques described in section 2.4 on simulated flows from water years 1986

through 2015. This period is slightly different than the 1990s climate normal (water years 1981-2010) over which the WRF-GCM simulations were evaluated because the PNNL-Obs timeseries is shorter in duration than the WRF-GCM forcings (PNNL-Obs begins 1/1/1981 whereas WRF-GCM forcings begin 1/1/1970). The delayed start allows adequate model spin up to establish reasonable soil saturation and snowpack prior to peak flow analysis. Threshold exceedances were counted over the 1990s, 2050s, and 2080s climate normals of each DHSVM simulation forced by WRF-GCM. An automated screening process was implemented to count individual peak flow exceedances regardless of the duration of the peak flow.

2.6 Assessing Peak Flow Generating Mechanisms

To assess peak flow generating mechanisms through time, I followed the methodology of Chegwiddden et al. (2020) who built from the methods of Berghuijs et al. (2016), Musselman et al. (2018) and Curry and Zwiers (2018). Flow generating mechanisms were qualified based on antecedent watershed conditions leading up to AMFs using an automated decision tree procedure (Figure 4). Possible flow generating mechanisms were: (1) extreme precipitation, (2) rain on snow, (3) snowmelt, or (4) other. The Stillaguamish watershed exhibits characteristics of rain-dominated and transitional rain-snow watersheds, making it susceptible to each of these mechanisms (Hamlet et al., 2013). The goal of this analysis was to evaluate how peak-flow generation is likely to change as the climate warms.

To qualify as a snowmelt event, basin-average snow water equivalent (SWE) had to exceed 0.1 m within 7-days prior to an AMF and SWE had to decline by at least 10% leading up to an AMF (Figure 4). To qualify as a rain on snow (ROS) event, an AMF had to follow within four days of a rain event equal to or exceeding 0.1 m depth (basin average), and snowmelt had to account for greater than 20% of the sum of precipitation and snowmelt. To qualify as an extreme precipitation event, an AMF had to follow within four days of a precipitation event with a magnitude above the 99th percentile for that given year. AMFs that did not meet any of these thresholds were qualified as “Other” and are most likely attributable to soil saturation from prolonged low-intensity rain events and/or snowmelt (Chegwiddden et al., 2020). Each AMF was attributed to a single flow generating mechanism. If multiple criteria were met, the assignment order was snowmelt, rain on snow, and lastly extreme precipitation. The purpose of this ordering is to better evaluate changes in peak-flow generating mechanisms through time. Extreme precipitation events are the most common driver of peak flows in present day and are likely to be

even more common in a warmer climate that produces less snow and more rain. Therefore, I biased the peak-flow mechanism decision tree towards rarer events (snowmelt and rain on snow) to highlight changes in peak-flow generating mechanisms through time.

3 Results

3.1 Changes in Climate

Analysis of the WRF-GCM ensemble indicates that mean annual air temperature in the Stillaguamish watershed will increase by 2.15 to 5.34 °C from the 1990s climate normal (1981-2010) to the 2080s climate normal (2070-2099; SM Figures 13 and 14). Precipitation also trends upwards, from an annual basin-average of 2.35 m in the 1990s climate normal to 2.56 m in the 2080s climate normal (an 8.9% increase, SM Figures 16 and 17). Precipitation intensity likewise trends upwards, with mean ensemble-average annual maximum 24-hour precipitation magnitude increasing from 0.10 m in the 1990s to 0.12 m in the 2080s (a 20 % increase, SM Figure 18) and fall and winter months showing the greatest relative increases in storm intensity (SM Figure 19). Generally, the ensemble shows that rare precipitation events (e.g., 10-year or greater) are becoming more intense over time while high frequency events remain relatively consistent.

3.2 Changes in Hydrology

Simulated hindcasts (1981-2010, the 1990s climate normal) for the WRF-GCM ensemble display hydrology characteristic of a rainy transitional watershed with elevated winter streamflows, a seasonal snowpack, moderate melt-derived spring streamflows, and low summer streamflows (Figures 5 & 6). By midcentury (2040-2069, the 2050s climate normal), in response to a reduced snowpack, simulated hydrographs show a gradational shift to a more rain-dominated signal with higher winter streamflows and lower spring and summer streamflows. These seasonal signals – higher winter streamflow and lower spring and summer streamflow - become even more apparent by the end of century (2070-2099, the 2080s climate normal), at which point a spring melting phase is no longer apparent in monthly hydrographs at the mouth of the watershed. Individual tributaries of the Stillaguamish River show similar trends depending on elevation. High elevation tributaries show the most pronounced changes as they lose a significant portion of their spring melt signal. Lower elevation tributaries display the least change over time (see Supplemental Materials section S3.1 and SM Figure 20).

To examine changes in snow accumulation and melt, I analyzed basin-average snowpack and snow melt in the model ensemble (Figure 6). Snowpack, measured as SWE, in the 1990s climate normal generally peaks around April 1st across all GCMs, consistent with regional observations in the Pacific Northwest (Curry and Zwiers, 2018; Mote et al., 2018). The range of maximum basin-average SWE for the 1990s climate normal ranges from 0.07 to 0.26 m with a mean of 0.15 m. By the 2050s, maximum SWE declines by about 65%, and by the 2080s by 79%. The average timing of peak snow accumulation also shifts 26 days earlier from March 28th in the 1990s to March 2 in the 2080s. SWE in hindcasts across the model ensemble varied significantly but generally seemed to be biased low compared to PNNL-Obs. ACCESS 1.0 generated the greatest overall snowpack and its hindcast April 1st basin-average SWE was most similar to PNNL-Obs. MRI-CGCM3 and NorESM1-M produced the least basin-average SWE (SM Figure 15). The overall negative bias in SWE generation in the model ensemble hindcasts is concerning. It indicates the model ensemble may be insensitive to the effects warming will have on snowpack generation and melt timing.

To assess spatial changes in snow accumulation, I examined DHSVM outputs of April 1st SWE for the ACCESS 1.0 simulation. I believe this GCM produced the most realistic hindcast snowpack for the 1990s climate normal because it produced slightly more SWE than PNNL-Obs, likely due to its cold bias (Bi et al., 2013; SM Figure 14, SM Figure 15). During DHSVM calibration, I observed that the PNNL-Obs calibrated DHSVM likely under-predicted April 1 SWE. Over the available calibration range, PNNL-Obs yielded a mean April 1 SWE of 0.6 m in an elevation band similar to two SNOTEL stations located in similar geographic settings outside of the basin which averaged 1.07 m of SWE over the same period (a 45% low bias, refer to SM 2.2.2 and SM Figure 8). In the ACCESS 1.0 simulation, mean April 1 SWE in the 1990s climate normal is equal to or greater than 0.01 m in depth over an area of 666 square kilometers (km²) of the 1,724 km² watershed (39%; Figure 7). By the 2050s, this value declines to 444 km (26% of the watershed), and by the 2080s to 174 km (10% of the watershed). In terms of elevation, the April 1 snowline in the Stillaguamish recedes from about 800 m above sea level in the 1990s to about 1100 m above sea level in the 2080s.

Basin-average snow melt shows similar trends to basin average snow accumulation (Figure 8). Peak snow melt in the 1990s climate normal spans November through May. By the 2050s, significantly less melting occurs in late autumn and late spring as a function of warmer air

temperatures truncating the snow accumulation season (note that average precipitation for these periods does not decline; SM Figure 16). By the 2080s, snow melt peaks from December through March, with average annual melt over the period declining by about 60% compared to the 1990s climate normal.

3.3 Changes in Peak Flow Magnitude

Peak flows are projected to increase basin-wide for almost all WRF-GCM simulations, regardless of flow duration or return period (Table 4). There is a wide range in projected peak flow magnitudes across the WRF-GCM ensemble. To normalize for individual biases between GCMs, I compared projected peak flows to their relative hindcast (e.g., ACCESS1.0 in the 1990s versus 2080s). At Stanwood, mean 3-hour peak flows are projected to increase by about +12.0% by the 2050s and +26.5% by the 2080s. The WRF-GCMs which project the greatest change in peak flow magnitude from the 1990s to the 2080s are CanESM2, BCC_CSM1.1, FGOALS_g2, and MIROC5; those projecting the least change are: ACCESS1.0, ACCESS1.3 and MRI_CGCM (Figures 9 and 10). The greatest range in projected change is for the rarest events (i.e., 100-year events).

3.4 Changes Peak Flow Frequency

An important factor for evaluating flood risk is flood frequency. The simulations indicate that projected peak flow magnitudes are not stationary through time, rather, they increase over time within individual WRF-GCM simulations. While my methods for calculating peak flow magnitude do incorporate return period, and thus implicitly factor in frequency changes, they do not directly consider how frequently modern extreme flows will occur in the future. To evaluate this metric, I counted the number of individual peak flows within each WRF-GCM simulation that were greater than the PNNL-Obs 10-year peak flow from 1986 through 2015. This threshold is the model equivalent to a modern 10-year event.

The 10-year PNNL-Obs peak flow is 1729 cubic meters per second (m^3s^{-1}). Given the return period and assuming climate stationarity, a flow of that magnitude should be exceeded about 3 times within a 30-year climate normal. A majority (9 of 12) of WRF-GCM simulations exceeded the historical 10-year threshold more than 3 times over a comparable timeframe (Figure 11), indicating that the WRF-GCM ensemble may be biased to produce higher peak flows than the downscaled PNNL-Obs forcings. Over the 2050s and 2080s climate normals, the

10-year PNNL-Obs threshold is exceeded more frequently by all WRF-GCM simulations, indicating that peak flow frequency is not stationary throughout the 21st century. By the 2080s, the 10-year event threshold is exceeded 2.4 times more frequently than in the 1990s.

3.5 Changes in Flow Generating Mechanisms

The dominant AMF generating mechanism in the Stillaguamish Watershed is extreme precipitation throughout the simulation span (Figure 12). In the 1990s climate normal, ROS events are also significant, accounting for 10.6% of AMFs. These ROS events are also larger on average than extreme precipitation events, with an average 24-hour magnitude of $1,553 \text{ m}^3\text{s}^{-1}$ compared to extreme precipitation events at $1230 \text{ m}^3\text{s}^{-1}$. By the 2050s climate normal, ROS events are rarer, accounting for 3.7% of AMFs. By the 2080s, they account for only 1.7% of AMFs, on average across all GCMs. The flow generating mechanism decision tree I used resulted in only one AMF qualifying as a snowmelt event and less than 2% of AMFs qualifying as other.

These results indicate that AMFs in the Stillaguamish watershed are most often associated with extreme precipitation. ROS events, a type of extreme precipitation event, are also a factor but are likely to become less common as the climate warms and the snowpack shrinks (Figures 6 & 7). The shift in flow generating mechanisms towards an overwhelming dominance of extreme precipitation corroborates the findings of Chegwiddden et al. (2020). Similarly, they also validate the findings of Warner et al. (2015) who found that atmospheric river events, the dominant extreme precipitation meteorological mechanism in the region, are projected to increase in intensity over time. The stronger precipitation events in the 2080s mean that even though ROS events are lost by the 2080s, the average streamflow magnitude resulting from extreme precipitation events increases in magnitude by about 26 %, roughly matching the average streamflow magnitude of ROS AMF events in the 1990s.

4 Discussion

Projected climate change will increase peak flows in the Stillaguamish River via two mechanisms: (1) by yielding higher air temperatures which in turn produce more rain and less snow and (2) by increasing extreme precipitation intensity. A shrinking snowpack will magnify peak flows by increasing the proportion of the watershed that receives rain during winter storm events. The ratio of land area that receives rain vs snow relates directly to the volume of water

supplied to streams and rivers during a flood event – rain migrates to stream channels on the order of hours to days; snow migrates to stream channels only when air temperatures are sufficiently high to produce melting – generally long after a storm event has passed. In short, shrinking snowpacks lead to greater runoff during and immediately after storm events. Snowpack has already declined significantly over recent decades (Mote et al. 2018) and my results indicate this trend will continue throughout the century. Atmospheric river events are projected to become more intense, particularly in the second half of this century (Warner et al. 2015; SM Figure 18). As with declines in winter snowpack, this translates directly to more water in streams during peak flows due to higher soil saturation and greater overland flow. Rain events exceeding soil infiltration capacity will become more common and exceed infiltration capacity by greater margins by the end of the century. Overall, my results indicate that peak flow magnitudes will increase substantially in the watershed, by about +12% by the 2050s and +26.5% by the 2080s, depending on river reach, return period, and flow duration. Historic extreme peak flows will also be exceeded more frequently.

This study is focused on peak flows which are a proxy for flood inundation. The hydraulic modeling required to derive flood inundation estimates based on my peak flow projections is beyond the scope of this research. Nonetheless, inferences regarding future flood likelihood and severity can be extrapolated from these results. Peak flows in the Stillaguamish watershed have seen a significant upward trend over the observed record and the majority of the changes have been attributed to changes in climate (Hall et al., 2014). Portions of the Stillaguamish watershed which are prone to periodic seasonal flooding are likely to experience more frequent and more severe flooding barring significant channel modification or upstream floodplain expansion. This will yield varying consequences across the watershed. There is significant human development and agriculture within the historic 100-year flood zones (FEMA, 2020) near the mouth of the Stillaguamish River (e.g., the town of Stanwood – Figure 1). These areas will likely experience significantly greater and more frequent inundation due to climate change later this century. Increased flood severity and susceptibility will yield greater risks for human lives (Han and Sharif, 2021), local ecosystems (Ward et al., 2015), and inflict greater costs on property owners and local municipalities (Winsemius et al., 2015). Increasing flood frequency and severity may also impact the health of downstream ecosystems and water users through introduction of additional contaminant pulses that originate from point sources (Kaushal

et al., 2014). Spawning habitat for endangered anadromous fish species is also likely to deteriorate due to increased channel bed scour during peak flow events (Gendaszek et al., 2017). Ongoing strategies such as engineered log jams (Roni et al., 2015), or other in-stream restoration strategies (Marttila et al., 2019) may provide some resilience to increased magnitude and incidence of peak streamflows.

In less developed portions of the watershed, greater peak flows and flooding have the potential to produce significant geomorphic change in the form of channel migration, aggradation, and/or incision (Richter and Thomas, 2007; Wicherski et al., 2017; Pfeiffer et al., 2019). Though there will be significant negative societal outcomes associated with increasing peak flows, increased flooding may provide some localized and long-term ecological benefits such as regenerating riparian areas (Death et al., 2015; Juracek and Fitzpatrick, 2022) and reconnecting fragmented aquatic ecosystems (Talbot et al., 2018). Managing flood inundation via floodplain reconnection is a potential mechanism for improving ecosystem resilience and salmonid survival rates while also reducing downstream flood risks (Beechie et al., 2013). Floodplain reconnection may also provide other important benefits such as increased groundwater-surface water connectivity and improved aquifer recharge (Wohl, 2021).

The focus of this research is extreme events (e.g., 10-year, 50-year, and 100-year events) which are rare, making them difficult to quantify with a limited set of models and timeseries. Extreme peak flows are controlled by a combination of random variability superimposed on longer-term trends. This analysis is based on 30-year climate normals since this period should encompass natural decadal climate variability. However, the 30-year period also limits the accuracy of the most extreme (e.g., 50- and 100-year) peak flow estimates since they are purely extrapolations from empirical Gumbel extreme value functions. My analysis of changes in peak flow magnitude is limited to individual parent GCMs. Each of the 12 GCMs in the ensemble produced a different range of AMFs. By focusing on peak flow changes within GCMs, I limited the capacity of one or more extreme events within a discrete set of GCMs to unduly affect my analysis. However, I did not evaluate any of the GCMs to determine which set of projections best match historical hydrological observations within the watershed. On average, my model ensemble likely underpredicted snow accumulation (Figure 5). This means that the model ensemble hindcasts (i.e., climate and streamflows for the 1990s climate normal) may be more reflective of a slightly warmer climate. This may mean that the projections underestimate the

effect of warming. Regardless, the conclusions are the same: warming will drive an increase in peak flow magnitude and a shift away from snow-related peak flow generating mechanisms.

The limitations of this study are inherent to many physically based modeling endeavors. The downscaling approach with WRF limited the spatial resolution of projections to 12-kilometers. This resolution can produce accurate basin-wide weather but may lack the resolution required to account for micro-climates and localized storm events like thunderstorms which are rare in the region but may impact future peak streamflows (Zhao et al. 2009). The watershed model, DHSVM, is limited to a single landcover layer (i.e., the model cannot account for changes in development/logging practices) and does not consider the effect of deep groundwater interactions. Groundwater is unlikely to affect peak flows, but it could have a significant influence on spring and summer streamflows which my projections indicate will decline sharply due to losses in snowpack. Lastly, the DHSVM, like many complex hydrologic models, is prone to over-parameterization (Beven, 2006). Throughout the calibration process, I attempted to avoid over-parameterization by using literature values when possible and manually altering sensitive watershed parameters within realistic bounds even if it meant achieving poorer calibration statistics. Despite these efforts, I cannot be sure that the model is the most accurate representation possible of the actual Stillaguamish watershed.

My results indicate that the 12 GCMs in the model ensemble produce a wide range of snowpacks in their hindcast simulations, a critical component of regional hydrology in the western Cascades (SM Figure 15). Moreover, most of the hindcasts appear to be biased towards producing less snow than likely exists in the watershed in present day. By analyzing individual GCMs through time, I parsed relative changes over time from the simulations; however, the simulated hindcasts for the model ensemble indicate a bias towards a rainier, less snowy climate than available historical observations suggest is reasonable. Future work could focus on a discrete set of GCMs with less of a warm-bias to match historical signals for the watershed, or the development of a more robust bias correction process or reanalysis methodology aimed at producing hindcasts across the ensemble that are more representative of the present climate in the watershed.

5 Conclusions

I developed and applied dynamically downscaled climate projections generated with WRF to a DHSVM of the Stillaguamish Watershed to analyze how a warming climate would

affect streamflows in the watershed. To calibrate the DHSVM, I iteratively altered key meteorological and hydrological parameters, and evaluated model skill using statistical methods. My coupled WRF-DHSVM models produced “good” to “satisfactory” calibration results (Moriassi et al., 2015) compared to recorded streamflow at gauging sites throughout the watershed. After calibrating the DHSVM and developing a meteorologic basis for bias correcting climate projections, I applied 12 RCP8.5 projections to the DHSVM to simulate hydrological response from 2070 through 2099. I analyzed trends across the model ensemble in terms of climate, hydrology, peak flow magnitude and frequency, and flow generating processes. My projections indicate that the Stillaguamish will experience significant warming, increases in extreme precipitation incidence, and increases in peak flows on the order of +10 to +19% by the 2050s and +23 to +39% by the 2080s.

This research provides significant evidence for how and why peak flows are changing in the Stillaguamish Watershed. Put simply, a warming climate is yielding more rapid runoff and larger floods that occur with greater frequency. Flood generating mechanisms are changing along with the climate, making antecedent snowpack conditions less relevant to peak flow generation. Besides these applied findings, this research can also guide future efforts aimed at regionalizing GCM projections and coupling WRF and DHSVM to inform other watershed-scale planning efforts.

6 References

- Abatzoglou JT, Rupp DE, Mote PW (2014). Seasonal Climate Variability and Change in the Pacific Northwest of the United States. *Journal of Climate* 27(5):2125–2142. <https://doi.org/10.1175/JCLI-D-13-00218.1>
- Ashley ST, Ashley WS (2008). Flood Fatalities in the United States. *Journal of Applied Meteorology and Climatology* 47(3):805–818. <https://doi.org/10.1175/2007JAMC1611.1>
- Beamer EM, Pess GR (1999). Effects of peak flows on Chinook *Oncorhynchus tshawytscha* spawning success in two Puget Sound river basins. In: *Watershed Management to Protect Declining Species*. American Water Resources Association
- Beechie T, Imaki H, Greene J, Wade A, Wu H, Pess G, Roni P, Kimball J, Stanford J, Kiffney P, Mantua N (2013). Restoring salmon habitat for a changing climate. *River Restoration Applications* 29(8):939–960. <https://doi.org/10.1002/rra.2590>
- Berghuijs WR, Woods RA, Hutton CJ, Sivapalan M (2016). Dominant flood generating mechanisms across the United States. *Geophysical Research Letters* 43(9):4382–4390. <https://doi.org/10.1002/2016GL068070>
- Bevin, K (2006). A manifesto for the equifinality thesis. *Journal of Hydrology* 320(1-2): 18-36.
- Bi D, Dix M, Marsland S, O’Farrell S, Rashid H, Uotila P, Hirst A, Kowalczyk E, Golebiewski M, Sullivan A, Yan H, Hannah N, Franklin C, Sun Z, Vohralik P, Watterson I, Zhou X, Fiedler R, Collier M, Ma Y, Noonan J, Stevens L, Uhe P, Zhu H, Griffies S, Hill R, Harris C, Puri K (2013). The ACCESS coupled model: description, control climate and evaluation. *a* 63(1):41–64. <https://doi.org/10.22499/2.6301.004>
- Booth, D.B., Haugerud, R.A., and Troost, K.G. (2003). *The geology of Puget lowland rivers: Restoration of Puget Sound rivers*. University of Washington Press, Seattle, p. 14–45
- Bowling LC, Lettenmaier DP (2001). The Effects of Forest Roads and Harvest on Catchment Hydrology in a Mountainous Maritime Environment. In: *Land Use and Watersheds: Human Influence on Hydrology and Geomorphology in Urban and Forest Areas*. American Geophysical Union (AGU), pp 145–164
- Brewer MC, Mass CF (2016). Projected Changes in Western U.S. Large-Scale Summer Synoptic Circulations and Variability in CMIP5 Models. *Journal of Climate* 29(16):5965–5978. <https://doi.org/10.1175/JCLI-D-15-0598.1>
- Chegwidden SO, Rupp DE, Nijssen B (2020). Climate change alters flood magnitudes and mechanisms in climatically-diverse headwaters across the northwestern United States. *Environ Res Lett* 15(9):094048. <https://doi.org/10.1088/1748-9326/ab986f>

- Chen B, Krajewski WF, Liu F, Fang W, Xu Z (2017). Estimating instantaneous peak flow from mean daily flow. *Hydrology Research* 48(6):1474–1488. <https://doi.org/10.2166/nh.2017.200>
- Chen X, Leung LR, Gao Y, Liu Y, Wigmosta M, Richmond M (2018). Predictability of Extreme Precipitation in Western U.S. Watersheds Based on Atmospheric River Occurrence, Intensity, and Duration. *Geophysical Research Letters* 45(21):11,693–11,701. <https://doi.org/10.1029/2018GL079831>
- Clarke, K. (2020). Modeling the effects of climate change on streamflow and stream temperature in the South Fork of the Stillaguamish River. Western Washington University. 75 p.
- Cristea NC, Lundquist JD, Loheide II SP, Lowry CS, Moore CE (2014). Modelling how vegetation cover affects climate change impacts on streamflow timing and magnitude in the snowmelt-dominated upper Tuolumne Basin, Sierra Nevada. *Hydrological Processes* 28(12):3896–3918. <https://doi.org/10.1002/hyp.9909>
- Curry CL, Zwiers FW (2018). Examining controls on peak annual streamflow and floods in the Fraser River Basin of British Columbia. *Hydrology and Earth System Sciences* 22(4):2285–2309. <https://doi.org/10.5194/hess-22-2285-2018>
- Cunnane, C (1989). Statistical Distributions for Flood Frequency Analysis. Operational Hydrology Report No. 33. World Meteorological Organization, Geneva, Switzerland.
- Du E, Link TE, Gravelle JA, Hubbart JA (2014). Validation and sensitivity test of the distributed hydrology soil-vegetation model (DHSVM) in a forested mountain watershed. *Hydrological Processes* 28(26):6196–6210. <https://doi.org/10.1002/hyp.10110>
- Dymond SF, Aust WM, Prislely SP, Eisenbies MH, Vose JM (2014). Application of a Distributed Process-Based Hydrologic Model to Estimate the Effects of Forest Road Density on Stormflows in the Southern Appalachians. *Forest Science* 60(6):1213–1223. <https://doi.org/10.5849/forsci.13-605>
- Elsner MM, Cuo L, Voisin N, Deems JS, Hamlet AF, Vano JA, Mickelson KEB, Lee S-Y, Lettenmaier DP (2010). Implications of 21st century climate change for the hydrology of Washington State. *Climatic Change* 102(1–2):225–260. <https://doi.org/10.1007/s10584-010-9855-0>
- FEMA (2020). Flood Insurance Study for Snohomish County, Washington and Incorporated Areas, Volumes 1 – 3. Department of Homeland Security. Accessed June 2022 via <https://www.snohomishwa.gov/DocumentCenter/View/6231/53061CV001B-FIS-Vol-1>
- Freeman, K. (2019). Modeling the Effects of Climate Variability on Hydrology and Stream Temperatures in the North Fork of the Stillaguamish River. Western Washington University. 88 p.

- Embrey, S.S. (1987). The relation of streamflow to habitat for anadromous fish in the Stillaguamish River basin, Washington (Water-Resources Investigations Report No. 86–4326). Tacoma, WA: USGS and Stillaguamish Indian Tribe. <https://doi.org/10.3133/wri864326>
- Friedman JM, Lee VJ (2002). Extreme Floods, Channel Change, and Riparian Forests Along Ephemeral Streams. *Ecological Monographs* 72(3):409–425. [https://doi.org/10.1890/0012-9615\(2002\)072\[0409:EFCCAR\]2.0.CO;2](https://doi.org/10.1890/0012-9615(2002)072[0409:EFCCAR]2.0.CO;2)
- Gao Y, Lu J, Leung LR, Yang Q, Hagos S, Qian Y (2015). Dynamical and thermodynamical modulations on future changes of landfalling atmospheric rivers over western North America. *Geophys Res Lett* 42(17):7179–7186. <https://doi.org/10.1002/2015GL065435>
- Gendaszek, A.& Burton, K., Magirl, C., Konrad, C. (2017). Streambed scour of salmon spawning habitat in a regulated river influenced by management of peak discharge. *Freshwater Biology*. 63. 10.1111/fwb.12987.
- Greene CM, Jensen DW, Pess GR, Steel EA, Beamer E (2005). Effects of Environmental Conditions during Stream, Estuary, and Ocean Residency on Chinook Salmon Return Rates in the Skagit River, Washington. *Transactions of the American Fisheries Society* 134(6):1562–1581. <https://doi.org/10.1577/T05-037.1>
- Gumbel EJ (1941). The Return Period of Flood Flows. *Annals of Math Statistics*. 12(2). 28 p. <https://doi.org/10.1214/aoms/1177731747>
- Gupta HV, Kling H, Yilmaz KK, Martinez GF (2009). Decomposition of the mean squared error and NSE performance criteria: Implications for improving hydrological modelling. *Journal of Hydrology* 377(1–2):80–91. <https://doi.org/10.1016/j.jhydrol.2009.08.003>
- Hall, J. E., Beechie, T. J., Pess, G. R. (2014). Influence of climate and land cover on river discharge in the North Fork Stillaguamish River. Northwest Fisheries Science Center, NOAA Fisheries. Final Contract Report to Stillaguamish Tribe of Indians. 41 p.
- Hamlet AF, Lettenmaier DP (2007). Effects of 20th century warming and climate variability on flood risk in the western U.S. *Water Resources Research* 43(6). <https://doi.org/10.1029/2006WR005099>
- Hamlet AF, Elsner MM, Mauger GS, Lee S-Y, Tohver I, Norheim RA (2013). An Overview of the Columbia Basin Climate Change Scenarios Project: Approach, Methods, and Summary of Key Results. *Atmosphere-Ocean* 51(4):392–415. <https://doi.org/10.1080/07055900.2013.819555>
- Han Z, Sharif HO (2021). Analysis of Flood Fatalities in the United States, 1959–2019. *Water* 13(13):1871. <https://doi.org/10.3390/w13131871>
- Hosking JRM (1990). L-Moments: Analysis and Estimation of Distributions Using Linear Combinations of Order Statistics. *Journal of the Royal Statistical Society: Series B (Methodological)* 52(1):105–124. <https://doi.org/10.1111/j.2517-6161.1990.tb01775.x>

- Hosking, JRM (2019). L-moments. R package version 2.8. <https://cran.r-project.org/package=lmom>
- Ikeda, K., R. Rasmussen, C. Liu, A. Newman, F. Chen, M. Barlage, E. Gutmann, J. Dudhia, A. Dai, C. Luce, and K. Musselman. (2021). Snowfall and snowpack in the Western U.S. as captured by convection permitting climate simulations: current climate and pseudo global warming future climate. *Climate Dynamics*
- IPCC, 2021: Climate Change (2021): The Physical Science Basis. Contribution of Working Group I to the Sixth Assessment Report of the Intergovernmental Panel on Climate Change [Masson-Delmotte, V., P. Zhai, A. Pirani, S.L. Connors, C. Péan, S. Berger, N. Caud, Y. Chen, L. Goldfarb, M.I. Gomis, M. Huang, K. Leitzell, E. Lonnoy, J.B.R. Matthews, T.K. Maycock, T. Waterfield, O. Yelekçi, R. Yu, and B. Zhou (eds.)]. Cambridge University Press. In Press.
- Jongman B, Ward PJ, Aerts JCJH (2012). Global exposure to river and coastal flooding: Long term trends and changes. *Global Environmental Change* 22(4):823–835.
<https://doi.org/10.1016/j.gloenvcha.2012.07.004>
- Juracek KE, Fitzpatrick FA (2022). Geomorphic responses of fluvial systems to climate change: A habitat perspective. *River Research and Applications* 38(4):757–775.
<https://doi.org/10.1002/rra.3938>
- Kaushal SS, Mayer PM, Vidon PG, Smith RM, Pennino MJ, Newcomer TA, Duan S, Welty C, Belt KT (2014). Land Use and Climate Variability Amplify Carbon, Nutrient, and Contaminant Pulses: A Review with Management Implications. *J Am Water Resour Assoc* 50(3):585–614.
<https://doi.org/10.1111/jawr.12204>
- Knoben WJM, Freer JE, Woods RA (2019). Technical note: Inherent benchmark or not? Comparing Nash-Sutcliffe and Kling-Gupta efficiency scores. *Catchment hydrology/Modelling approaches*.
<https://doi.org/10.5194/hess-2019-327>
- Lapointe M, Eaton B, Driscoll S, Latulippe C (2011). Modelling the probability of salmonid egg pocket scour due to floods. *Canadian Journal of Fisheries and Aquatic Sciences*.
<https://doi.org/10.1139/f00-033>
- Lee SY, Mauger G, Won J (2018). Effect of Climate Change on Flooding in King County Rivers. Climate Impacts Group, University of Washington. Seattle.
- Leibowitz SG, Wigington Jr. PJ, Schofield KA, Alexander LC, Vanderhoof MK, Golden HE (2018). Connectivity of Streams and Wetlands to Downstream Waters: An Integrated Systems Framework. *JAWRA Journal of the American Water Resources Association* 54(2):298–322.
<https://doi.org/10.1111/1752-1688.12631>
- Lorente-Plazas R, Mitchell TP, Mauger G, Salathé EP (2018). Local Enhancement of Extreme Precipitation during Atmospheric Rivers as Simulated in a Regional Climate Model. *Journal of Hydrometeorology* 19(9):1429–1446. <https://doi.org/10.1175/JHM-D-17-0246.1>

- Lundquist JD, Dickerson-Lange SE, Lutz JA, Cristea NC (2013). Lower forest density enhances snow retention in regions with warmer winters: A global framework developed from plot-scale observations and modeling: *Forests and Snow Retention*. *Water Resour Res* 49(10):6356–6370. <https://doi.org/10.1002/wrcr.20504>
- Mantua N, Tohver I, Hamlet A (2010). Climate change impacts on streamflow extremes and summertime stream temperature and their possible consequences for freshwater salmon habitat in Washington State. *Climatic Change* 102(1–2):187–223. <https://doi.org/10.1007/s10584-010-9845-2>
- Mass C (1981). Topographically Forced Convergence in Western Washington State. *Monthly Weather Review* 109(6):1335–1347. [https://doi.org/10.1175/1520-0493\(1981\)109<1335:TFCIWW>2.0.CO;2](https://doi.org/10.1175/1520-0493(1981)109<1335:TFCIWW>2.0.CO;2)
- Mass C, Salathé EP, Steed R, Baars J (2022). The Mesoscale Response to Global Warming over the Pacific Northwest Evaluated Using a Regional Climate Model Ensemble. *Journal of Climate* 35(6):2035–2053. <https://doi.org/10.1175/JCLI-D-21-0061.1>
- Marttila M, Louhi P, Huusko A, Vehanen T, Mäki-Petäys A, Erkinaro J, Syrjänen JT, Muotka T (2019). Synthesis of habitat restoration impacts on young-of-the-year salmonids in boreal rivers. *Rev Fish Biol Fisheries* 29(3):513–527. <https://doi.org/10.1007/s11160-019-09557-z>
- Mauger GS, Casola JH, Morgan HA, Strauch RL, Jones B, Curry B, Busch Isaksen TM, Whitely Binder L, Krosby MB, Snover AK (2015). *State of Knowledge: Climate Change in Puget Sound*. Climate Impacts Group, University of Washington, Seattle, Washington
- Mesinger F, DiMego G, Kalnay E, Mitchell K, Shafran PC, Ebisuzaki W, Jović D, Woollen J, Rogers E, Berbery EH, Ek MB, Fan Y, Grumbine R, Higgins W, Li H, Lin Y, Manikin G, Parrish D, Shi W (2006) North American Regional Reanalysis. *Bull Amer Meteor Soc* 87(3):343–360. <https://doi.org/10.1175/BAMS-87-3-343>
- Minder JR, Durran DR, Roe GH, Anders AM (2008) The climatology of small-scale orographic precipitation over the Olympic Mountains: Patterns and processes. *Quarterly Journal of the Royal Meteorological Society* 134(633):817–839. <https://doi.org/10.1002/qj.258>
- Moriasi DN, Arnold JG, Liew MWV, Bingner RL, Harmel RD, Veith TL (2007). Model evaluation guidelines for systematic quantification of accuracy in watershed simulations. *Transactions of the ASABE* 50:16
- Moriasi DN, Gitau MW, Pai N, Daggupati P (2015). Hydrologic and Water Quality Models: Performance Measures and Evaluation Criteria. *Trans ASABE* 58(6):1763–1785. <https://doi.org/10.13031/trans.58.10715>
- Mote PW, Li S, Lettenmaier DP, Xiao M, Engel R (2018). Dramatic declines in snowpack in the western US. *npj Clim Atmos Sci* 1(1):2. <https://doi.org/10.1038/s41612-018-0012-1>

- Musselman KN, Lehner F, Ikeda K, Clark MP, Prein AF, Liu C, Barlage M, Rasmussen R (2018). Projected increases and shifts in rain-on-snow flood risk over western North America. *Nature Clim Change* 8(9):808–812. <https://doi.org/10.1038/s41558-018-0236-4>
- Nash JE, Sutcliffe JV (1970). River flow forecasting through conceptual models part I — A discussion of principles. *Journal of Hydrology* 10(3):282–290. [https://doi.org/10.1016/0022-1694\(70\)90255-6](https://doi.org/10.1016/0022-1694(70)90255-6)
- Neiman PJ, Ralph FM, Wick GA, Lundquist JD, Dettinger MD (2008). Meteorological Characteristics and Overland Precipitation Impacts of Atmospheric Rivers Affecting the West Coast of North America Based on Eight Years of SSM/I Satellite Observations. *Journal of Hydrometeorology* 9(1):22–47. <https://doi.org/10.1175/2007JHM855.1>
- NWS (National Weather Service). (2021). Weather Related Fatality and Injury Statistics. Available online: <https://www.weather.gov/hazstat/#> (accessed on 1 January 2021).
- Pfeiffer AM, Collins BD, Anderson SW, Montgomery DR, Istanbuluoglu E (2019). River Bed Elevation Variability Reflects Sediment Supply, Rather Than Peak Flows, in the Uplands of Washington State. *Water Resour Res* 55(8):6795–6810. <https://doi.org/10.1029/2019WR025394>
- PRISM Climate Group. 2014. Average Annual Precipitation (1981-2010), Washington: Oregon State University. Accessed June 2020 via: http://prism.oregonstate.edu/projects/gallery_view.php?state=WA
- R Core Team (2020). R: A language and environment for statistical computing. R Foundation for statistical computing, Vienna, Austria. <https://www.R-project.org/>
- Ralph FM, Dettinger M, Lavers D, Gorodetskaya IV, Martin A, Viale M, White AB, Oakley N, Rutz J, Spackman JR, Wernli H, Cordeira J (2017) Atmospheric Rivers Emerge as a Global Science and Applications Focus. *Bulletin of the American Meteorological Society* 98(9):1969–1973. <https://doi.org/10.1175/BAMS-D-16-0262.1>
- Richter B, Thomas G (2007). Restoring Environmental Flows by Modifying Dam Operations. *Ecology and Society* 12(1). <https://doi.org/10.5751/ES-02014-120112>
- Rogers M and Mauger GS (2021). Pacific Northwest Climate Projection Tool. University of Washington Climate Impacts Group. Accessed June 2022 via https://public.tableau.com/views/PNWClimateProjectionTool/StorySheet?:language=en-US&publish=yes&:display_count=n&:origin=viz_share_link
- Roe GH, Montgomery DR, Hallet B (2003). Orographic precipitation and the relief of mountain ranges. *Journal of Geophysical Research: Solid Earth* 108(B6). <https://doi.org/10.1029/2001JB001521>

- Roni P, Beechie T, Pess G, Hanson K (2015). Wood placement in river restoration: fact, fiction, and future direction. *Can J Fish Aquat Sci* 72(3):466–478. <https://doi.org/10.1139/cjfas-2014-0344>
- Rupp DE, Abatzoglou JT, Hegewisch KC, Mote PW (2013). Evaluation of CMIP5 20th century climate simulations for the Pacific Northwest USA. *Journal of Geophysical Research: Atmospheres* 118(19):10,884–10,906. <https://doi.org/10.1002/jgrd.50843>
- Rutz JJ, Steenburgh WJ, Ralph FM (2014). Climatological Characteristics of Atmospheric Rivers and Their Inland Penetration over the Western United States. *Monthly Weather Review* 142(2):905–921. <https://doi.org/10.1175/MWR-D-13-00168.1>
- Ryberg, K.; Goree, B.; Williams-Sether, T.; Mason, R. (2017). The U.S. Geological Survey Peak-Flow File Data Verification Project, 2008-16 (Scientific Investigations Report No. 2017–5119) (p. 76). USGS.
- Salathé EP, Hamlet AF, Mass CF, Lee S-Y, Stumbaugh M, Steed R (2014). Estimates of Twenty-First-Century Flood Risk in the Pacific Northwest Based on Regional Climate Model Simulations. *Journal of Hydrometeorology* 15(5):1881–1899. <https://doi.org/10.1175/JHM-D-13-0137.1>
- Skamarock WC, Klemp JB, Dudhia J, Gill DO, Barker DM, Duda MG, Huang X-Y, Wang W, Powers JG (2008). A Description of the Advanced Research WRF Version 3. NCAR Technical Note :125
- Stewart IT, Cayan DR, Dettinger MD (2004). Changes in Snowmelt Runoff Timing in Western North America under a 'Business as Usual' Climate Change Scenario. *Climatic Change* 62(1–3):217–232. <https://doi.org/10.1023/B:CLIM.0000013702.22656.e8>
- Stillaguamish Implementation Review Committee (SIRC) (2005). Stillaguamish Watershed Chinook Salmon Recovery Plan. Snohomish County Department of Public Works, Surface Water Management Division, Everett, Washington. Accessed via <https://www.snohomishcountywa.gov/Archive.asp?ADID=2163>, May, 2020.
- Storck P, Bowling L, Wetherbee P, Lettenmaier D (1998). Application of a GIS-based distributed hydrology model for prediction of forest harvest effects on peak stream flow in the Pacific Northwest. *Hydrological Processes* 12(6):889–904. [https://doi.org/10.1002/\(SICI\)1099-1085\(199805\)12:6<889::AID-HYP661>3.0.CO;2-P](https://doi.org/10.1002/(SICI)1099-1085(199805)12:6<889::AID-HYP661>3.0.CO;2-P)
- Sun N, Yan H, Wigmosta MS, Leung LR, Skaggs R, Hou Z (2019). Regional Snow Parameters Estimation for Large-Domain Hydrological Applications in the Western United States. *J Geophys Res Atmos* 124(10):5296–5313. <https://doi.org/10.1029/2018JD030140>
- Talbot CJ, Bennett EM, Cassell K, Hanes DM, Minor EC, Paerl H, Raymond PA, Vargas R, Vidon PG, Wollheim W, Xenopoulos MA (2018). The impact of flooding on aquatic ecosystem services. *Biogeochemistry* 141(3):439–461. <https://doi.org/10.1007/s10533-018-0449-7>

- Taylor K, Ronald S, Meehl G (2011). An overview of CMIP5 and the Experiment Design. *Bulletin of the American Meteorological Society* 93:485–498. <https://doi.org/10.1175/BAMS-D-11-00094.1>
- Thomaz SM, Bini LM, Bozelli RL (2007). Floods increase similarity among aquatic habitats in river-floodplain systems. *Hydrobiologia* 579(1):1–13. <https://doi.org/10.1007/s10750-006-0285-y>
- Tohver IM, Hamlet AF, Lee S-Y (2014). Impacts of 21st-Century Climate Change on Hydrologic Extremes in the Pacific Northwest Region of North America. *JAWRA Journal of the American Water Resources Association* 50(6):1461–1476. <https://doi.org/10.1111/jawr.12199>
- Turnipseed DP, Sauer VB (2010). Discharge Measurements at Gaging Stations. Chapter 8 of Book 3, Section A. Techniques and Methods 3-AB. USGS. US Department of the Interior: 106pp
- USGS. 2001. 10-meter Digital Elevation Model Datasets for Washington State. Accessed November 2019 via: <http://gis.ess.washington.edu/data/raster/tenmeter/byquad/index.html>
- USGS. (2017). Revisiting the Oso Landslide. Accessed October 2019 via: <https://www.usgs.gov/news/revisiting-oso-landslide>.
- USGS.(2016). National Water Information System data available on the World Wide Web, Station 12170300, Accessed June 2022 via https://waterdata.usgs.gov/nwis/uv?site_no=12170300
- Van Vuuren DP, Edmonds J, Kainuma M, Riahi K, Thomson A, Hibbard K, Hurtt GC, Kram T, Krey V, Lamarque J-F, Masui T, Meinshausen M, Nakicenovic N, Smith SJ, Rose SK (2011). The representative concentration pathways: an overview. *Climatic Change* 109(1):5. <https://doi.org/10.1007/s10584-011-0148-z>
- Ward EJ, Anderson JH, Beechie TJ, Pess GR, Ford MJ (2015). Increasing hydrologic variability threatens depleted anadromous fish populations. *Global Change Biology* 21(7):2500–2509. <https://doi.org/10.1111/gcb.12847>
- Warner MD, Mass CF, Salathé EP (2015). Changes in Winter Atmospheric Rivers along the North American West Coast in CMIP5 Climate Models. *Journal of Hydrometeorology* 16(1):118–128. <https://doi.org/10.1175/JHM-D-14-0080.1>
- Wartman J, Montgomery DR, Anderson SA, Keaton JR, Benoît J, dela Chapelle J, Gilbert R (2016). The 22 March 2014 Oso landslide, Washington, USA. *Geomorphology* 253:275–288. <https://doi.org/10.1016/j.geomorph.2015.10.022>
- Whitney WM, Doherty RL, Colman BR (1993). A Methodology for Predicting the Puget Sound Convergence Zone and Its Associated Weather. *Weather and Forecasting* 8(2):214–222. [https://doi.org/10.1175/1520-0434\(1993\)008<0214:AMFPTP>2.0.CO;2](https://doi.org/10.1175/1520-0434(1993)008<0214:AMFPTP>2.0.CO;2)

- Widmann M, Bretherton CS, Salathé EP (2003). Statistical Precipitation Downscaling over the Northwestern United States Using Numerically Simulated Precipitation as a Predictor. *Journal of Climate* 16(5):799–816. [https://doi.org/10.1175/1520-0442\(2003\)016<0799:SPDOTN>2.0.CO;2](https://doi.org/10.1175/1520-0442(2003)016<0799:SPDOTN>2.0.CO;2)
- Wigmosta M.S., Vail LW, Lettenmaier DP (1994). A distributed hydrology soil vegetation model for complex terrain. *Water Resources Research*, 30 (6), 1665-1679.
- Wigmosta M.S., B. Nijssen, and P. Storck. (2002). The Distributed Hydrology Soil Vegetation Model. In *Mathematical Models of Small Watershed Hydrology and Applications*, edited by VP Singh & DK Frevert. 7-42. Highlands Ranch, Colorado:Water Resources Publications. PNNL-SA-36347.
- Winsemius HC, Aerts JCJH, van Beek LPH, Bierkens MFP, Bouwman A, Jongman B, Kwadijk JCJ, Ligtvoet W, Lucas PL, van Vuuren DP, Ward PJ (2016). Global drivers of future river flood risk. *Nature Clim Change* 6(4):381–385. <https://doi.org/10.1038/nclimate2893>
- Wohl E (2021). An Integrative Conceptualization of Floodplain Storage. *Reviews of Geophysics* 59(2):e2020RG000724. <https://doi.org/10.1029/2020RG000724>
- Yapo PO, Gupta HV, Sorooshian S (1998). Multi-objective global optimization for hydrologic models. *Journal of Hydrology* 204(1):83–97. [https://doi.org/10.1016/S0022-1694\(97\)00107-8](https://doi.org/10.1016/S0022-1694(97)00107-8)
- Zhao Q, Liu Z, Ye B, Qin Y, Wei Z, Fang S (2009). A snowmelt runoff forecasting model coupling WRF and DHSVM. *Hydrol Earth Syst Sci* 13(10):1897–1906. <https://doi.org/10.5194/hess-13-1897-2009>
- Zhang G, Kang S, Cuo L, Qu B (2016). Modeling hydrological process in a glacier basin on the central Tibetan Plateau with a distributed hydrology soil vegetation model: APPLICATION OF DHSVM AT A GLACIER BASIN. *J Geophys Res Atmos* 121(16):9521–9539. <https://doi.org/10.1002/2016JD025434>

Tables

Table 1 The twelve general circulation models (GCMs) used as input to the regional Weather Research and Forecasting (WRF) model simulations applied in this study. Horizontal resolution is given in degrees latitude and longitude. Vertical levels refer to the number of layers in each GCM. All simulations described in this study are based on the high-emissions Representative Concentration Pathway 8.5 greenhouse gas scenario.

Model	Parent Research Center, location	Resolution	Vertical Levels
ACCESS1-0	Commonwealth Scientific and Industrial Research Organization (CSIRO), Australia/ Bureau of Meteorology, Australia	1.25° × 1.88°	38
ACCESS1-3	Commonwealth Scientific and Industrial Research Organization (CSIRO), Australia/ Bureau of Meteorology, Australia	1.25° × 1.88°	38
bcc-csm1-1	Beijing Climate Center (BCC), China Meteorological Administration	2.8° × 2.8°	26
CanESM2	Canadian Centre for Climate Modeling and Analysis	2.8° × 2.8°	35
CCSM4	National Center of Atmospheric Research (NCAR), USA	1.25° × 0.94°	26
CSIRO-Mk3-6-0	Commonwealth Scientific and Industrial Research Organization (CSIRO) / Queensland Climate Change Centre of Excellence, Australia	1.8° × 1.8°	18
FGOALS-g2	LASG, Institute of Atmospheric Physics, Chinese Academy of Sciences	2.8° × 2.8°	26
GFDL-CM3	NOAA Geophysical Fluid Dynamics Laboratory, USA	2.5° × 2.0°	48
GISS-E2-H	NASA Goddard Institute for Space Studies, USA	2.5° × 2.0°	40
MIROC5	Atmosphere and Ocean Research Institute (The University of Tokyo), National Institute for Environmental Studies, and Japan Agency for Marine-Earth Science and Technology	1.4° × 1.4°	40
MRI-CGCM3	Meteorological Research Institute, Japan	1.1° × 1.1°	48
NorESM1-M	Norwegian Climate Center, Norway	2.5° × 1.9°	26

Table 2 Bias-corrections applied to the PNNL-Obs (historical) forcings. These were applied uniformly to all PNNL-Obs grid points and timesteps prior to hydrologic model calibration. Bias corrections were based on iterative evaluation of annual and seasonal trends in PNNL-Obs compared to regional weather observations from 35 weather stations in and around the study area.

Variable	Scaling
Temperature	+ 0.2 °C
Precipitation	+ 15%
Wind	-40%
Shortwave Radiation	- 10%

Table 3 – Model evaluation scores for the Stillaguamish DHSVM. Simulated streamflows were compared to observations at four gauging stations in the watershed (Figure 1, Figure 2, and SM Figures 8 through 11) which are operated by the Washington Department of Ecology (Ecology) and the United States Geological Survey (USGS). The “Calibration Water Years” column lists the available overlapping period between historical meteorological forcings (PNNL-Obs) and recorded observations. Daily/monthly average statistics are reported for percent bias, coefficient of determination (R^2), Nash-Sutcliffe Efficiency (NSE), and Kling-Gupta Efficiency (KGE). Qualitative statistical descriptors for model skill from Moriasi et al., 2015 are shown in the bottom row. *A qualitative descriptor is not available for KGE, but it is a metric similar to NSE so the same parameter thresholds as NSE are listed for reference.

Site Name (Agency, ID No.)	Calibration Water Years	Daily / Monthly Calibration Statistics			
		% Bias	R^2	NSE	KGE
Silvana (Ecology 05A070)	2010-2015	-9.3 / -9.2	0.624 / 0.806	0.592 / 0.779	0.763 / 0.814
NFArlington (USGS 12167000)	2005-2015	-11.3 / -11.3	0.622 / 0.755	0.572 / 0.723	0.760 / 0.805
SFJordanRd (Ecology 05A105)	2005-2015	-21.4 / -21.3	0.649 / 0.794	0.607 / 0.669	0.698 / 0.709
Pilchuck626 (Ecology 05D070)	2005-2015	2.1 / 2.2	0.560 / 0.764	0.560 / 0.761	0.636 / 0.781
	Very Good	$X < \pm 5$	$X \geq 0.85$	$X \geq 0.80$	* $X \geq 0.80$
	Good	$\pm 5 \leq X < \pm 10$	$0.85 \geq X \geq 0.75$	$0.80 \geq X \geq 0.70$	$0.80 \geq X \geq 0.70$
	Satisfactory	$\pm 10 \leq X < \pm 15$	$0.75 \geq X \geq 0.60$	$0.70 \geq X \geq 0.50$	$0.70 \geq X \geq 0.50$
	Not Satisfactory	$X \geq \pm 15$	$X \leq 0.60$	$X \leq 0.50$	$X \leq 0.50$

Table 4. Table of minimum, average, and maximum percent change in simulated 3-hour peak flow magnitude across the model ensemble averaged (mean) across 2, 5, 10, and 20-year return periods. Percent change is relative to the 1990s climate normal (1981-2010) by the 2050s (2040-2069) and 2080s (2070-2099). See Figure 1 for map of locations.

Location	2050s % Change			2080s % Change		
	Min	Avg	Max	Min	Avg	Max
Stanwood	-18.8	+12.0	+38.3	+6.7	+26.5	+46.8
Pilchuck626	-22.8	+14.4	+47.9	-0.6	+29.9	+56.6
PortageCreek	-13.6	+18.2	+47.1	+5.0	+39.2	+81.2
NFArlington	-18.2	+10.8	+34.9	+3.8	+23.8	+45.6
NFBoulderCreek	-13.7	+13.7	+43.5	+8.4	+26.5	+48.7
NFDeerCreek	-15.7	+10.2	+30.2	-1.1	+22.2	+45.5
SFJordanRd	-17.0	+13.0	+41.3	+4.5	+24.9	+39.7
SFJimCreek	-16.0	+11.9	+29.1	+6.6	+27.6	+51.0
SFCanyonCreek	-15.3	+11.5	+30.3	+4.8	+23.0	+36.1

Figures

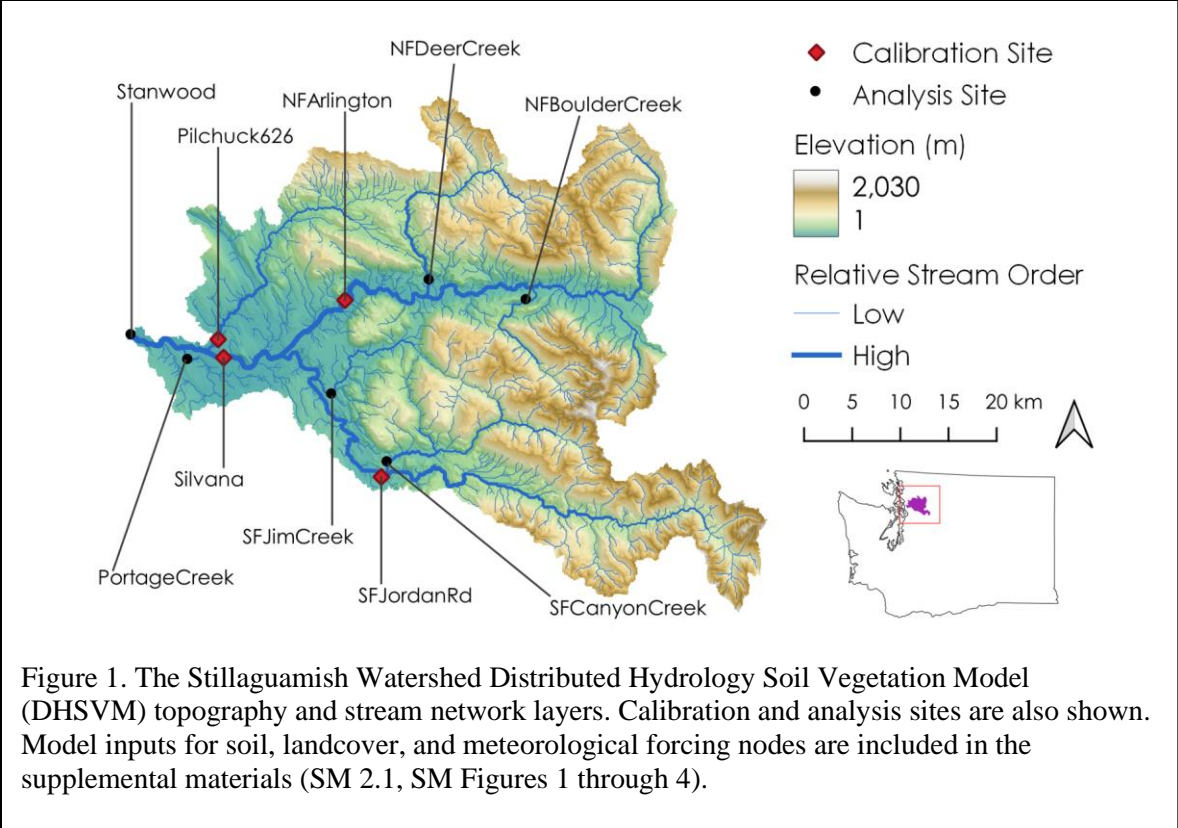
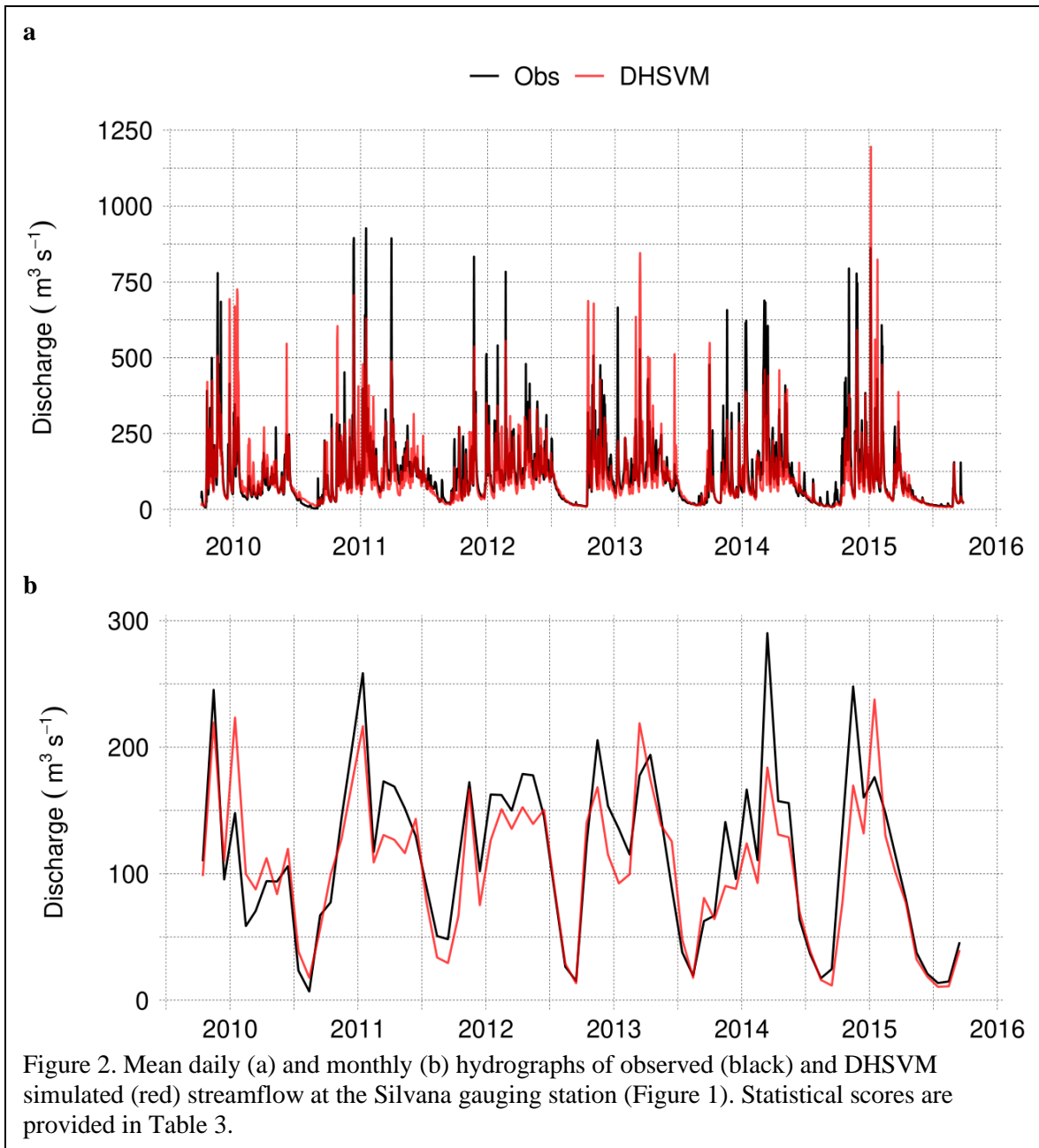
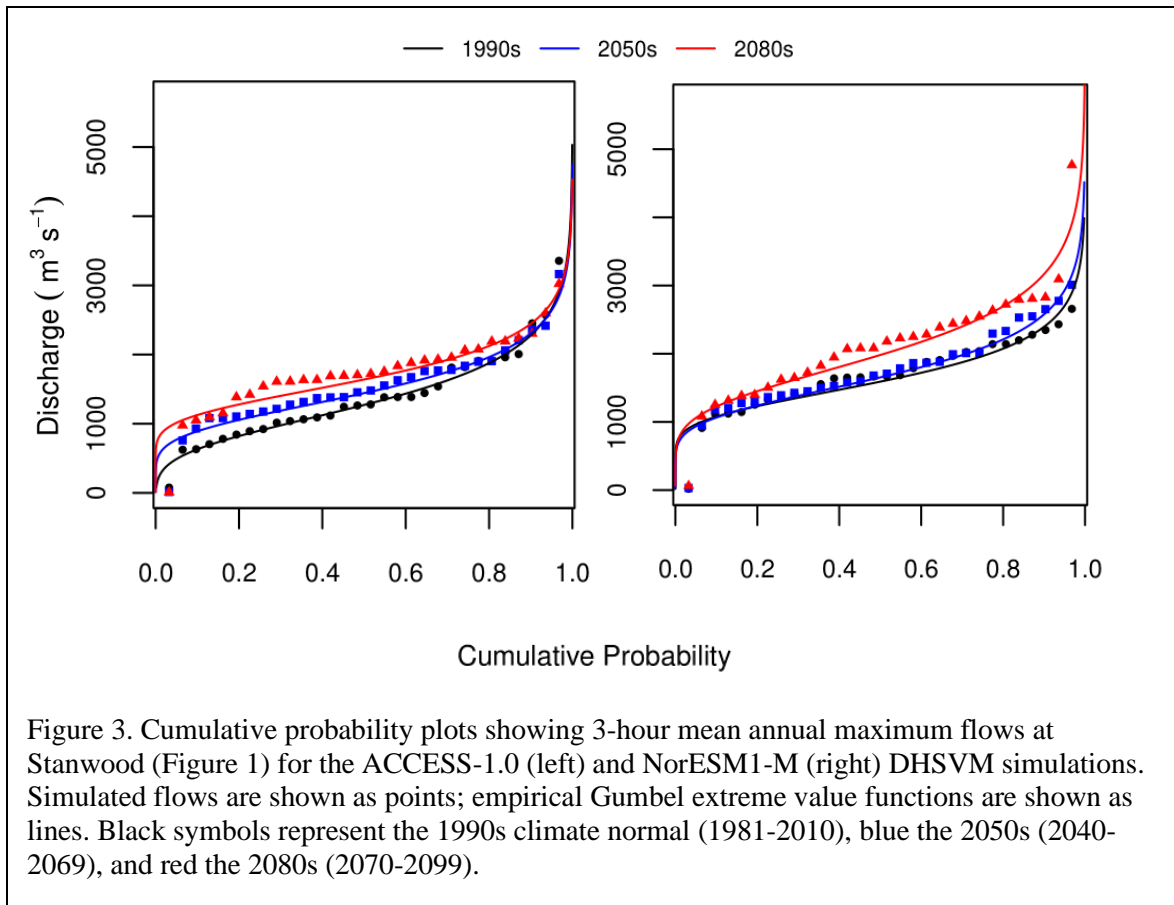


Figure 1. The Stillaguamish Watershed Distributed Hydrology Soil Vegetation Model (DHSVM) topography and stream network layers. Calibration and analysis sites are also shown. Model inputs for soil, landcover, and meteorological forcing nodes are included in the supplemental materials (SM 2.1, SM Figures 1 through 4).





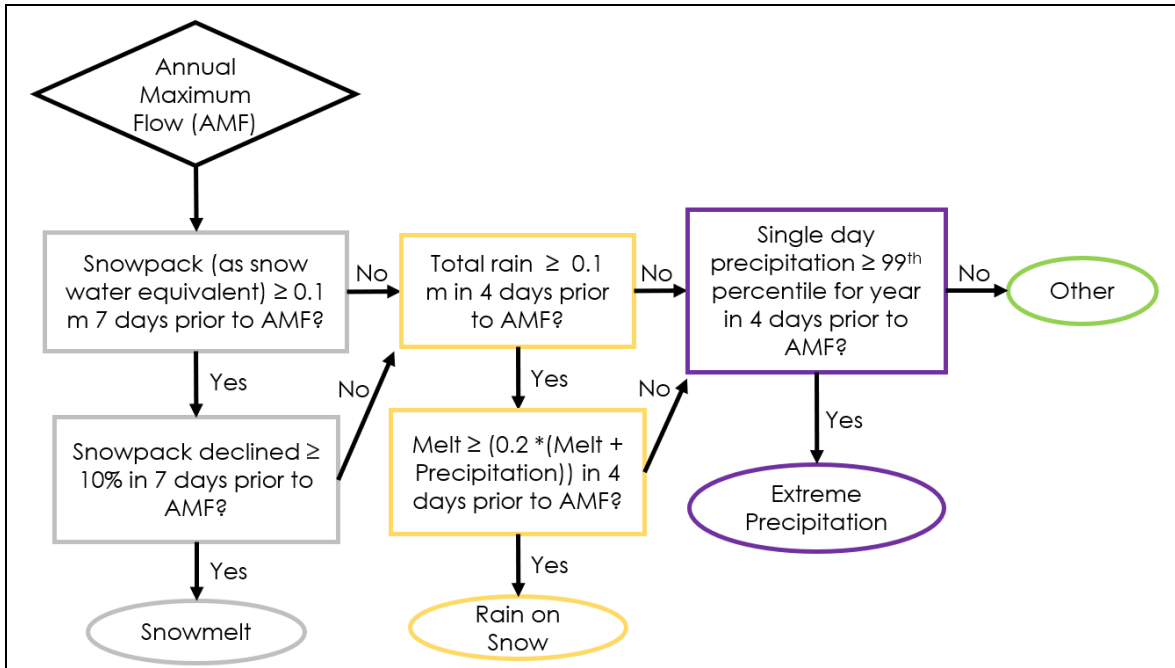


Figure 4. Flow generating mechanism decision tree. Annual maximum flows within the 1990s, 2050s and 2080s climate normals were assigned a single flow generating mechanism as shown. This logic is based on the work of Chegwiddden et al., 2020.

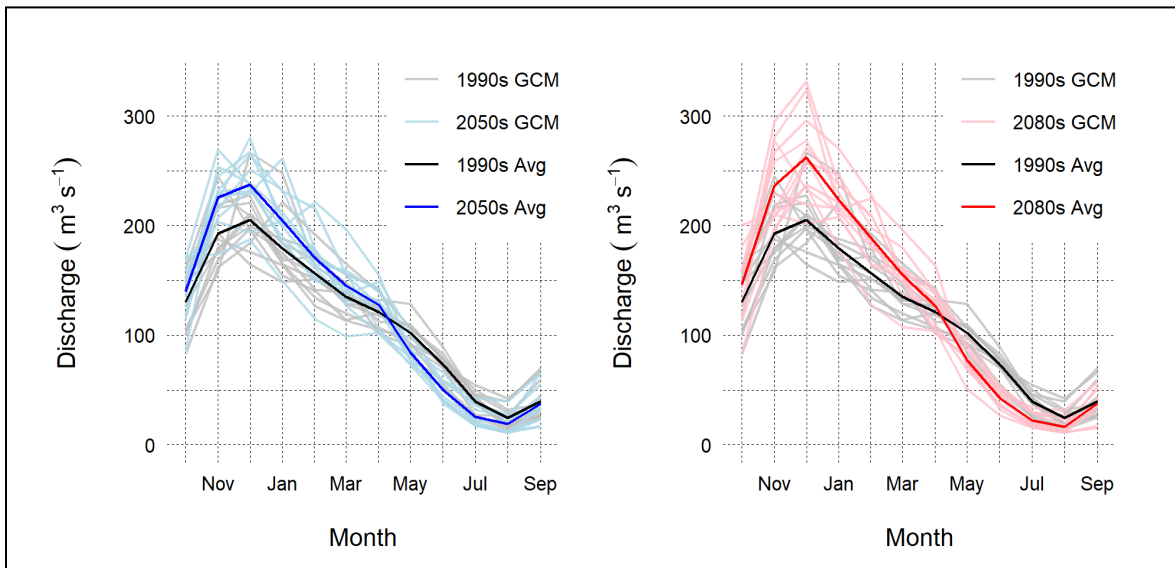


Figure 5. Mean monthly stream discharge at the mouth of the Stillaguamish River near Stanwood across climate normals for hydrologic simulations forced by individual general circulation models (GCM). Light gray, blue, and red lines represent individual GCM averages over 30-year climate normals for the 1990s and 2050s (left) and 2080s (right) respectively. Bolded black, blue, and red lines represent ensemble averages across all 12 GCMs.

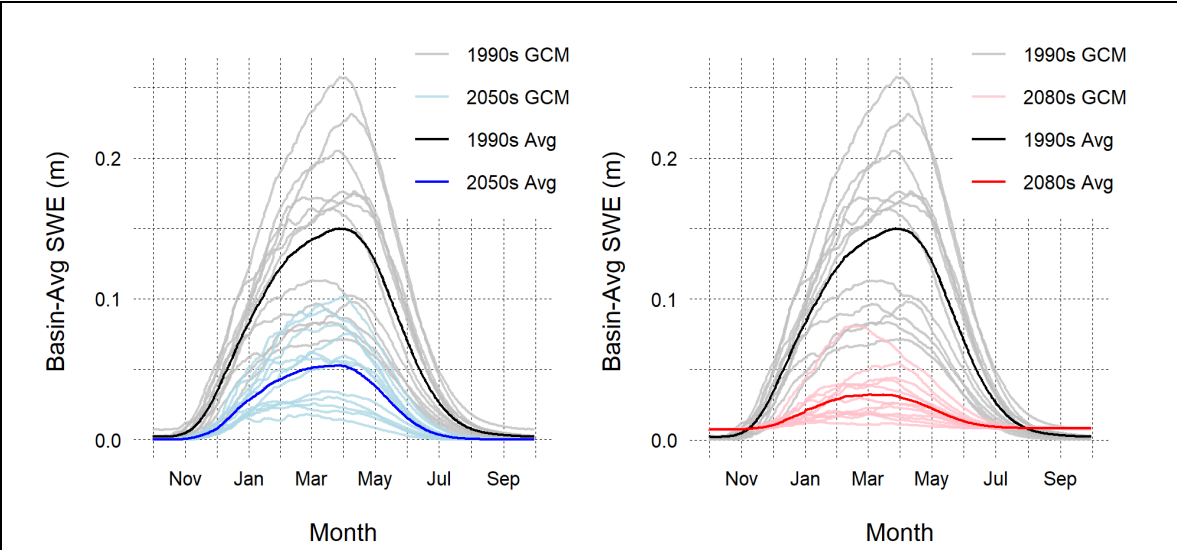


Figure 6. Mean daily snow water equivalent (SWE) watershed-wide across climate normals for hydrologic simulations forced by individual general circulation models (GCM). Light, blue, and red lines represent individual GCM averages over 30-year climate normals for the 1990s and 2050s (left) and 2080s (right) respectively. Bolded black, blue, and red lines represent ensemble averages across all 12 GCMs.

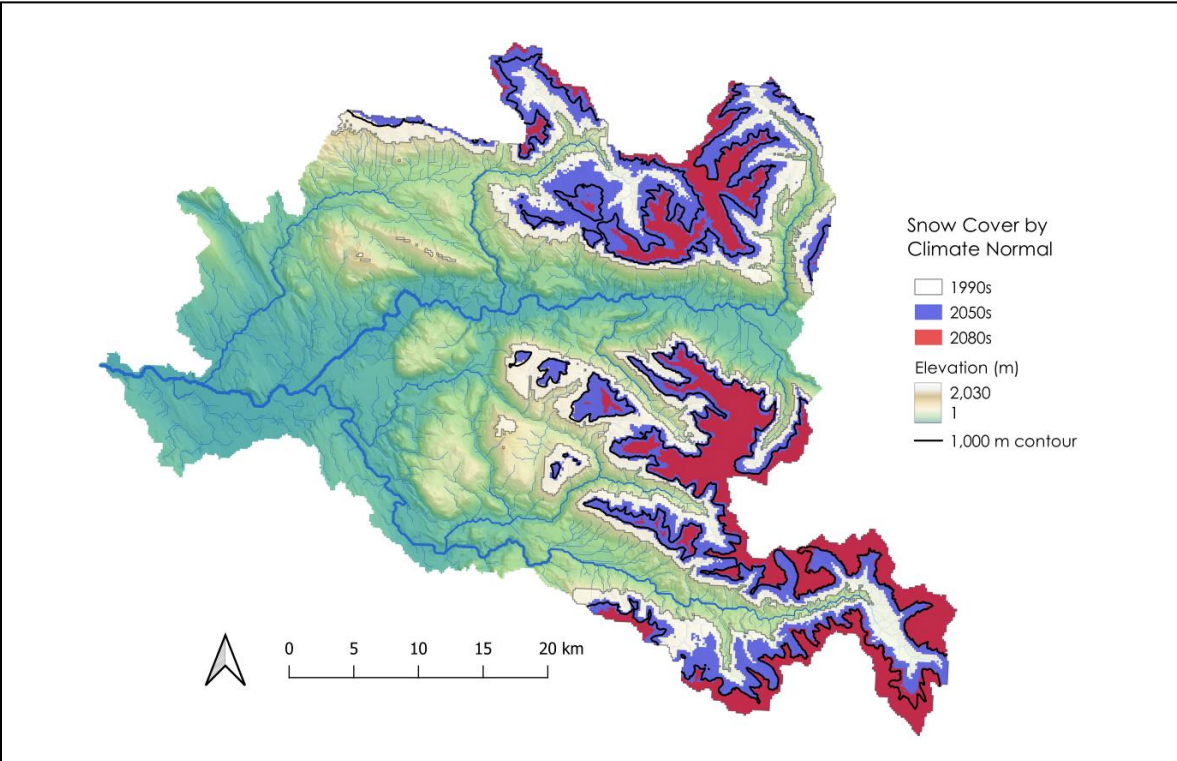
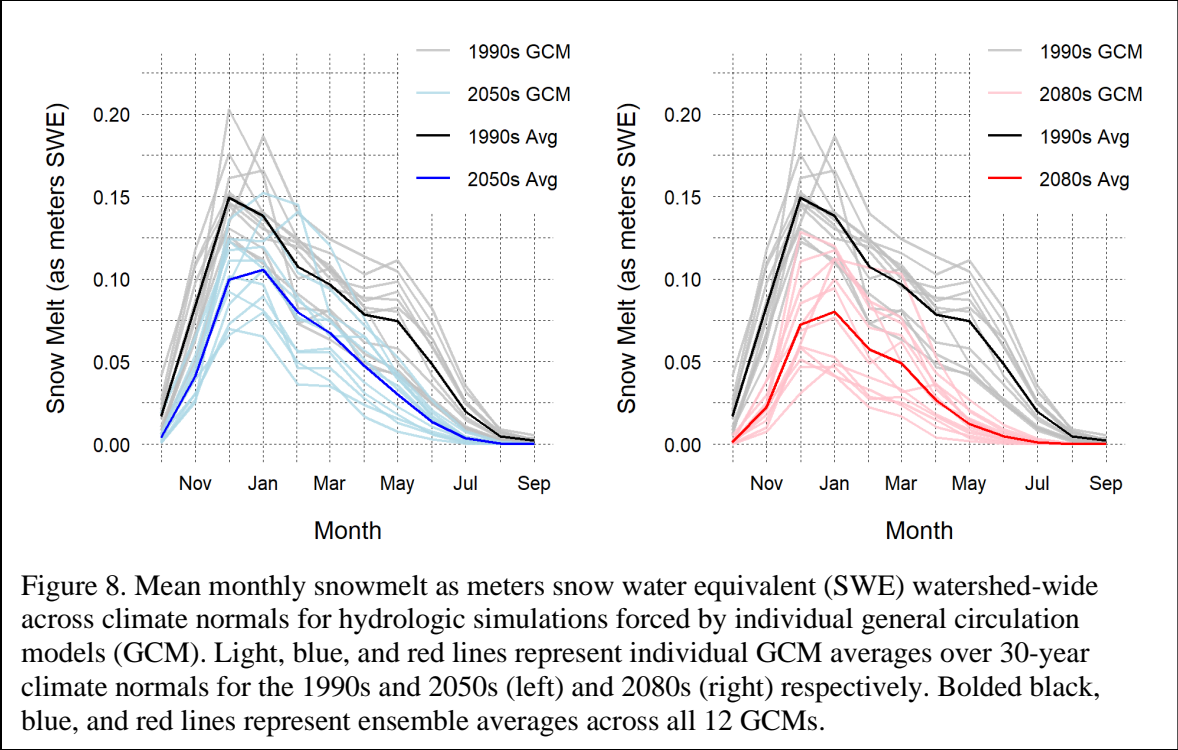


Figure 7. April 1 snowline by climate normal for the DHSVM simulation forced by the ACCESS 1.0. The 1,000 m elevation contour is shown for reference. ACCESS 1.0 is shown because its hindcast snowline is the most similar to PNNL-Obs.



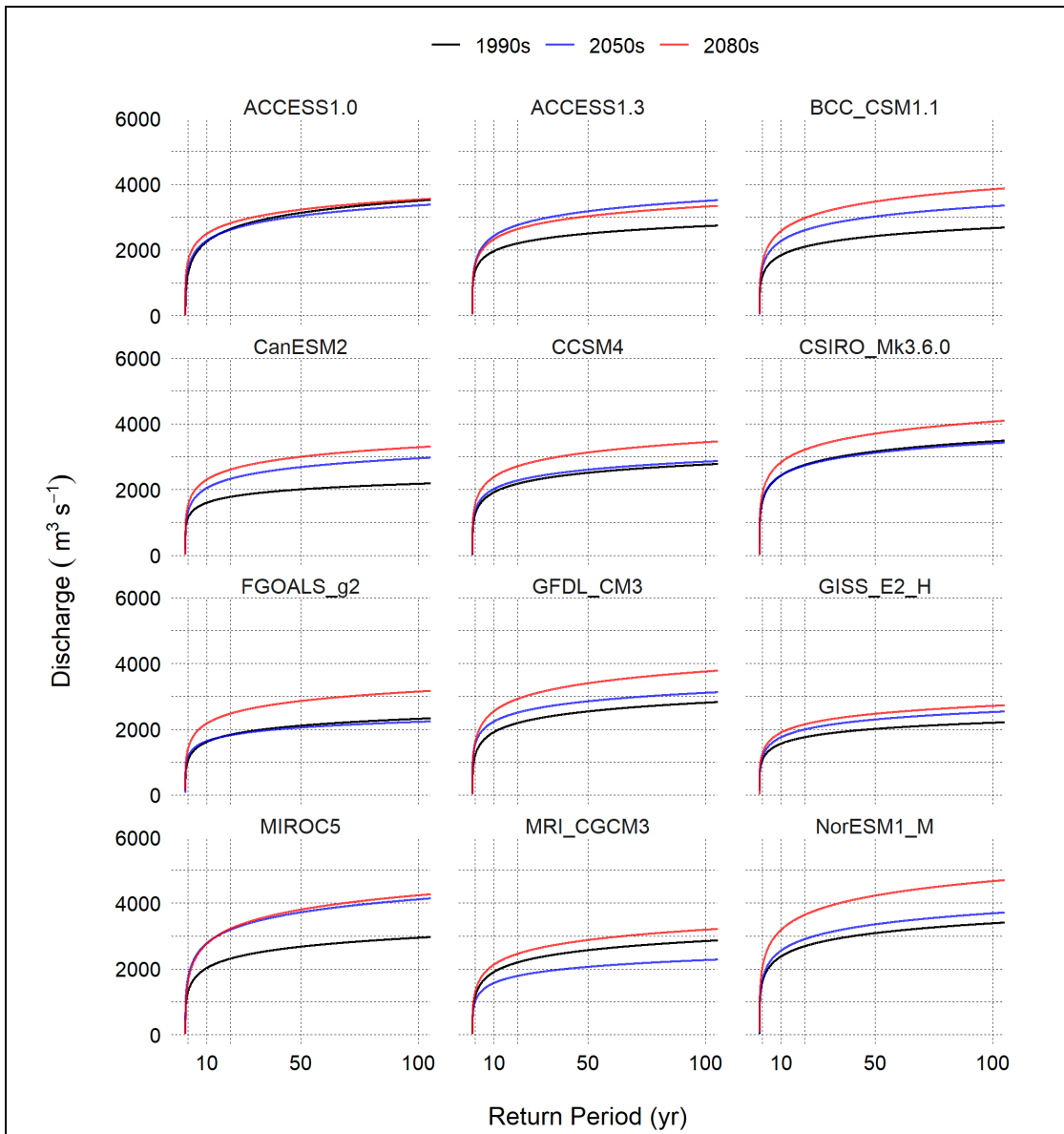


Figure 9. Discharge versus return period from empirical Gumbel extreme value functions for 3-hour annual maximum flows at the Stanwood (Figure 1). The black line represents the 1990s climate normal (1981-2010); blue the 2050s (2040-2069), and red the 2080s (2070-2099). Each plot shows the empirical Gumbel extreme value function for parent general circulation model simulations. Vertical lines are shown for 2, 10, 20, 50, and 100-year return periods.

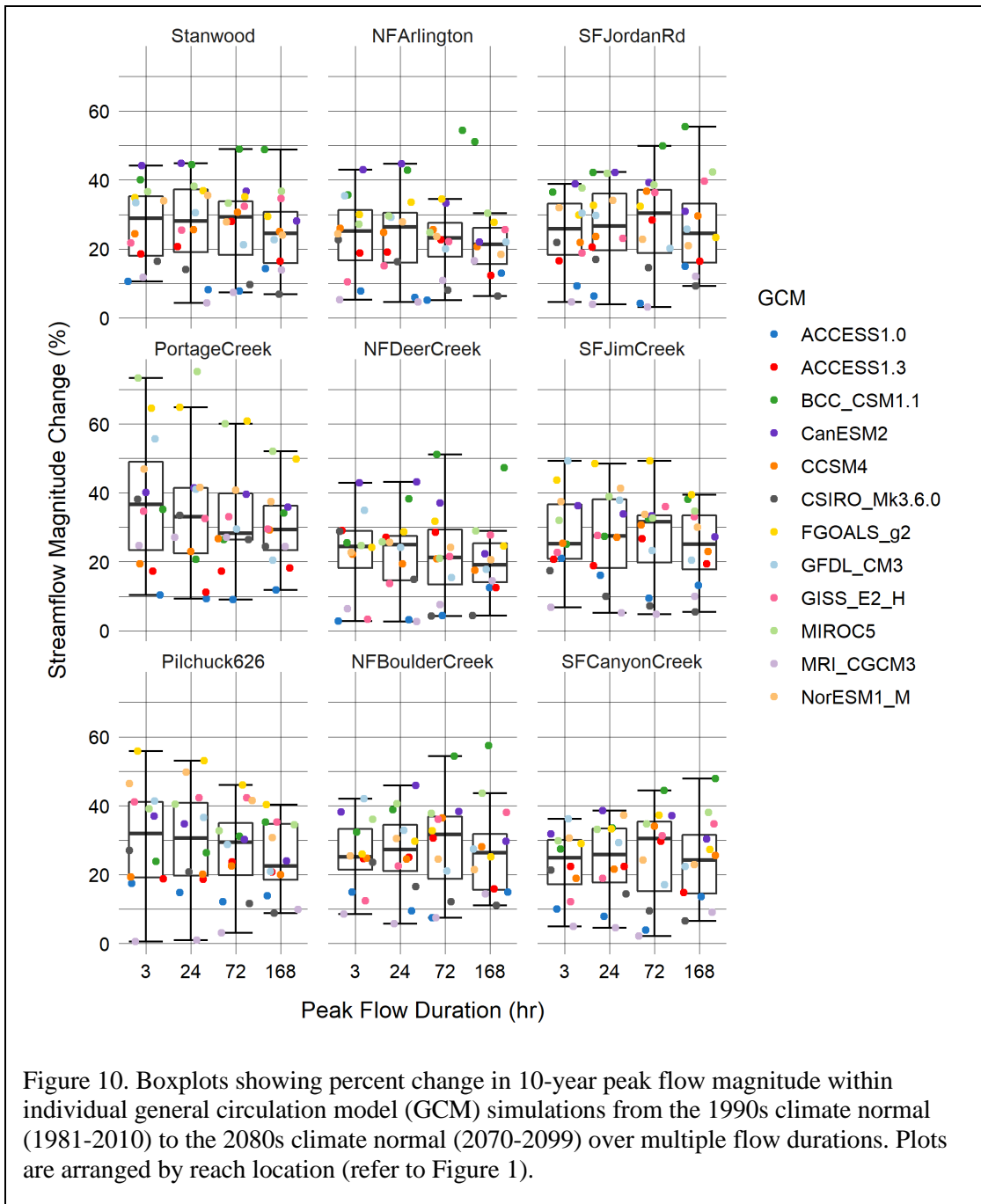


Figure 10. Boxplots showing percent change in 10-year peak flow magnitude within individual general circulation model (GCM) simulations from the 1990s climate normal (1981-2010) to the 2080s climate normal (2070-2099) over multiple flow durations. Plots are arranged by reach location (refer to Figure 1).

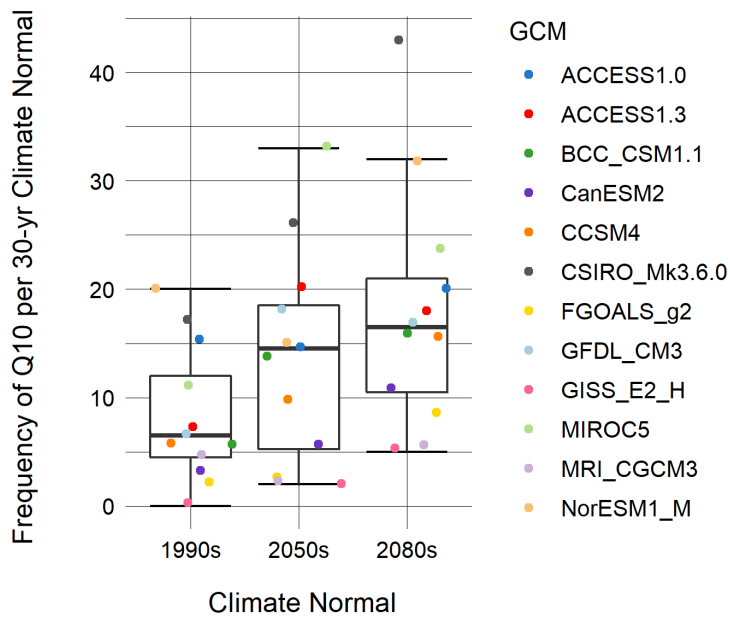
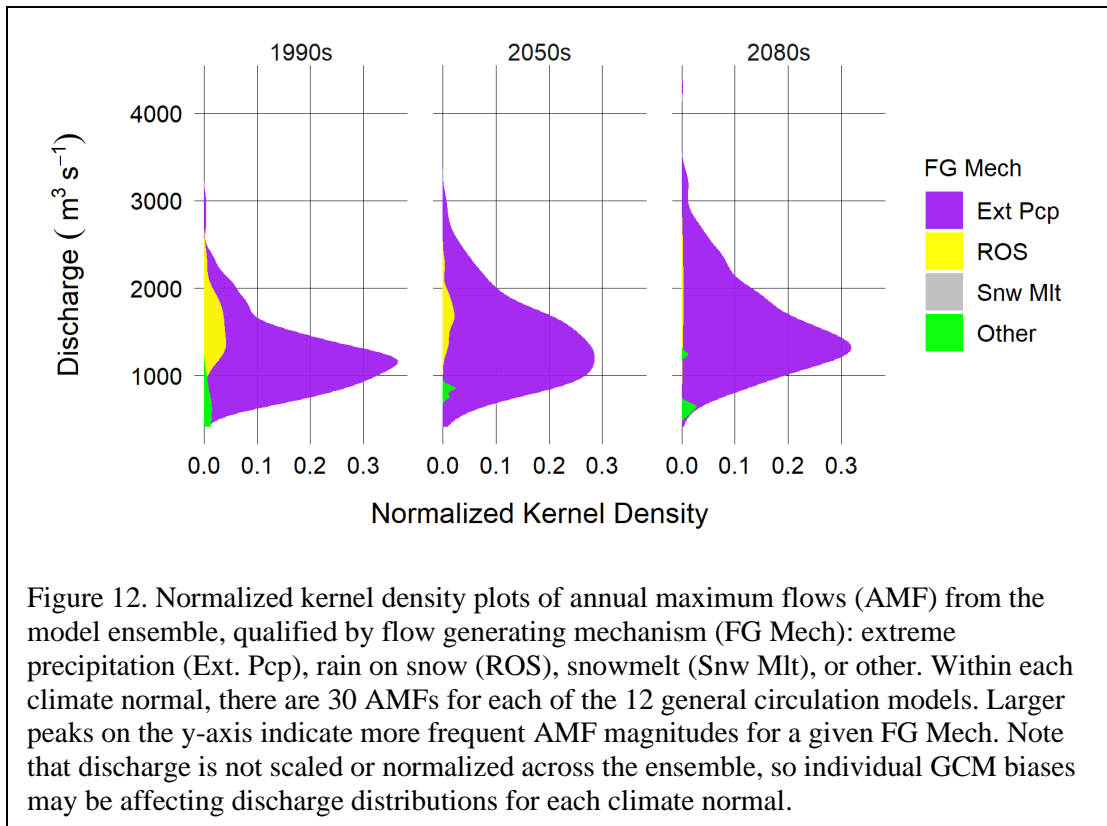


Figure 11. Frequency of 3-hour 10-year peak flow occurrence per 30-year climate normal at Stanwood by general circulation model (GCM). The 10-year peak flow threshold is $1729 \text{ m}^3\text{s}^{-1}$ which was calculated from the empirical Gumbel extreme value function for the PNNL-Obs simulation from 1985-2015. Each climate normal encompasses 30 years. On average, a 10-year flow should occur about 3 times per 30-year climate normal. This figure illustrates the positive bias most WRF-GCMs have in comparison to PNNL-Obs. The relative increase in frequency of threshold occurrence over time illustrates the effects of a warmer climate on peak flows.



Supplemental Materials

Supplemental Materials

Table of Contents

SM1	Additional Context on Peak Flows in the Stillaguamish Watershed	1
SM2	Building the DHSVM and WRF Forcings	1
SM2.1	Hydrologic Model Inputs.....	2
SM2.2	Meteorological Data Bias Correction and Hydrologic Model Calibration.....	3
SM2.2.1	Historical Meteorological Data Bias Correction	3
SM 2.2.2	Hydrologic Model Calibration	5
SM2.3	Flood Frequency Analysis on Simulated Peak Flows	6
SM3	Additional Results	7
SM3.1	Projected Flow Changes in Tributaries of the Stillaguamish River	8
SM3.2	Seasonal Changes in Peak Flow Threshold Exceedance.....	9
SM4	References	9

Tables

Figures

List of Tables and Figures

- SM Table 1: Weather Stations Used to Evaluate Historical Meteorological Forcings
- SM Table 2: SNOTEL Stations Used to Evaluate DHSVM Snow Production
- SM Table 3: Lapse Rates and Rain/Snow Thresholds in Stillaguamish Model
- SM Table 4: Parameterization Changes from Baseline to Final Calibration
- SM Table 5: Stream Channel Hydraulic Geometry Classes in Final Calibration

- SM Figure 1: Topography of the Stillaguamish Watershed and WRF Forcing Nodes
- SM Figure 2: Simulated Soil Thickness in the Stillaguamish DHSVM
- SM Figure 3: Soil Types in the Stillaguamish DHSVM
- SM Figure 4: Landcover Classes in the Stillaguamish DHSVM
- SM Figure 5: Temperature Biases for PNNL-Obs
- SM Figure 6: Precipitation Biases for PNNL-Obs
- SM Figure 7: Windspeed and Shortwave Radiation Biases for PNNL-Obs
- SM Figure 8: Map of April 1 Snow Water Equivalent for the Stillaguamish DHSVM
- SM Figure 9: Daily Calibration Hydrographs for Silvana and NF Arlington
- SM Figure 10: Daily Calibration Hydrographs for SFJordanRd and Pilchuck626
- SM Figure 11: Monthly Calibration Hydrographs for Silvana and NF Arlington
- SM Figure 12: Monthly Calibration Hydrographs for SFJordanRd and Pilchuck626
- SM Figure 13: Simulated Air Temperature Timeseries for the Model Ensemble
- SM Figure 14: Simulated Monthly Air Temperature for the Model Ensemble
- SM Figure 15: Simulated Snow Water Equivalent by GCM and Normal
- SM Figure 16: Simulated Monthly Precipitation Magnitude for the Model Ensemble
- SM Figure 17: Simulated Monthly Precipitation Magnitude Boxplots
- SM Figure 18: Simulated Maximum Daily Precipitation Magnitude by Normal and GCM
- SM Figure 19: Simulated Maximum Daily Precipitation by Month and Normal
- SM Figure 20: Simulated Monthly Mean Streamflow, High and Low Elevation Tributaries
- SM Figure 21: Monthly Frequency of 3-hour, 10-year Peak Flow Occurrence per Normal

SM1 Additional Context on Peak Flows in the Stillaguamish Watershed

In the Stillaguamish Watershed, peak flows are common in late fall and winter months following rain and snowmelt events (Hall et al., 2014; Clark et al., 2019; Freeman, 2019). Hall et al. (2014) completed a statistical analysis of historical peak flows in the North Fork of the Stillaguamish and their relation to climate and landcover factors. They found that 1-day maximum annual streamflows observed at the Arlington, WA USGS stream gauging station (NFArlington in Figure 1) exhibited an increasing trend over the historical record with a linear best fit line ranging from about 13,000 cubic feet per second (cfs; or 370 cubic meters per second [cms]) in 1929 to about 22,000 cfs (625 cms) in 2009. Over the same period, a slight decline in base flows was observed. Peak flow magnitude in other gauged streams in Washington generally exhibited weaker trends through time (Mastin, et al., 2017), perhaps indicating unique climate factors are at play in the Stillaguamish Watershed. Hall et al. (2014) also analyzed the meteorological record at Darrington, WA (located near the mouth of Boulder Creek, Figure 1) and determined that annual rainfall magnitude has trended upward while snowfall magnitude (as snow water equivalence) has trended downward. They found a statistically significant correlation between peak flows and annual rainfall magnitude, but no such correlation was observed between landcover changes and streamflows. Hall et al. (2014) developed and tested a variety of statistical models to predict 1-day maximum annual flows. The most skillful model they developed relied on day-of precipitation and 5-day antecedent precipitation magnitudes to predict streamflows, indicating that precipitation is far and away the most predictive parameter controlling peak flows in the watershed.

SM2 Building the DHSVM and WRF Forcings

Considerable effort is required to use the models described in this work. The Distributed Hydrology Soil Vegetation Model (DHSVM) is maintained by the Pacific Northwest National Laboratory. DHSVM version 3.2 was used in this research. The Weather Research and Forecasting (WRF) model is maintained by the National Center for Atmospheric Research. WRF version 3.2 was used in this research. Both models are open source. Construction and parameterization of these models and their outputs is described in this section.

SM2.1 Hydrologic Model Inputs

The DHSVM requires digital grids for elevation, soil type, soil thickness, landcover, and stream networks. I generated these grids at a 150-meter resolution using publicly available data, ESRI ArcGIS, and QGIS. Meteorology is forced over these digital grids at a constant timestep. A description of the datasets is provided below:

Topography – I used 10-meter digital elevation models (DEM) produced by USGS (2001) and available for download at the following URL:

<http://gis.ess.washington.edu/data/raster/tenmeter/byquad/index.html>. To generate the DHSVM topography grid. I resampled a mosaic of 10-meter DEMs that encompassed the Stillaguamish Watershed to 150-meter resolution using bilinear interpolation (SM Figure 1).

Watershed bounds and stream network – I generated the stream network for the Stillaguamish watershed using hydrology geoprocessing tools in ESRI ArcGIS and a Python script that executes ArcMap processes to build a stream network with a user-specified minimum source area (SM Figure 1). I elected to use a source area of 500,000 square meters because it provided adequate resolution to model high alpine streams without generating superfluous broken stream segments in the lowlands of the watershed. The Python script also generates a soil thickness map as a function of relief (higher relief areas have thinner soil layers to simulate alpine environments; SM Figure 2) and assigns user-specified hydraulic geometries to individual stream segments as a product of slope and drainage area. I specified the minimum and maximum soil thicknesses as 1 and 5 meters and created a hydraulic geometry classification based on visual assessment and measurement of satellite imagery. The python script is available for download here: https://github.com/pnnl/DHSVM-PNNL/tree/master/CreateStreamNetwork_PythonV

Meteorology – Meteorological forcings were generated using the Weather Research and Forecasting (WRF) model. The historic (i.e., calibration/PNNL-Obs) meteorologic forcings were generated with WRF at 6-km horizontal resolution and have a 1-hour timestep. The projected meteorologic forcings (i.e., downscaled general circulation models [GCM]) were generated with WRF at 12-km horizontal resolution and have 1-hour timesteps. The 12-km WRF-GCM grid was transferred to the PNNL-Obs 6-km grid via bilinear interpolation (SM Figure 1).

Soil Types – I used the STATSGO dataset produced by a partnership of federal, regional, state and local agencies known as the National Cooperative Soil Survey (NCSS). In its native form, STATSGO data are coarse (i.e., state-wide) vector data. I reclassified STATSGO soil units into

seven distinct DHSVM soil classes (SM Figure 3). I downloaded STATSGO data for Washington state using Penn State's data portal:

http://www.soilinfo.psu.edu/index.cgi?soil_data&statsgo.

Landcover – I used the 2016 Coastal Change Analysis Program (C-CAP) dataset which is a NOAA product produced from Landsat Imagery. C-CAP landcover data are classified based on observed spectral reflectance characteristics and standardized for the contiguous United States. I reclassified C-CAP units into ten distinct DHSVM landcover types (SM Figure 4). C-CAP data are available via: <https://coast.noaa.gov/ccapftp/#/>

SM2.2 Meteorological Data Bias Correction and Hydrologic Model Calibration

The meteorologic forcings used in this project are from an effort that involved modeling peak flows in the Stillaguamish and Snohomish watersheds (Mauger et al., 2021). Meteorologic forcing preparation methodology was the same for both watersheds, therefore details pertaining to both watersheds are discussed in section 2.2.1. The hydrologic models for both watersheds were calibrated individually, therefore, only details pertaining to the Stillaguamish River model are discussed in section 2.2.2.

SM2.2.1 Historical Meteorological Data Bias Correction

Prior to calibrating the hydrologic models, the historical meteorological forcings (PNNL-Obs) were evaluated to quantify their biases and determine how best to correct them to minimize the effect of these biases on the hydrologic simulations. This was done in two ways:

1. By comparing WRF with surface weather observations, and
2. By using WRF to simulate snowpack and comparing the results to observations.

Together this allowed us to identify key biases and correct for them prior to embarking on hydrologic model calibration.

Comparison with surface weather observations

PNNL-Obs results were compared with surface observations from the 35 weather stations listed in SM Table 1. Observations were obtained from three sources:

1. GHCN-D (Global Historical Climate Network - Daily; (Lawrimore et al., 2011). This dataset includes daily observations of total precipitation, minimum temperature, and maximum temperature.

2. SNOTEL-BCQC (Snow Telemetry Bias Correction and Quality Control; Sun et al. 2019). This dataset includes daily observations of total precipitation, minimum temperature, and maximum temperature.
3. AWN (Ag Weather Net; <http://weather.wsu.edu>). This dataset includes hourly observations of precipitation, temperature, humidity, and shortwave radiation.

These observations were compared against results from the nearest grid cell in the PNNL-Obs forcings. To account for elevation differences between WRF grid cells and the observations, temperatures were adjusted based on seasonal lapse rates (SM Table 3). Biases were calculated by comparing the full PNNL-Obs simulation (1981-2015) with all valid observational data from 1970 to 2019, for each weather station. This analysis included annual and seasonal averages as well as extreme metrics.

SM Figure 5 shows the comparison between the annual average of daily minimum and maximum temperatures. Although the biases are similar for the two maps, they differ substantially among stations and do not exhibit a clear geographic pattern. On average the comparisons suggest a slight cold bias in the PNNL-Obs simulation. SM Figure 6 shows the comparison with annual precipitation and the top 1% of precipitation events in each year. These show a much clearer pattern, relatively consistent among both metrics, of a dry bias in the PNNL-Obs simulation. Based on these comparisons, a simplified approach to bias correcting WRF results was completed, where a uniform scaling was applied based on the average bias among all comparisons across the two watersheds. The same approach was used for wind and shortwave radiation which were both generally overestimated in PNNL-Obs (SM Figure 7). Due to the small number of available comparison data for wind and shortwave radiation, statewide data were used to develop their scaling factors.

The bias corrections applied to the PNNL-Obs are listed in Table 2 of the primary document. Humidity estimates from WRF were not bias-corrected. Although observations are available, tests indicated that adjustments to humidity could frequently lead to over-saturated air or other physically implausible conditions. Future work could develop an improved approach, in which the relative humidity is corrected, then converted to vapor pressure deficit as used by the hydrologic model. Regardless of the approach, adjustments to humidity are unlikely to have a large effect on flood peaks.

No observational comparisons were made for longwave radiation because very few observations exist. Instead, longwave estimates were estimated using an empirical formulation

(Dilly and O'Brien, 1998; Unsworth and Monteith, 1975), which previous research suggests is superior to WRF longwave estimates (Currier et al. 2017).

SM 2.2.2 Hydrologic Model Calibration

There are no SNOTEL stations within the Stillaguamish watershed. As a consequence, I relied on watershed-adjacent NRCS SNOTEL stations (SM Table 2) and observed historical streamflow to calibrate the Stillaguamish model. Our baseline parameterization started from prior DHSVM-based studies in the North and South Forks of the Stillaguamish (Freeman, 2019; Clarke, 2020). From there I iteratively altered meteorology, soil, snow, and vegetation parameters based in part on Sun et al. (2019).

Parameterizing meteorological constants within DHSVM proved to be the most challenging aspect of Stillaguamish DHSVM calibration. The goal for meteorological parameterization was to produce model estimates of SWE that were similar to those observed at the Skookum Creek and Alpine Meadows NRCS SNOTEL stations within a similar elevation band. Although they are located outside of the Stillaguamish watershed (within 100 km), I considered these SNOTEL stations to be proxies for the Stillaguamish watershed given their similar geographic settings. I achieved a qualitatively satisfactory SWE calibration using the seasonal temperature lapse rates and snow and rain temperature thresholds shown in SM Table 3.

Generally, the Stillaguamish model produced less SWE with this parameterization than what was observed at the Skookum Creek and Alpine Meadows SNOTEL stations (SM Figure 8); however, SWE can vary over similar geographies and altitudes due to unique alpine microclimates, so this bias may be inconsequential or simply a limitation of model resolution. I selected seasonal lapse rates based on iterative testing and literature values for similar watersheds (Minder et al. 2010). I was able to improve peak April 1 SWE and spring freshet using higher temperature lapse rates in winter months (to produce colder temps at higher elevations) and lower temperature lapse rates in late spring/summer months (to promote snowmelt in late spring/early summer).

The most sensitive soil parameters in the Stillaguamish were lateral conductivity, exponential decrease, and porosity of the major soil units in the watershed (Upland Bedrock/Loam, Gravel Loam, and Silt; SM Figure 3; SM Table 4). Field capacity was also sensitive but generally related to porosity for each unit (i.e., when porosity was greater, field capacity also needed to be greater). Compared to literature values (e.g., Du et al. 2014, Beckers

et al. 2004, Freeman 2019, Clarke 2020), our calibrated soil porosities are low; however, this is likely a function of the goals of our research: to produce a model skilled at producing accurate peak flows and therefore potentially biased towards inducing overland flow/soil saturation. Soil thickness bounds were also a moderately sensitive parameter. I settled on minimum and maximum bounds of 1 and 5 meters based on iterative testing. Thinner soil limits generally produced inadequate low flows during summer months. Thicker soil limits did not yield significant effects.

Vegetation parameters were generally less sensitive than meteorological or soil parameters in the Stillaguamish; however, I did perform some iterative sensitivity testing and parameterization of overstory leaf area index (LAI) and LAI multipliers for coniferous forests (the dominant landcover unit in the watershed, SM Figure 4). Select parameterization changes from baseline through calibration are shown in SM Table 4.

Stream channel geometry was a moderately sensitive model parameter when maintained within realistic bounds. The classification schema I used is based on slope and drainage area associated with a given stream channel reach (Table 5). This schema was spot checked for accuracy by comparing simulated reach geometry with aerial images of select reaches within primary tributaries and the main stem of the Stillaguamish River.

Daily and monthly average hydrographs of observed and simulated flows are provided in SM Figures 9 through 12 for the four calibration gauging sites in the watershed (Figure 1 in the primary document). Model skill is best at the North Fork of the Stillaguamish River (NFArlington) and the Main Stem of the Stillaguamish River (Silvana; Table 3 in the primary document). The South Fork of the Stillaguamish River (SFJordanRd) presented challenges, particularly for low flows which were generally under-simulated. Pilchuck Creek (Pilchuck626) presented opposite issues as low flows were generally over-simulated while peak flows were generally under-simulated.

SM2.3 Flood Frequency Analysis on Simulated Peak Flows

Flood frequency analysis is a broad set of statistical methods for quantifying extreme flood and/or streamflow magnitude relative to likelihood. The methods allow one to statistically extrapolate flood/streamflow magnitude beyond the historical observation range. For instance, in the United States, stream gauging stations often have a historical record for 30 years or fewer. Large infrastructure projects are typically designed for 50 or 100-year events. These event

magnitudes are typically estimated using flood frequency analysis with observed annual maximum flows (AMF).

In my flood frequency analysis, I used simulated AMFs within 30-year climate normals from each WRF-GCM simulation to statistically extrapolate peak flow magnitudes for 2- to 100-year return periods. Our statistical evaluation is based on the Gumbel distribution, also known as the type-1 extreme value distribution. The Gumbel distribution requires two parameters: location and scale. The Gumbel cumulative distribution function is given as:

$$\text{CDF} = e^{-e^{-(x-\mu)/\beta}}$$

where CDF is the distribution, x is a random variable, μ is the location parameter, and β is the scale parameter. I defined these parameters using L-moments, which are linear combinations of order statistics (Hosking, 1990).

Our data processing sequence is provided below:

1. Average hourly flows across selected duration (e.g., 3-hour, 1-day, 1-week)
2. Select AMFs and group them into 30-year sample sets (i.e., climate normals)
3. Rank annual maximum flows by magnitude within each 30-year sample set
4. Compute L-moment parameters for Gumbel distribution
5. Derive Gumbel cumulative distribution function from L-moment parameters (i.e., probability vs flow magnitude)
6. Derive return period from as $1/(1-P)$ where P is cumulative probability of a flow being less than a given magnitude
7. Compute percent change in flow magnitude for select event size (e.g., 2-year, 10-year, 100-year) from the 1990s climate normal to 2050s and 2080s climate normal.

SM3 Additional Results

Air temperature is a primary control on precipitation phase. Our simulations show significant increases in temperature by the 2050s and 2080s across the model ensemble (SM Figures 13 and 14). In our model ensemble, mean annual air temperature is 8.02 °C in the 1990s (1981-2010), 10.27 °C in the 2050s (2040-2069), and 11.86 °C in the 2080s (2070-2099). The coldest and hottest GCMs in the 1990s are ACCESS1-0 and NorESM1-M, respectively. In the 2080s, the coldest GCM is GISS-E2-H and the warmest is CanESM2. The GCMs with greatest

and least average temperature change from the 1990s to the 2080s are CanESM2 (+5.34 °C increase) and GISS-E2-H (+2.15 °C increase).

Our calibrated DHSVM has a rain/snow threshold of 1°C (i.e., precipitation in grid cells with air temperatures above 1 °C receive rain; below 1 °C receive snow). In the 1990s climate normal, a majority of GCMs produce basin-average temperatures below the rain/snow threshold in December and January; some GCMs also fall below the threshold in February (SM Figure 13). By the 2050s, only one GCM in January is below this threshold. By the 2080s, all GCMs have monthly mean temperatures well above the rain-snow threshold. Snow still accumulates during winter months in high elevation portions of the watershed in each WRF-GCM simulation, but the spatial distribution shrinks dramatically from the 1990s to the 2050s (Figure 5 of the primary document). Highlighting the control of temperature on snowpack, SWE across the model ensemble declines significantly by the 2050s for each GCM (SM Figure 15).

Mean annual precipitation across the model ensemble increases from 2.35 m in the 1990s to 2.57 m in the 2080s. The wettest months across WRF-GCM ensemble are November, December and January. These are also the months that see the most substantial increases in average precipitation over time (SM Figures 16 and 17). Modest increases in precipitation are also evident in early fall (September and October) and late winter/early spring (February, March, and April). Modest declines in precipitation are evident in summer months (June, July, and August).

Annual maximum precipitation intensity increases across the model ensemble by about 21% (SM Figures 18 and 19). The most significant changes are in fall and winter months (September through February). November shows the most significant change from the 1990s to the 2080s, with a relative increase in ensemble-average in 24-hour maximum precipitation magnitude of 21%.

SM3.1 Projected Flow Changes in Tributaries of the Stillaguamish River

In addition to examining trends in flows at the mouth of the Stillaguamish River near Stanwood, I examined trends in projected flows elsewhere in the watershed. High elevation transitional rain-snow tributaries in the watershed (e.g., Boulder Creek and Deer Creek in the North Fork; Canyon Creek and Jim Creek in the South Fork; Figure 1) generally show a more rapid increase in average winter streamflow magnitude than rain-dominated portions of the watershed (i.e., Pilchuck Creek) by the 2050s. By the 2080s, this remains the case but elevated

winter streamflows are also apparent in the rain-dominated portions of the watershed (SM Figure 20).

SM3.2 Seasonal Changes in Peak Flow Threshold Exceedance

I evaluated seasonal changes in peak flow threshold exceedance by counting the times a historic 10-year flow would be exceeded per month (SM Figure 21). The historic-10-year flow threshold I used is based on a 30-year PNNL-Obs simulation spanning water years 1985-2015. The months most capable of maintaining high average streamflows due to seasonal precipitation trends (November through February; SM Figures 16 and 17) also see the most frequent extreme peak flow threshold exceedances. November and December have the most exceedances in the 1990s climate normal and show the most significant increases by the 2080s climate normal. In the 1990s climate normal, the 10-year flow threshold is exceeded on average 2.5 times per 30 years during November and 3 times during December. By the 2080s, the 10-year flow threshold is exceeded 5 times per 30 years during November (a 100% increase) and 4 times per 30 years during December (a 25% increase; refer to SM Figure 21). These findings corroborate those of Warner et al. 2015 who evaluated the seasonal timing of heavy precipitation events in projected meteorology in the Pacific Northwest, finding that late fall and early winter months show the most dramatic increases in storm intensity through time.

SM4 References

- Beckers, J., & Alila, Y. (2004). A model of rapid preferential hillslope runoff contributions to peak flow generation in a temperate rain forest watershed. *Water Resources Research*, 40(3). <https://doi.org/10.1029/2003WR002582>
- Clarke, K. Modeling the effects of climate change on streamflow and stream temperature in the South Fork of the Stillaguamish River. Western Washington University. 75 p.
- Currier, W. R., Thorson, T., & Lundquist, J. D. (2017). Independent evaluation of frozen precipitation from WRF and PRISM in the Olympic Mountains. *Journal of Hydrometeorology*, 18(10), 2681-2703. <https://doi.org/10.1175/JHM-D-17-0026.1>
- Dilley, A. C., & O'Brien, D. M. (1998). Estimating downward clear sky long-wave irradiance at the surface from screen temperature and precipitable water. *Quarterly Journal of the Royal Meteorological Society*, 124(549), 1391-1401.
- Du, E., Link, T. E., Gravelle, J. A., & Hubbart, J. A. (2014). Validation and sensitivity test of the distributed hydrology soil-vegetation model (DHSVM) in a forested mountain watershed. *Hydrological Processes*, 28(26), 6196–6210. <https://doi.org/10.1002/hyp.10110>

- Freeman, K. 2019. Modeling the Effects of Climate Variability on Hydrology and Stream Temperatures in the North Fork of the Stillaguamish River. Western Washington University. 88 p.
- Hall, J. E., Beechie, T. J., Pess, G. R. 2014. Influence of climate and land cover on river discharge in the North Fork Stillaguamish River. Northwest Fisheries Science Center, NOAA Fisheries. Final Contract Report to Stillaguamish Tribe of Indians. 41 p.
- Lawrimore JH, Menne MJ, Gleason B, Williams CN, Wuertz DB, Vose RS, Rennie J (2011): Global Historical Climatology Network - Daily (GHCN-M), Version 3. NOAA National Centers for Environmental Information. doi:10.7289/V5X34VDR
- Mastin, M.C., Konrad, C.P., Veilleux, A.G., and Tecca, A.E. (2016). Magnitude, frequency, and trends of floods at gaged and ungaged sites in Washington, based on data through water year 2014 (ver 1.2, November 2017): U.S. Geological Survey Scientific Investigations Report 2016-5118, <http://dx.doi.org/10.3133/sir20165118>
- Mauger, G.S., J. Robinson, R.J. Mitchell, J. Won, and N. Cristea (2021). New Flood Projections for Snohomish County: Fine-scale Modeling and Dynamically-Downscaling. Report prepared for Snohomish County. Climate Impacts Group, University of Washington.
- Minder, J. R., Mote, P. W., & Lundquist, J. D. (2010). Surface temperature lapse rates over complex terrain: Lessons from the Cascade Mountains. *Journal of Geophysical Research: Atmospheres*, 115(D14). <https://doi.org/10.1029/2009JD013493>
- Sun, N., Yan, H., Wigmosta, M.S., Leung, L.R., Skaggs, R., and Hou, Z. (2019). Regional Snow Parameters Estimation for Large-Domain Hydrological Applications in the Western United States: *Journal of Geophysical Research: Atmospheres*, v. 124, p. 5296–5313, doi:10.1029/2018JD030140.
- Unsworth, M. H., & Monteith, J. L. (1975). Long-wave radiation at the ground I. Angular distribution of incoming radiation. *Quarterly Journal of the Royal Meteorological Society*, 101(427), 13-24. <https://doi.org/10.1002/qj.49710142703>
- USGS. 2001. 10-meter Digital Elevation Model Datasets for Washington State. Accessed November 2019 via: <http://gis.ess.washington.edu/data/raster/tenmeter/byquad/index.html>
- Warner MD, Mass CF, Salathé EP (2015) Changes in Winter Atmospheric Rivers along the North American West Coast in CMIP5 Climate Models. *Journal of Hydrometeorology* 16(1):118–128. <https://doi.org/10.1175/JHM-D-14-0080.1>

SM Tables

SM Table 1. Weather stations used to evaluate downscaled historical meteorological forcing (PNNL-Obs) biases.

Source	ID	Name	Lat.	Lon.	Elv (m)	Years
AWN	330169	Arlington	48.20	-122.22	10	2017-2019
AWN	330021	Fir Island	48.35	-122.42	0	2008-2019
AWN	300214	Langley	48.00	-122.43	51	2014-2019
AWN	330101	Mt. Vernon	48.43	-122.38	7	1993-2019
AWN	330159	Sakuma	48.49	-122.37	9	2006-2019
AWN	330092	Seattle	47.65	-122.28	9	2011-2019
AWN	330162	Snohomish	47.90	-122.11	0	2006-2019
AWN	330026	Woodinville	47.74	-122.15	14	2008-2019
GHCND	USC00450257	Arlington	48.20	-122.12	31	1922-2019
GHCND	USC00450456	Baring	47.77	-121.48	235	1970-2019
GHCND	USC00451233	Cedar Lake HCN	47.41	-121.75	476	1898-2019
GHCND	USC00451992	Darrington RS	48.26	-121.60	168	1911-2019
GHCND	USC00452675	Everett HCN	47.97	-122.19	18	1894-2019
GHCND	USW00024222	Everett-Snohomish	47.90	-122.28	185	1948-2019
GHCND	USR0000WFIN	Finney Cr WA	48.40	-121.79	579	1985-2019
GHCND	USR0000WGOH	Gold Hill WA	48.20	-121.50	1036	1990-2019
GHCND	USC00454169	Kent	47.41	-122.24	9	1912-2019
GHCND	USC00454486	Landsburg	47.37	-121.96	163	1903-2019
GHCND	USC00455525	Monroe	47.84	-121.99	37	1929-2019
GHCND	USC00455678	Mt Vernon 3-WNW	48.44	-122.38	4	1956-2005
GHCND	USC00456295	Palmer 3-ESE	47.30	-121.85	280	1924-2019
GHCND	USW00094248	Renton Muni Ap	47.49	-122.21	9	1998-2019
GHCND	USW00024234	Seattle Boeing Fld	47.53	-122.30	6	1948-2019
GHCND	USW00094290	Seattle Sand Pt	47.68	-122.25	18	1986-2019
GHCND	USW00024233	Seattle-Tacoma Intl	47.44	-122.31	113	1948-2019
GHCND	USC00457507	Sedro-Woolley HCN	48.49	-122.23	18	1896-2019
GHCND	USC00457773	Snoqualmie Falls	47.54	-121.83	134	1898-2019
GHCND	USC00458034	Startup 1-E	47.86	-121.71	52	1924-2019
GHCND	USC00458508	Tolt S Fk RSVR	47.70	-121.69	610	1962-2019
SNOTEL	908	Alpine Meadows	47.78	-121.70	1067	1994-2018
SNOTEL	898	Mount Gardner	47.36	-121.57	890	1993-2018
SNOTEL	672	Olallie Meadows	47.37	-121.44	1228	1980-2018
SNOTEL	911	Rex River	47.30	-121.60	1161	1995-2018
SNOTEL	912	Skookum Creek	47.68	-121.61	1009	1995-2018
SNOTEL	899	Tinkham Creek	47.33	-121.47	911	1993-2018

SM Table 2. Watershed-adjacent Snowpack Telemetry (SNOTEL) sites used to evaluate DHSVM snow production.

SNOTEL Site	ID	Lat. / Lon.	Elv (m)	Years
Skookum Creek	912	47.68N / 121.61W	1009	1995-2018
Alpine Meadows	908	47.78N / 121.7W	1067	1994-2018

SM Table 3. Lapse rates and rain/snow thresholds for the calibrated Stillaguamish DHSVM.

Parameter	Value	
Monthly Temperature Lapse Rate	Oct	-4.5°C/km
	Nov-Mar	-5.5°C/km
	Apr	-5.0°C/km
	May	-4.5°C/km
	Jun-Sep	-4.0°C/km
Precipitation Lapse Rate	0.0 m/km	
Snow Threshold	+1.0 °C	
Rain Threshold	+1.0 °C	

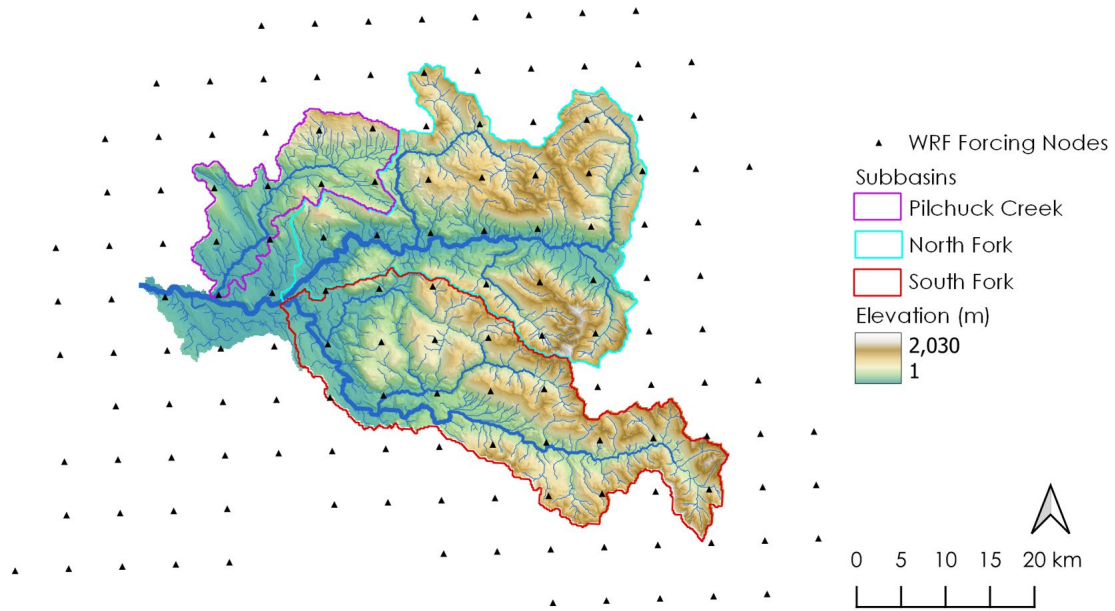
SM Table 4. Select parameterization changes from baseline to final calibration for the Stillaguamish DHSVM.

Parameterization	Baseline	Final	
Soils			
Upland	Lateral Conductivity	0.0001 m/s	0.0002 m/s
Bedrock/ Loam	Exponential Decrease	2.3	1.6
	Porosity (three layers)	0.3 / 0.3 / 0.3	0.26 / 0.25 / 0.25
Gravel Loam	Lateral Conductivity	0.0005 m/s	0.008 m/s
	Exponential Decrease	3	0.6
	Porosity (three layers)	0.45 / 0.45 / 0.45	0.26 / 0.23 / 0.23
Vegetation			
Rain/Snow LAI Multipliers		0.0003 / 0.0003	0.0001 / 0.0003
Conifer	Overstory LAI	12	8
Forests	Understory LAI	3	0.2

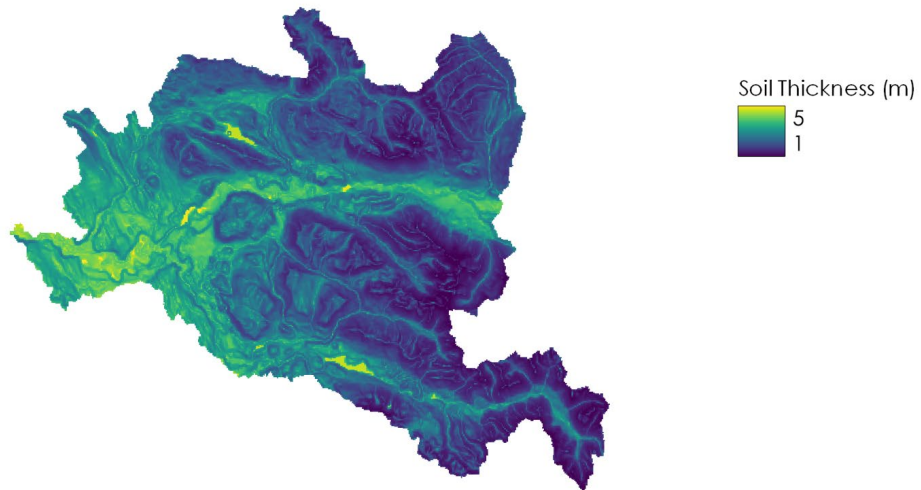
SM Table 5. Stream channel hydraulic geometry classes in the Stillaguamish DHSVM.

Slope		Drainage Area (m ²)		Channel Geometry			Manning's
Min	Max	Min	Max	Class	Width (m)	Depth (m)	n
-	0.0001	-	120,000	1	4.6	0.3	0.055
-	0.0001	120,000	500,000	2	8.4	0.6	0.050
-	0.0001	500,000	5,000,000	3	22.0	1.3	0.045
-	0.0001	5,000,000	20,000,000	4	40.0	2.2	0.040
-	0.0001	20,000,000	170,000,000	5	80.0	5.0	0.035
-	0.0001	170,000,000	-	6	100.0	6.0	0.035
0.0001	0.0025	-	120,000	7	4.3	0.3	0.055
0.0001	0.0025	120,000	500,000	8	7.9	0.6	0.050
0.0001	0.0025	500,000	5,000,000	9	20.6	1.2	0.045
0.0001	0.0025	5,000,000	20,000,000	10	37.5	2.1	0.040
0.0001	0.0025	20,000,000	170,000,000	11	75.0	4.7	0.035
0.0001	0.0025	170,000,000	-	12	93.8	5.6	0.035
0.0025	0.005	-	120,000	13	4.0	0.3	0.055
0.0025	0.005	120,000	500,000	14	7.4	0.5	0.050
0.0025	0.005	500,000	5,000,000	15	19.3	1.1	0.045
0.0025	0.005	5,000,000	20,000,000	16	35.0	1.9	0.040
0.0025	0.005	20,000,000	170,000,000	17	70.0	4.4	0.035
0.0025	0.005	170,000,000	-	18	87.5	5.3	0.035
0.005	0.015	-	120,000	19	3.5	0.2	0.055
0.005	0.015	120,000	500,000	20	6.3	0.5	0.050
0.005	0.015	500,000	5,000,000	21	16.5	1.0	0.045
0.005	0.015	5,000,000	20,000,000	22	30.0	1.7	0.040
0.005	0.015	20,000,000	170,000,000	23	60.0	3.8	0.035
0.005	0.015	170,000,000	-	24	75.0	4.5	0.035
0.015	0.035	-	120,000	25	2.9	0.2	0.055
0.015	0.035	120,000	500,000	26	5.3	0.4	0.050
0.015	0.035	500,000	5,000,000	27	13.8	0.8	0.045
0.015	0.035	5,000,000	20,000,000	28	25.0	1.4	0.040
0.015	0.035	20,000,000	170,000,000	29	50.0	3.1	0.035
0.015	0.035	170,000,000	-	30	62.5	3.8	0.035
0.035	0.035	-	120,000	31	2.3	0.2	0.055
0.035	0.035	120,000	500,000	32	4.2	0.3	0.050
0.035	0.035	500,000	5,000,000	33	11.0	0.7	0.045
0.035	0.035	5,000,000	20,000,000	34	20.0	1.1	0.040
0.035	0.035	20,000,000	170,000,000	35	40.0	2.5	0.035
0.035	0.035	170,000,000	-	36	50.0	3.0	0.035

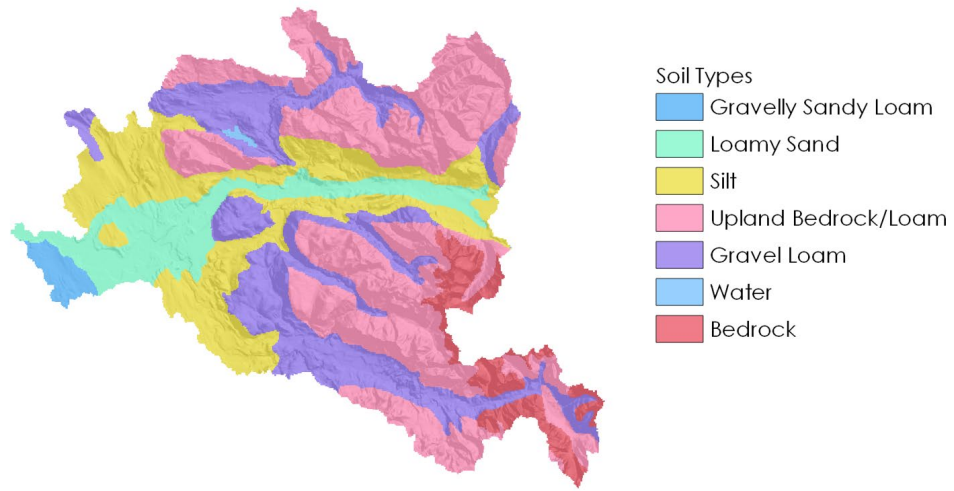
SM Figures



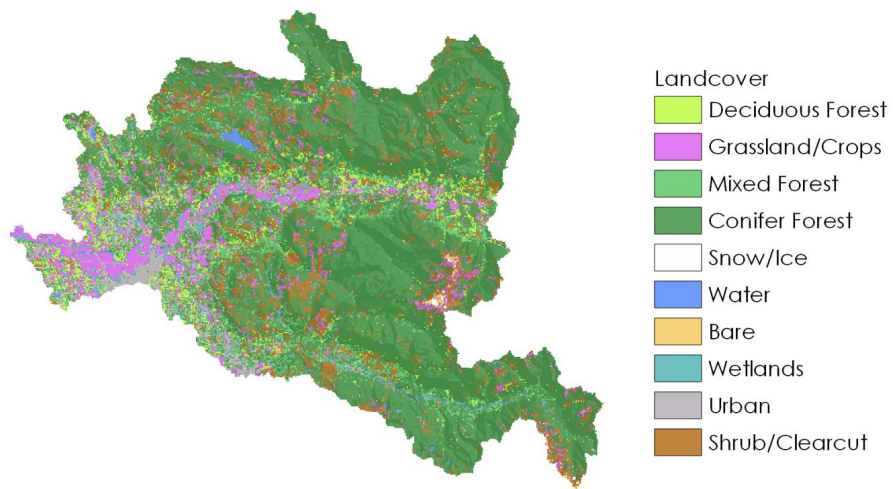
SM Figure 1. Topography of the Stillaguamish watershed DHSVM. Primary subbasins are outlined. Meteorologic forcing nodes at 6-kilometer resolution area also shown.



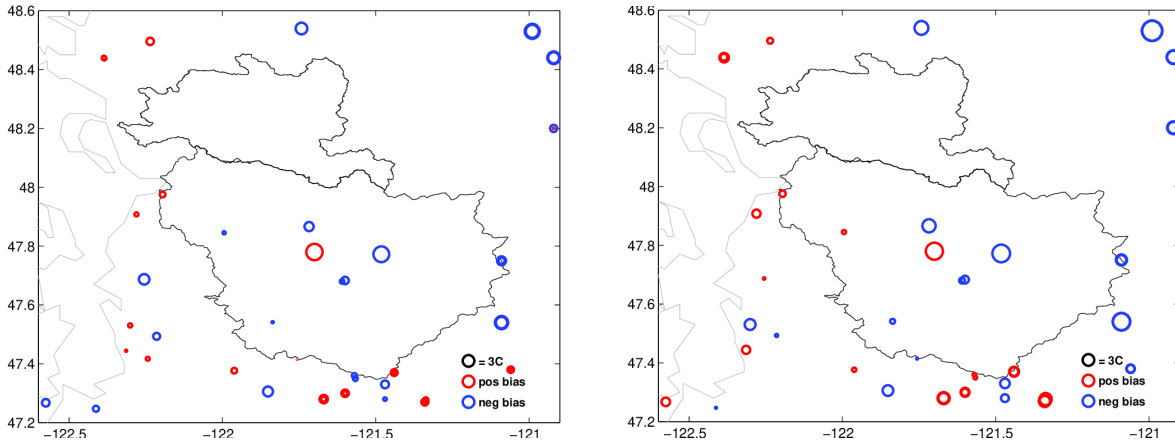
SM Figure 2. Simulated soil thickness in the Stillaguamish watershed DHSVM.



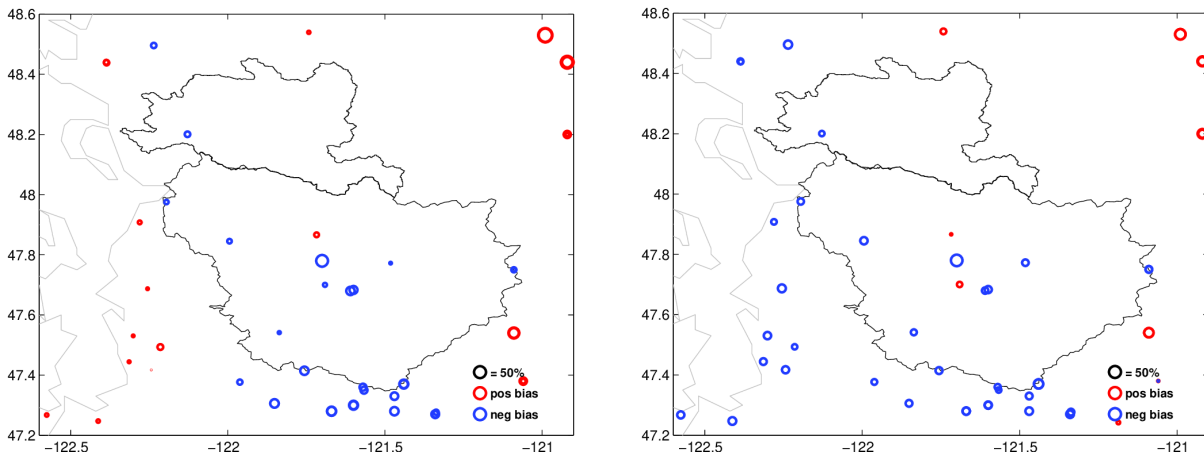
SM Figure 3. Soil types in the Stillaguamish watershed DHSVM.



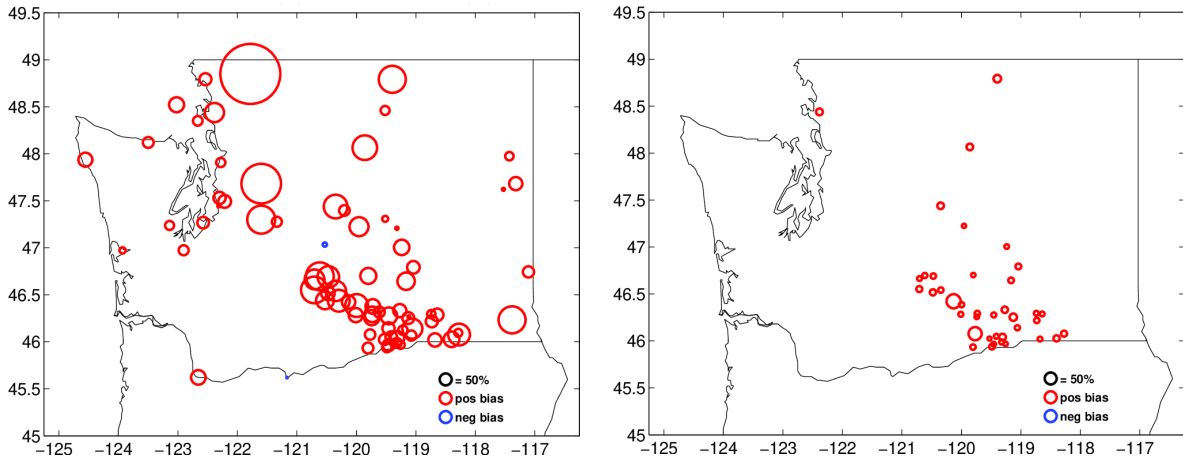
SM Figure 4. Landcover classes in the Stillaguamish watershed DHSVM.



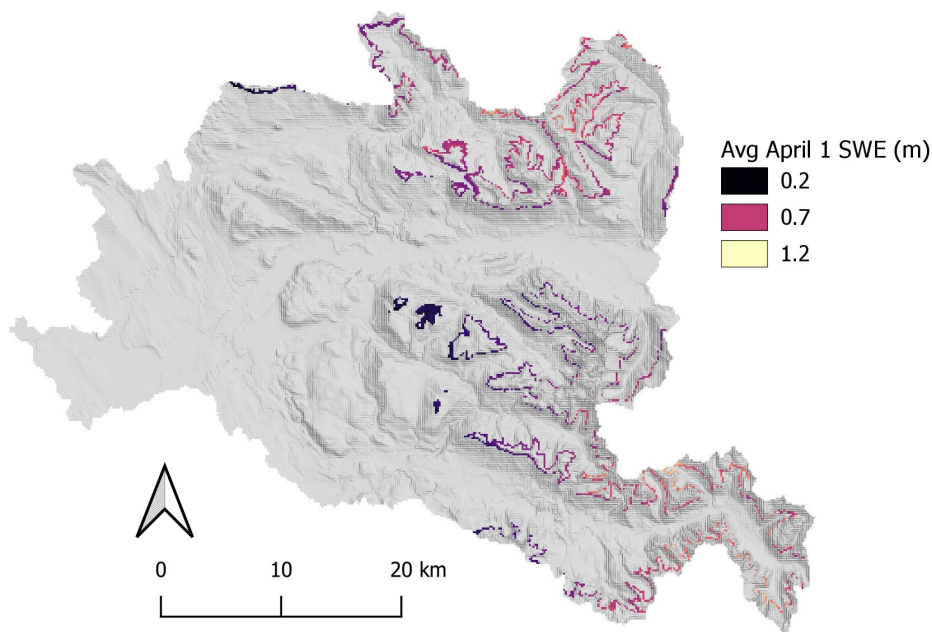
SM Figure 5. Map of annual average temperature biases for the PNNL-Obs simulation. The map to the left shows the bias for annual average daily temperature; the map on the right shows the same for maximum annual temperature. The size of each circle denotes the bias ($^{\circ}\text{C}$), while the color denotes the sign of the bias. The Stillaguamish and Snohomish watersheds are outlined in black, while the Puget Sound coastline is shown in grey.



SM Figure 6. As in SM Figure 5 except showing the annual average (left) and top 1% (right) precipitation biases (%) for the PNNL-Obs simulation.

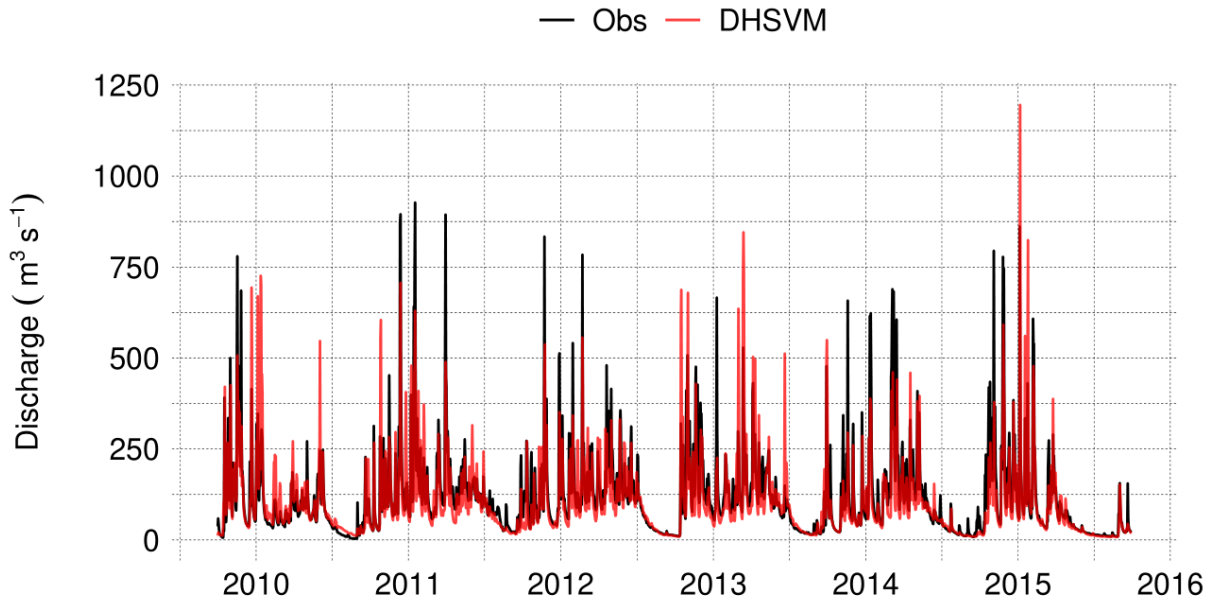


SM Figure 7. As in SM Figure 5 except showing the bias in annual average wind speed (left) and incoming shortwave radiation (right). Results are shown for the entire state of Washington since relatively fewer observations are available.

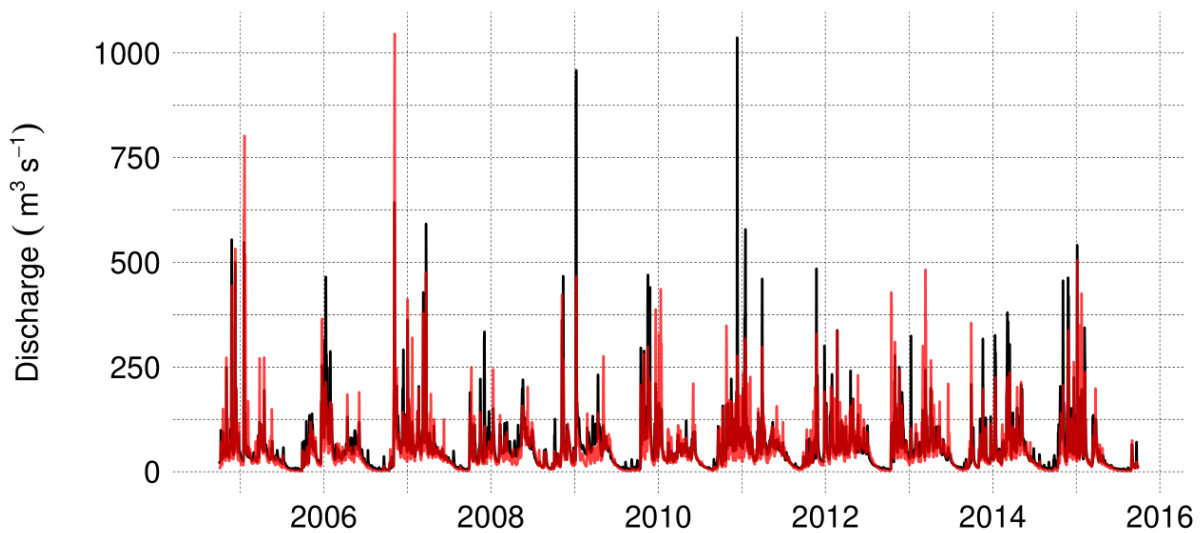


SM Figure 8. Map of mean April 1st simulated snow depth as snow water equivalent (SWE) for water years 2004 through 2015. Only pixels with elevations between 1005 and 1070 meters above sea level highlighted. This elevation band comprises the elevations of the Skookum Creek and Alpine Meadows SNOTEL stations in the adjacent Snohomish basin (SM Table 2). Mean simulated SWE for these pixels was 0.6 meters; mean observed SWE at the Skookum Creek and Alpine meadows stations over this same period was 1.07 m.

Silvana

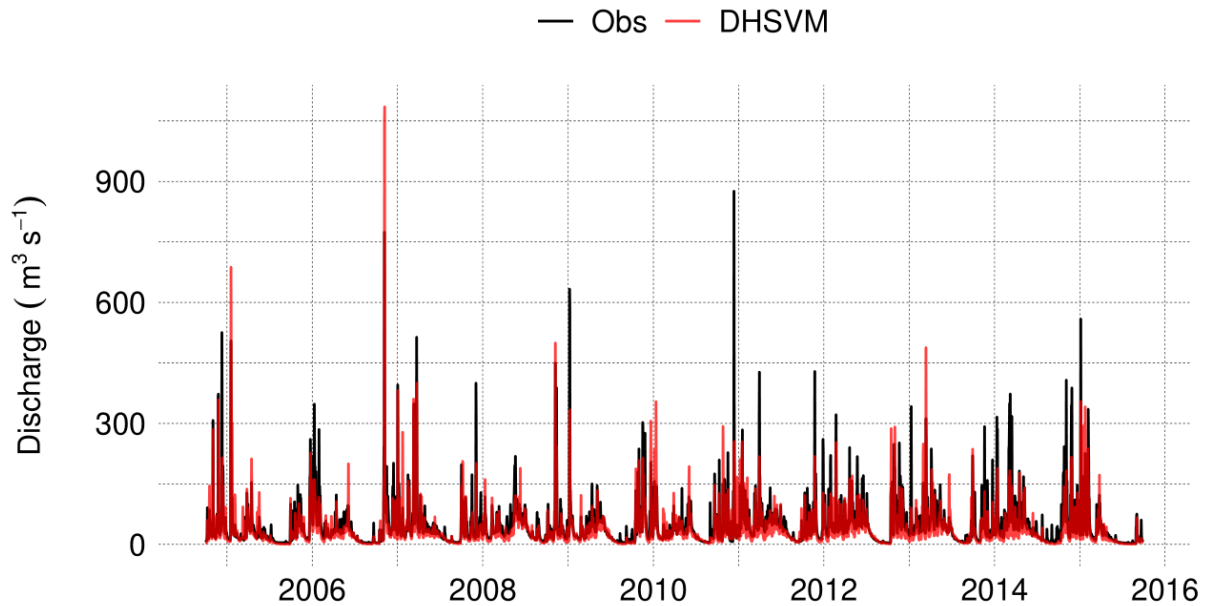


NFArlington

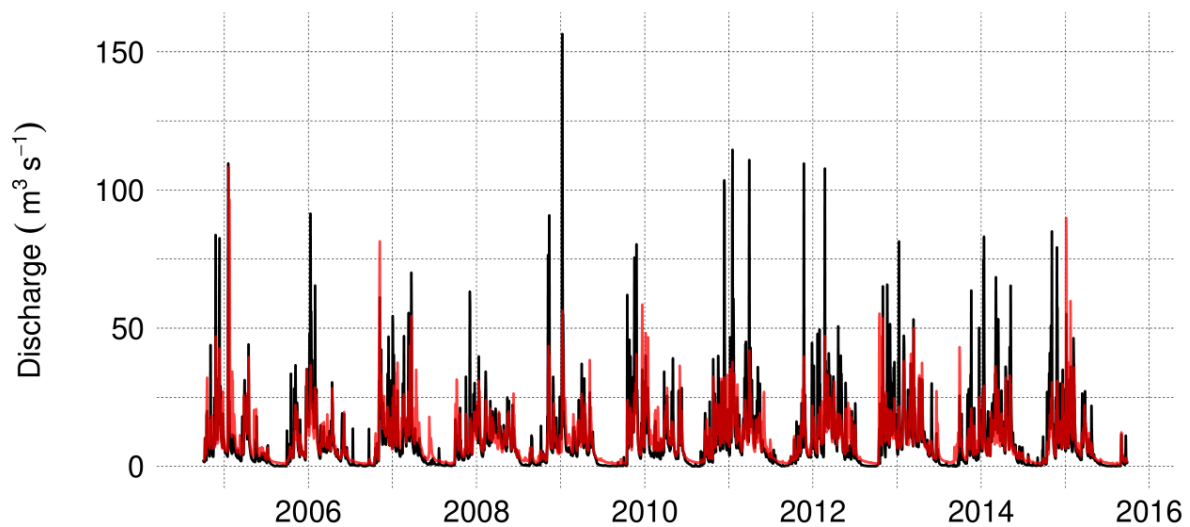


SM Figure 9. Daily mean hydrographs of observed flows (black) and DHSVM simulated flows (red) at the Silvana and NFArlington gauging stations in the Stillaguamish River (refer to Figure 1 of the primary document for locations). Statistical evaluation scores are provided in the Table 3 of the primary document.

SFJordanRd

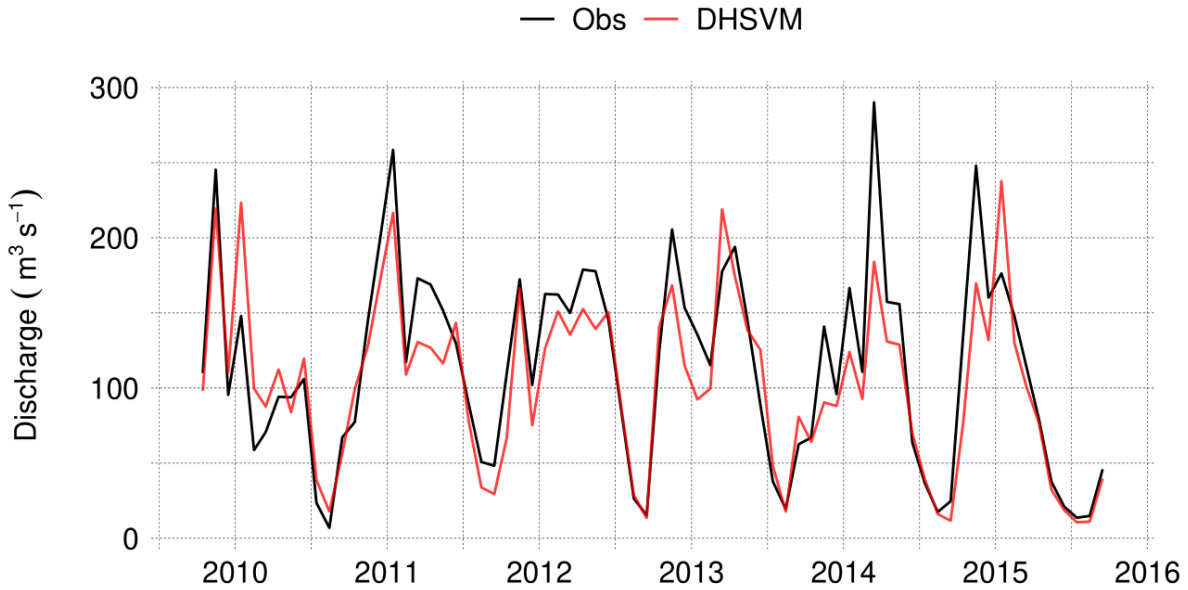


Pilchuck626

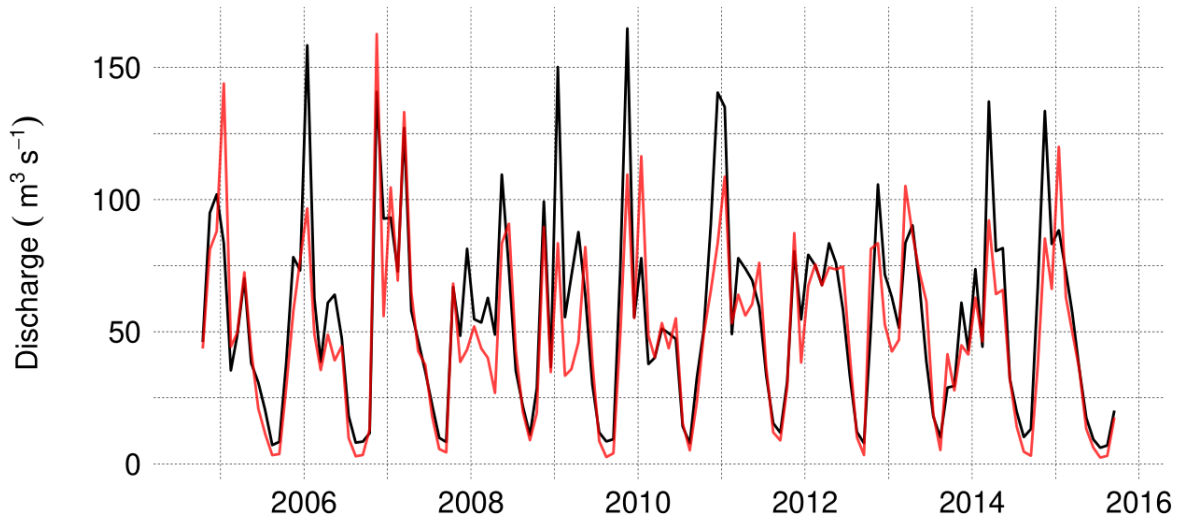


SM Figure 10. Daily mean hydrographs of observed flows (black) and DHSVM simulated flows (red) at the SFJordanRd and Pilchuck626 gauging stations in the Stillaguamish River (refer to Figure 1 of the primary document for locations). Statistical evaluation scores are provided in the Table 3 of the primary document.

Silvana

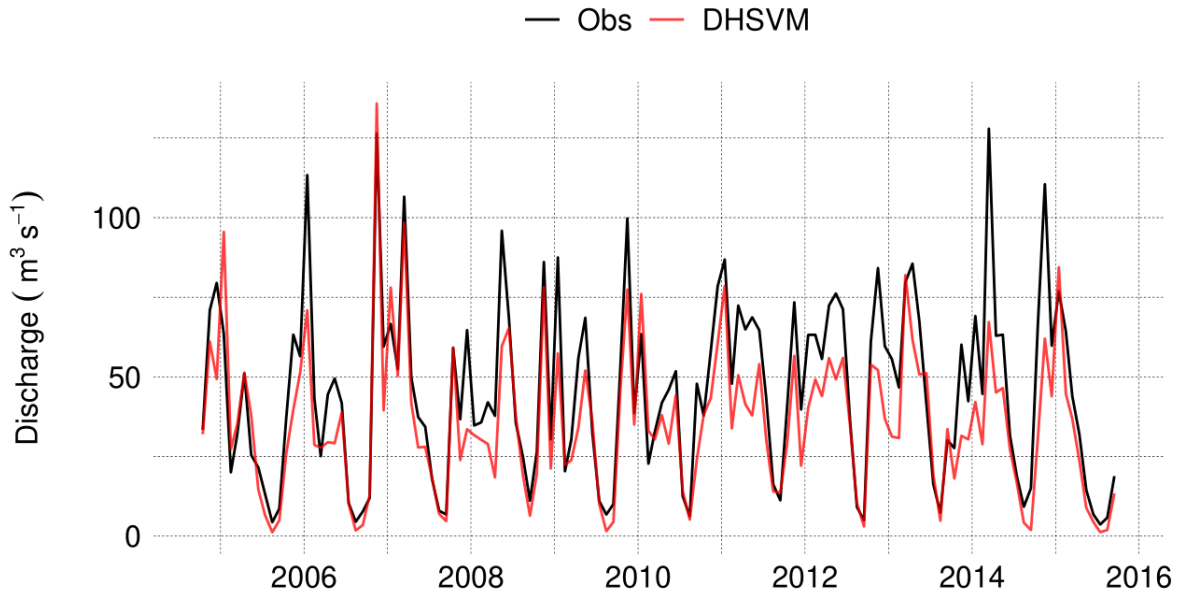


NFArlington

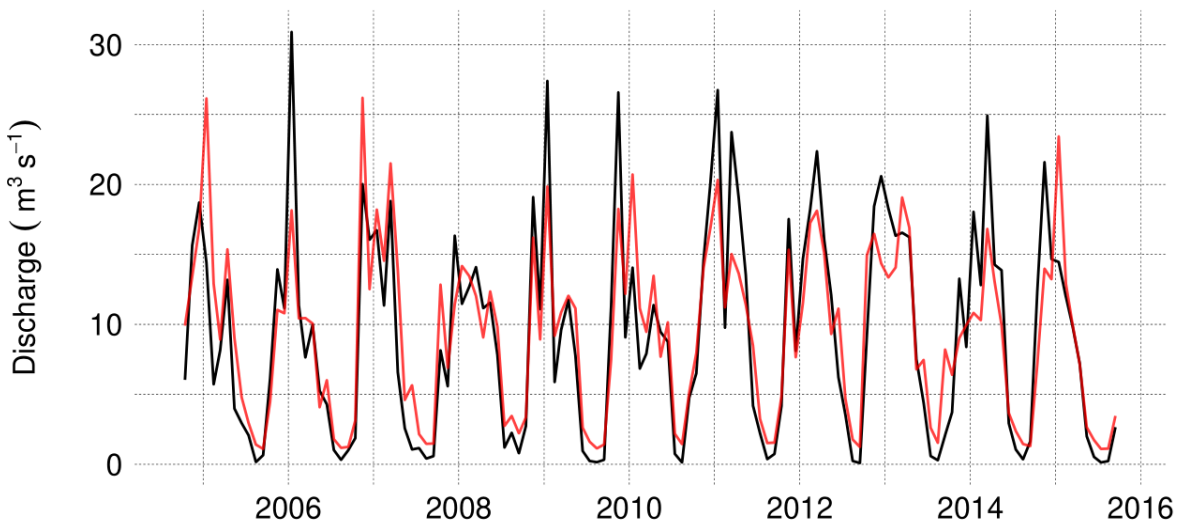


SM Figure 11. Monthly mean hydrographs of observed flows (black) and DHSVM simulated flows (red) at the Silvana and NFArlington gauging stations in the Stillaguamish River (refer to Figure 1 of the primary document for locations). Statistical evaluation scores are provided in the Table 3 of the primary document.

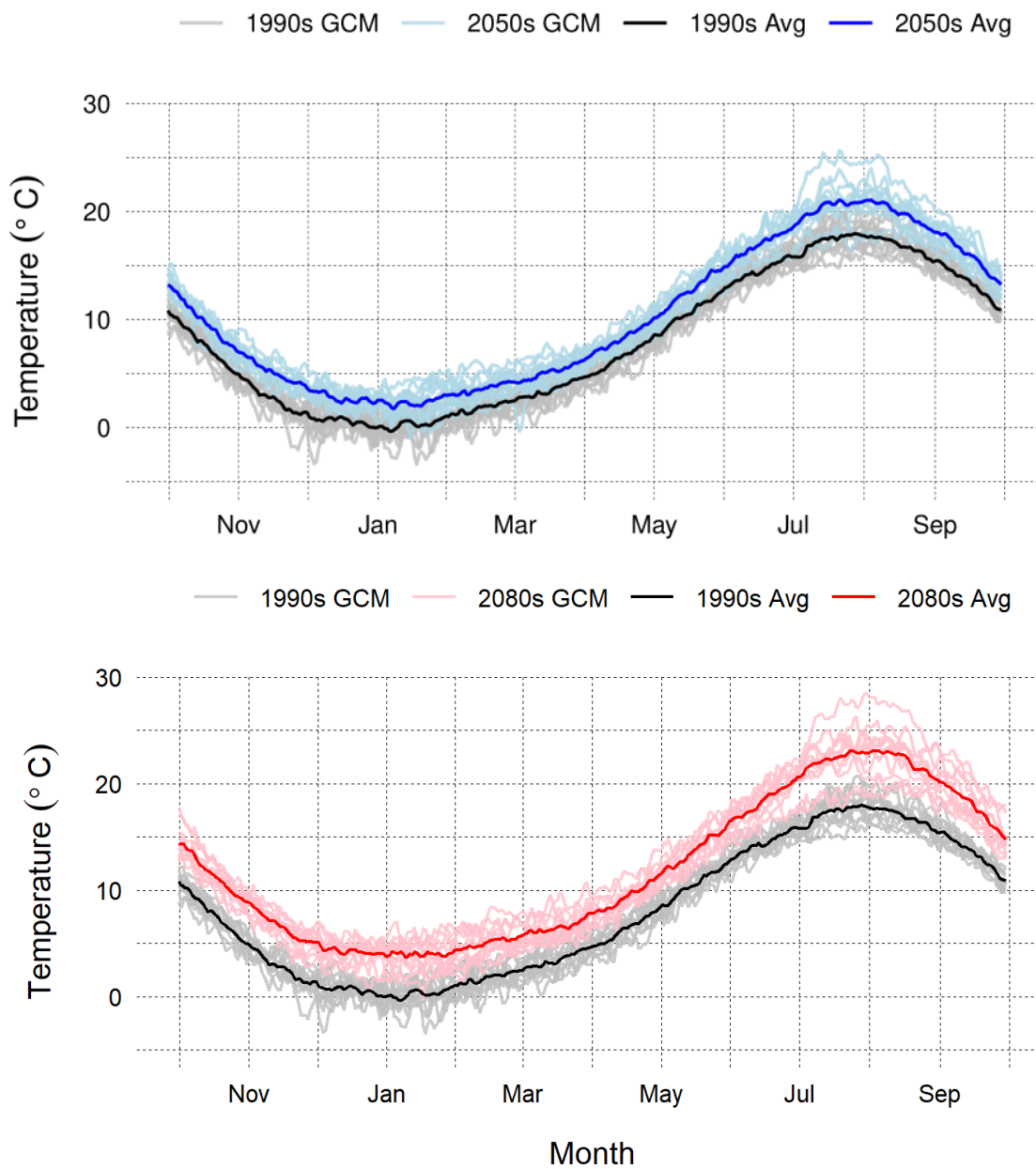
SFJordanRd



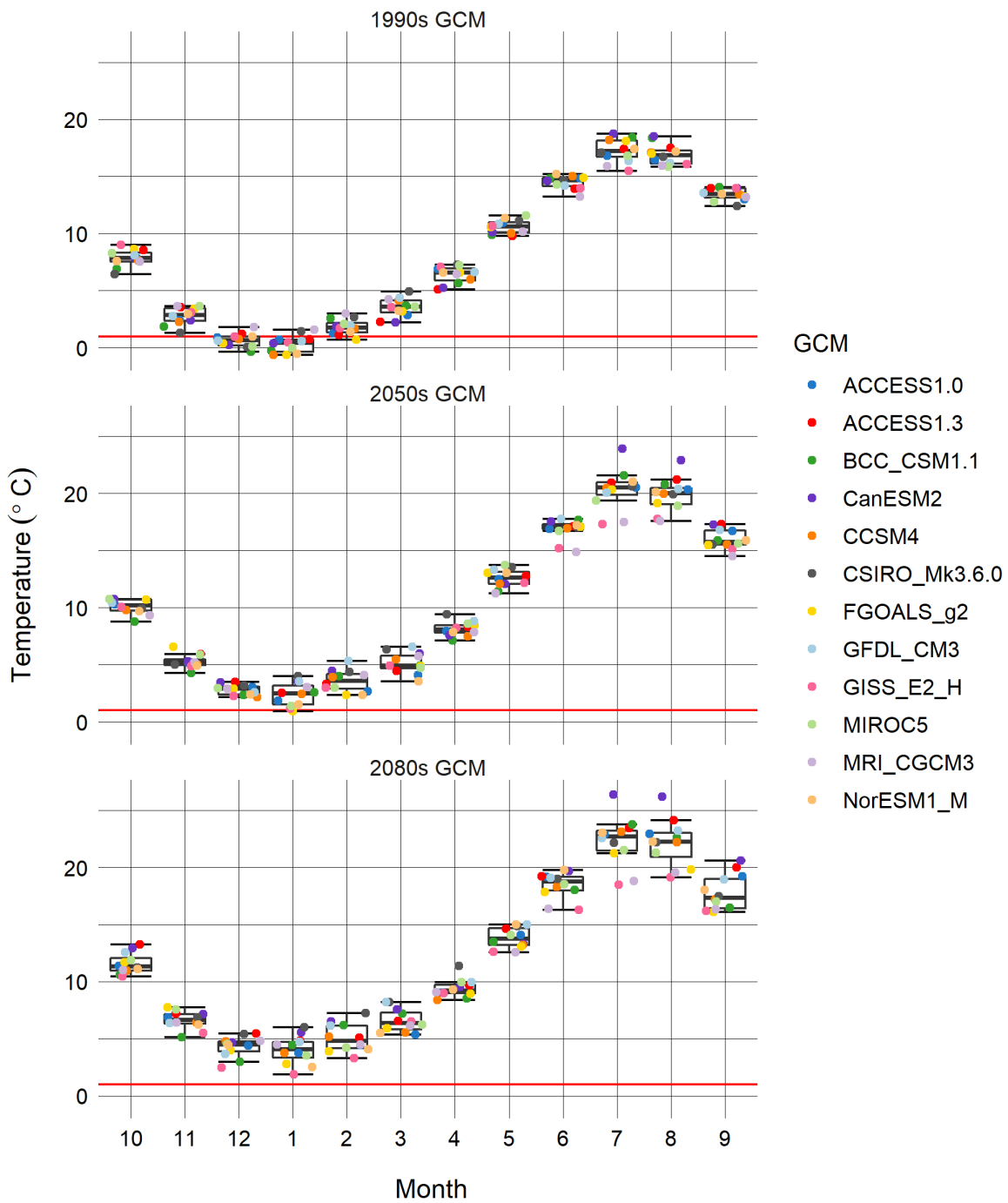
Pilchuck626



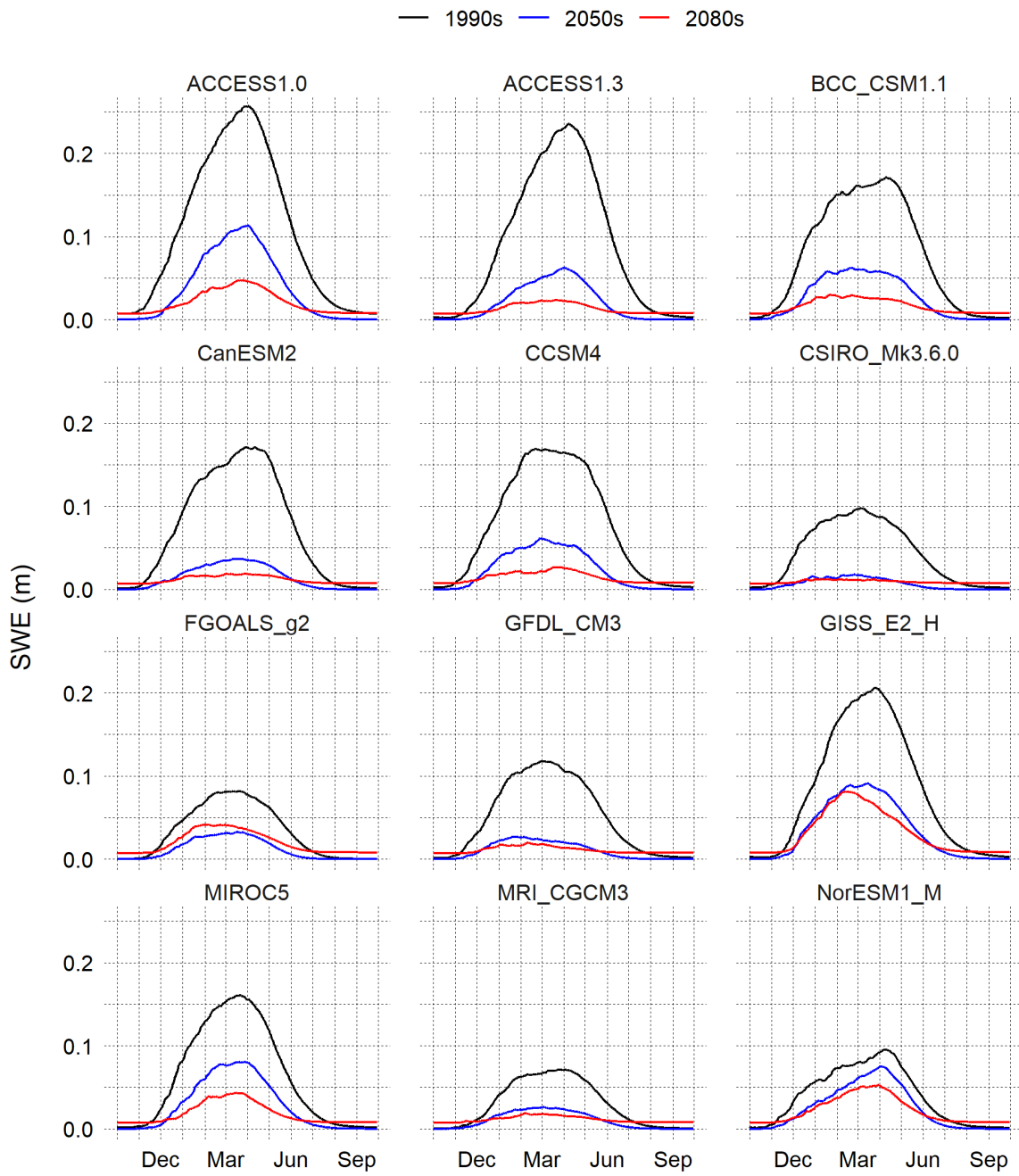
SM Figure 12. Monthly mean hydrographs of observed flows (black) and DHSVM simulated flows (red) at the SFJordanRd and Pilchuck626 gauging stations in the Stillaguamish River (refer to Figure 1 of the primary document for locations). Statistical evaluation scores are provided in Table 3 of the primary document.



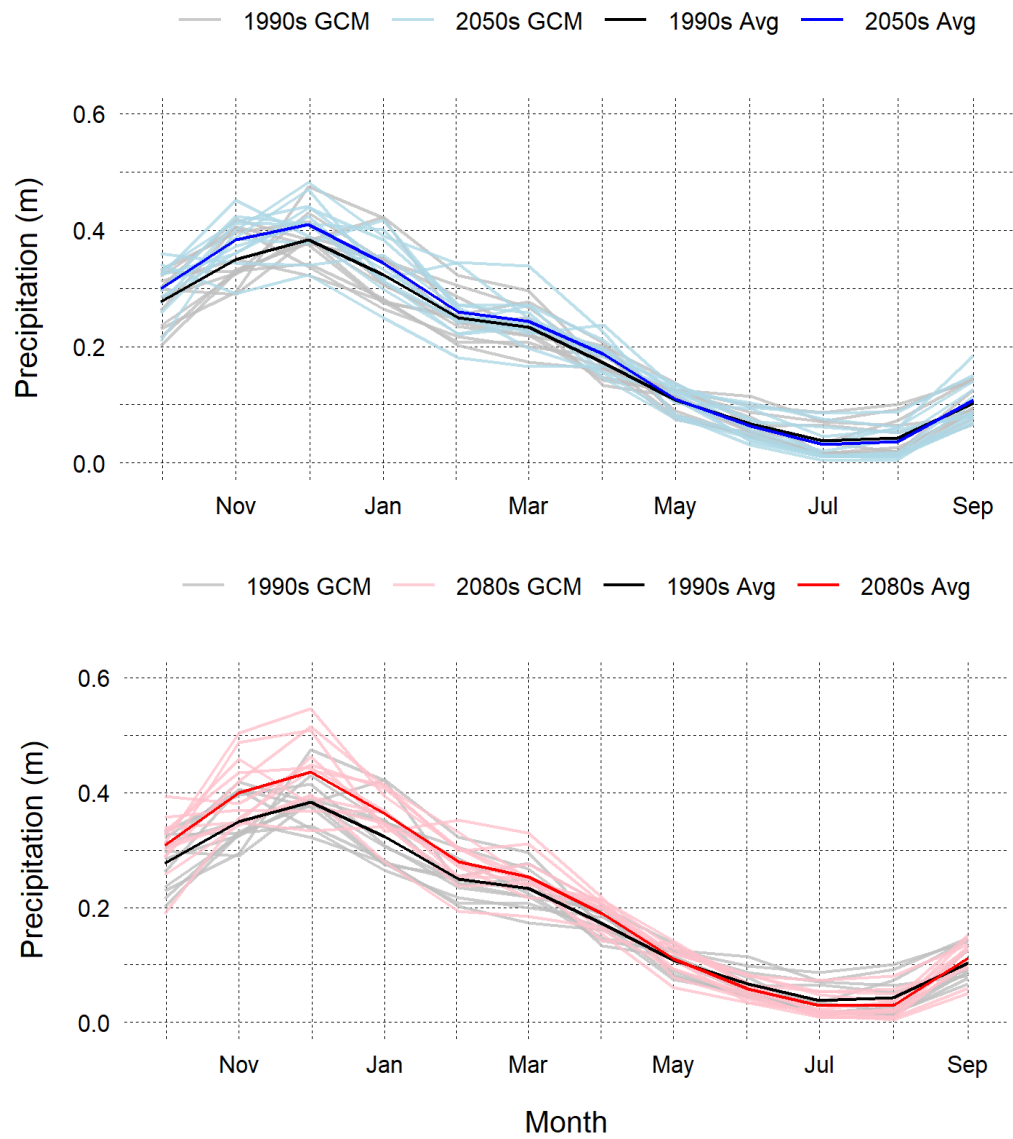
SM Figure 13. Simulated (basin average) mean daily air temperature in the Stillaguamish watershed. Light gray, blue, and red lines represent individual general circulation model (GCM) averages over 30-year climate normals for the 1990s and 2050s (top) and 2080s (bottom) respectively. Bolded black, blue, and red lines represent ensemble averages across all 12 GCMs.



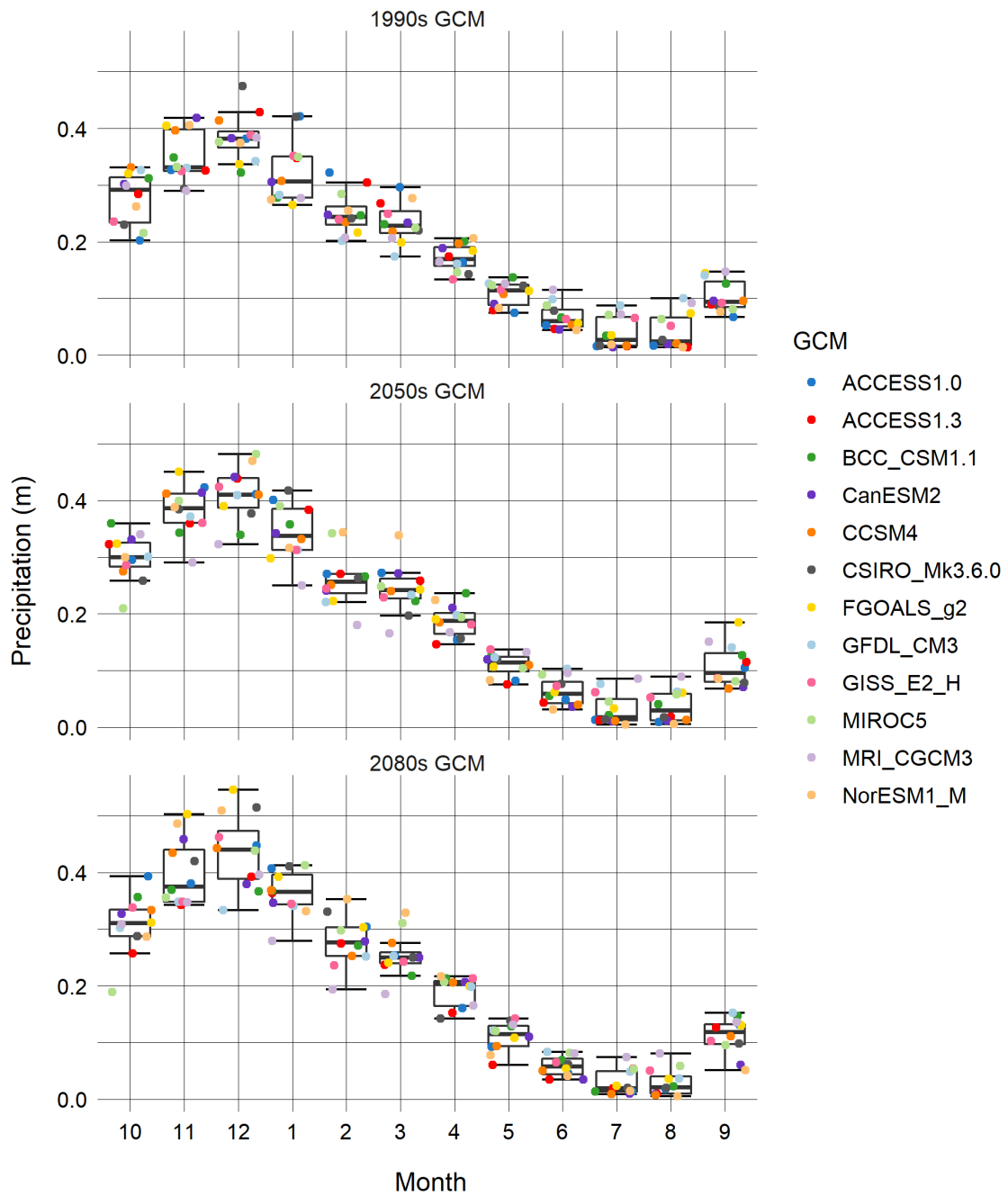
SM Figure 14. Simulated (basin average) mean monthly air temperature in the Stillaguamish watershed by parent general circulation model (GCM) and climate normal. The red line denotes rain/snow threshold in the hydrologic model.



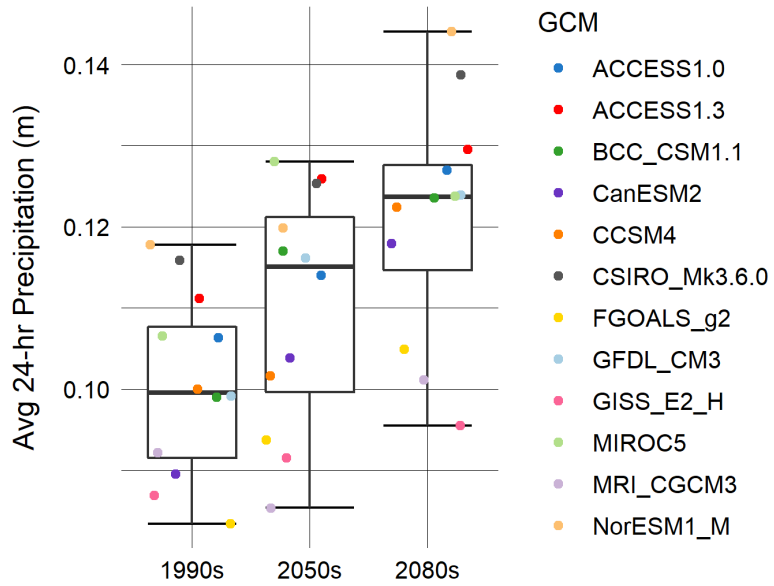
SM Figure 15. Simulated (basin average) mean annual snow water equivalent by parent general circulation model (GCM) and climate normal.



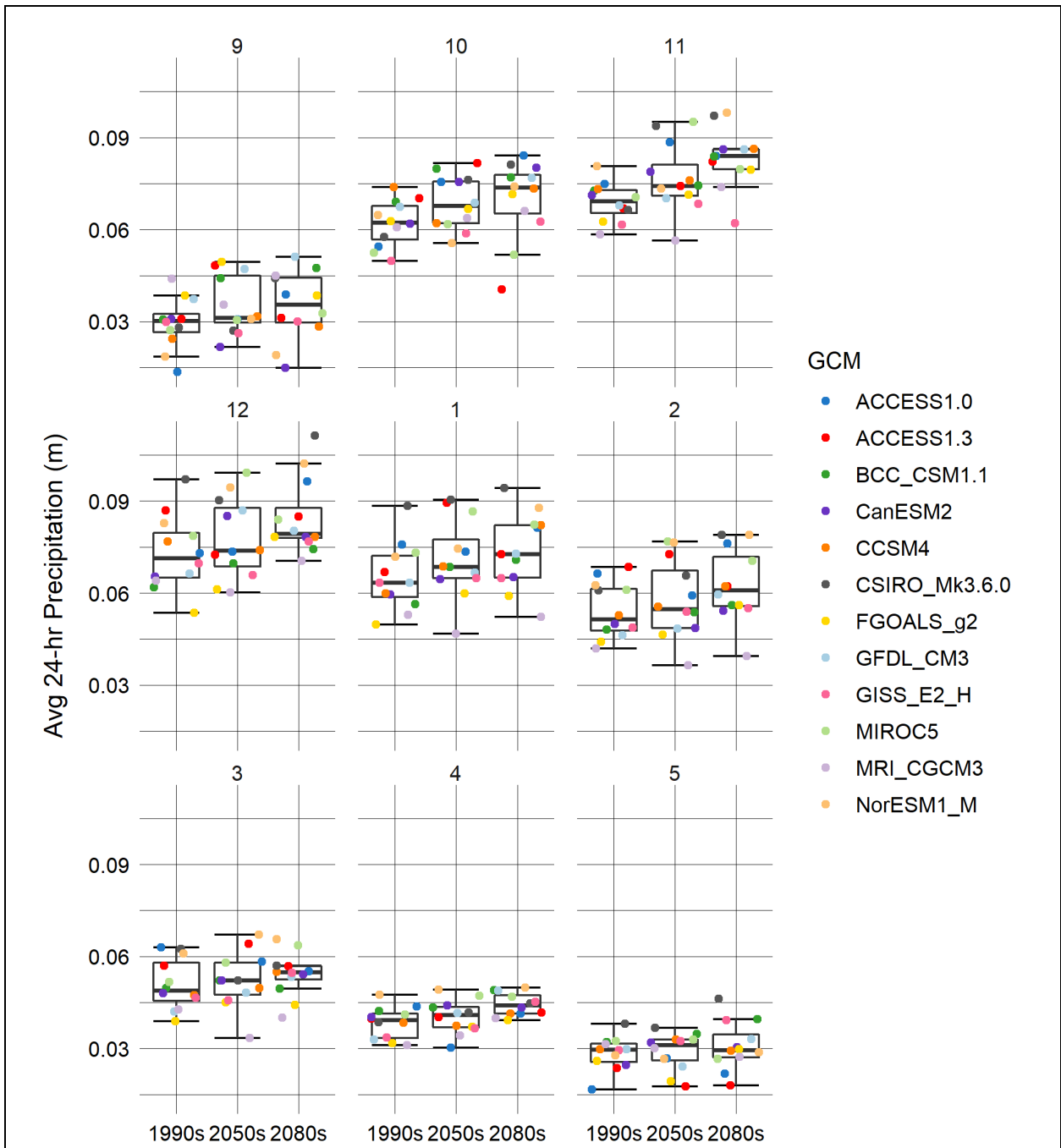
SM Figure 16. Simulated (basin average) mean monthly precipitation magnitude in the Stillaguamish watershed. Light gray, blue, and red lines represent individual general circulation model (GCM) averages over 30-year climate normals for the 1990s and 2050s (top) and 2080s (bottom) respectively. Bolded black, blue, and red lines represent ensemble averages across all 12 GCMs.



SM Figure 17. Simulated (basin average) mean monthly precipitation magnitude in the Stillaguamish watershed by parent general circulation model (GCM) and climate normal.

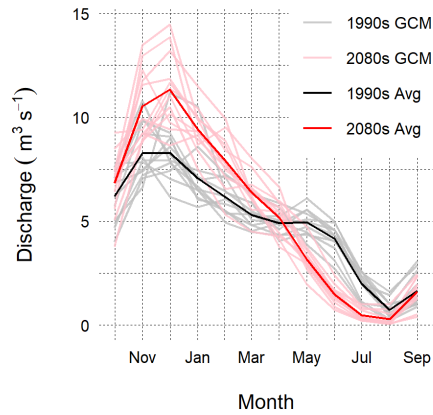
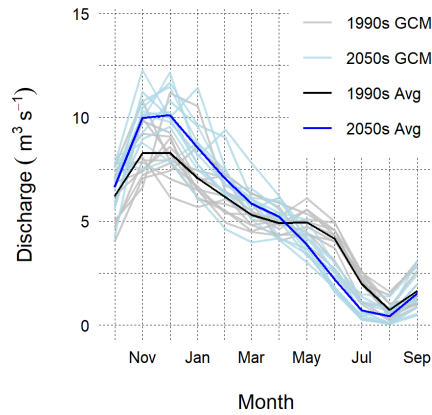


SM Figure 18. Simulated (basin average) mean annual maximum 24-hour precipitation magnitude by climate normal and parent general circulation model (GCM).

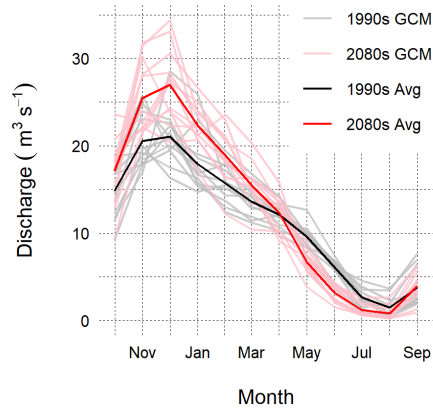
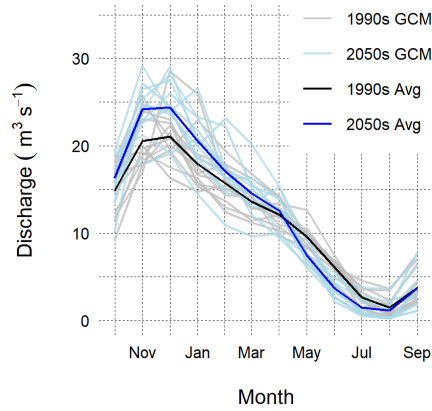


SM Figure 19. Simulated (basin average) mean month-annual maximum 24-hour precipitation magnitude for each climate normal and parent general circulation model (GCM). Each point represents the mean maximum precipitation magnitude within a given month over a 30-year climate normal period. Summer months (June through August) are omitted.

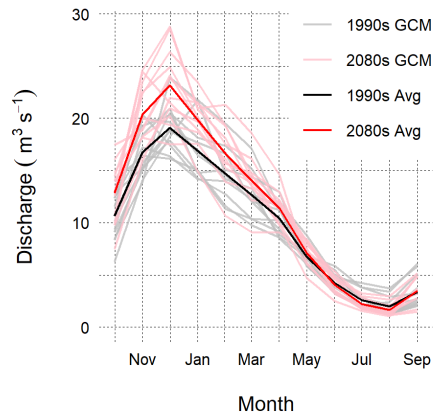
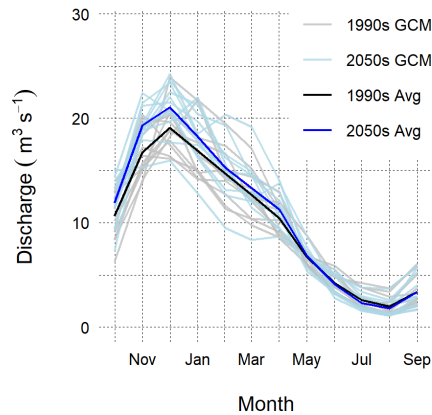
NFBoulderCreek



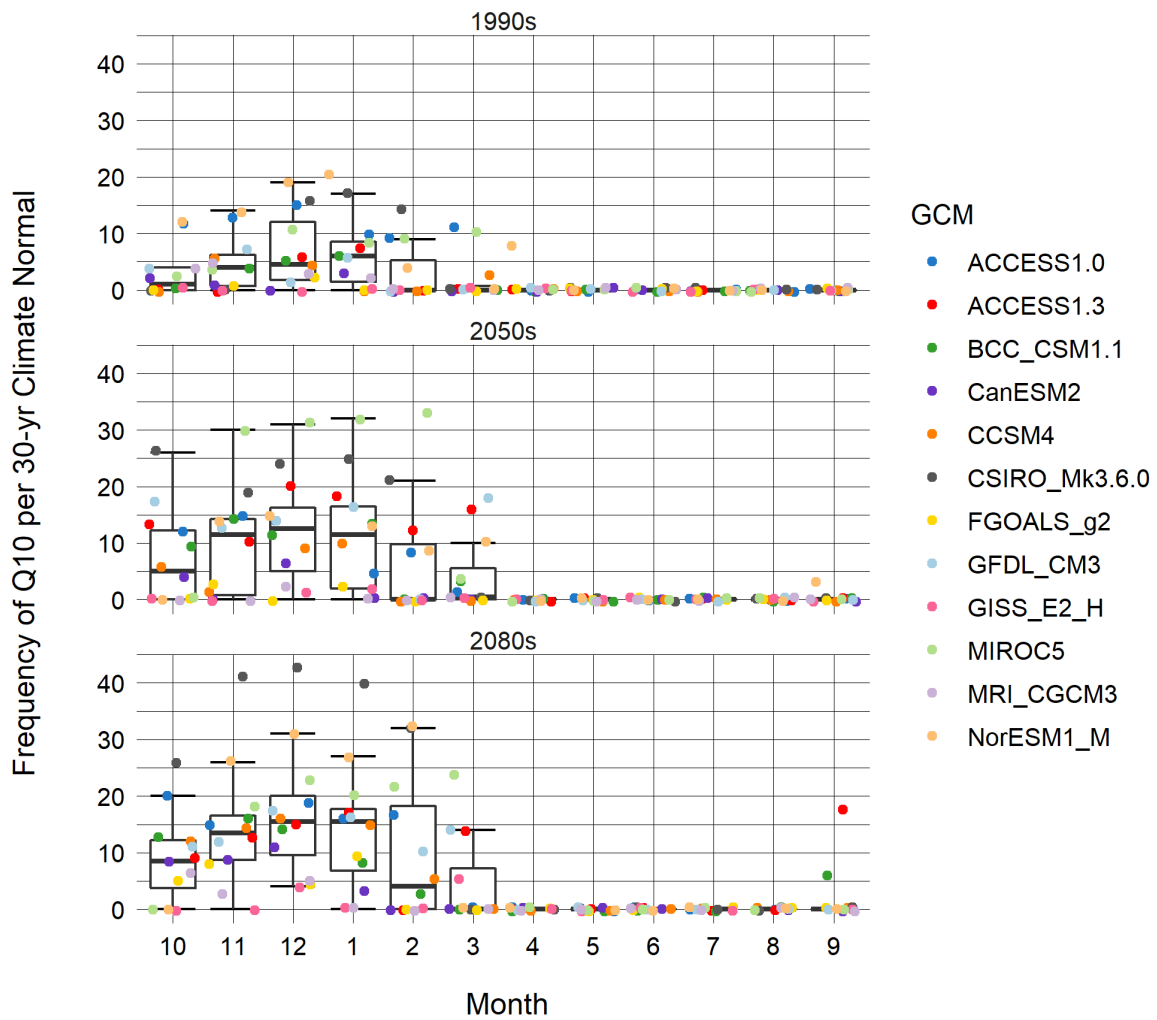
SFCanyonCreek



Pilchuck626



SM Figure 20. Simulated monthly mean stream discharge. Light gray, blue, and red lines represent individual general circulation model (GCM) averages over 30-year climate normals for the 1990s and 2050s (left) and 2080s (right) respectively. Bolded black, blue, and red lines represent ensemble averages across all 12 GCMs. NFBoulderCreek and SFCanyonCreek drain high elevation tributaries of the Stillaguamish River with substantial snowpack in 1990s hindcasts. Pilchuck626 drains a lower-relief rain-dominated tributary of the Stillaguamish River.



SM Figure 21. Monthly frequency of 3-hour 10-year peak flow occurrence per 30-year climate normal at Stanwood by general circulation model (GCM). The 10-year peak flow threshold is $1729 \text{ m}^3\text{s}^{-1}$ which was calculated from the empirical Gumbel extreme value function for the PNNL-Obs simulation from 1985-2015. Each climate normal encompasses 30 years. On average, a 10-year flow should occur about 3 times per 30-year climate normal.